# DESIGN AND DEVELOPMENT OF UNIVERSAL ANTIBIOFILM COATINGS FOR URINARY CATHETERS

by

Yan Mei

B.Eng., Wuhan University of Technology, 2009

M.Eng., Southeast University, 2012

A THESIS SUBMITTED IN PARTIAL FULFILLMENT OF

THE REQUIREMENTS FOR THE DEGREE OF

DOCTOR OF PHILOSOPHY

in

THE FACULTY OF GRADUATE AND POSTDOCTORAL STUDIES

(Pathology and Laboratory Medicine)

THE UNIVERSITY OF BRITISH COLUMBIA

(Vancouver)

March 2020

The following individuals certify that they have read, and recommend to the Faculty of Graduate and Postdoctoral Studies for acceptance, the dissertation entitled:

Design and development of universal antibiofilm coatings for urinary catheters

submitted by Yan Mei in partial fulfillment of the requirements for

the degree of Doctor of Philosophy

in Pathology and Laboratory Medicine

**Examining Committee:**

Jayachandran N. Kizhakkedathu, Professor, Pathology and Laboratory Medicine, UBC
Supervisor

Dirk Lange, Associate Professor, Department of Urologic Sciences, UBC
Supervisory Committee Member

Rizhi Wang, Professor, Department of Materials Engineering, UBC
University Examiner

Christian Kastrup, Associate Professor, Department of Biochemistry & Molecular Biology, UBC
University Examiner

**Additional Supervisory Committee Members:**

Donald E. Brooks, Professor, Department of Chemistry, UBC
Supervisory Committee Member

## Abstract

Catheter-associated urinary tract infection is one of the most common medical device-associated complications that has caused significant morbidity, mortality and costs. There is a significant need for new technologies to prevent such catheter-related infections. Despite advancements in the development of antimicrobial and antibiofilm coatings in recent years, current coating technologies to prevent biofilm formation fail to address all factors, including prevention of biological deposition, inhibition of bacterial colonization, adaptation to diverse materials, easy application to devices of various sizes and shapes, and stability of the coating. This thesis addresses my attempts to explore new knowledge and develop novel technologies to address this important medical need.

In Chapter 2, by using a high throughput screening method, we identified a highly durable thin hydrophilic coating which prevents biofilm formation over a long-term period (>4 weeks) in the presence of high concentration of bacteria. Furthermore, this coating can easily be applied to diverse substrates of varying shapes and material properties *via* a dip coating process and demonstrates a broad spectrum of bacterial adhesion resistance. When the coating was applied to commercial catheters, biofilm formation was consistently less with coated catheter than with uncoated catheters both *in vitro* and *in vivo*.

In Chapter 3, we propose a new mechanism for the stable coating formation between polycatecholamines and hydrophilic polymers. The hydrophilic polymers have an active role in the co-assembly and co-deposition process, which is influenced by the molecular weight and chemistry of the hydrophilic polymer. We determined that the self-assembly of different

polycatecholamines is influenced by different polymers but the nature of polycatecholamine is not the major factor that influences the final characteristics of the coating.

In Chapter 4, a facile layer-by-layer assembly process of a hydrophilic polymer with a natural polyphenol tannic acid was used to fabricate stable bacteria-resistant multilayers with controlled thickness. We demonstrated that the main driving force in this layer-by-layer assembly process is the hydrogen bonding between the polymers and tannic acid. This work demonstrates the fabrication of novel bacteria-resistant coatings and provides a potential platform incorporate antimicrobial agents for the development of multifunctional coatings.

## Lay Summary

Urological catheters are plastic tubes used to remove urine from patients undergoing surgery or have difficulty in urinating. Demand for urological catheters is growing large due to the increase in aging population. However, the use of catheters is associated with infection due to attachment of bacteria on the catheter surface, which is made of hydrophobic plastic materials, leading to the device removal and complications including poor quality of life and death in patients. Hence, this thesis aims to develop coatings that could prevent the incidence of such catheter infections. With the application of the new coating, catheters will behave like a non-stick material and thereby able to prevent the bacterial adhesion and growth on the surface. Interactions between the catheters and urine components will also be reduced. This study will largely improve the safety and performance of medical devices, thus improving patients' health.

## Preface

Ethics approval was received from the University of British Columbia for studies conducted at the Centre for Blood Research (UBC Ethics approval no: H07-02198). All animal work conducted for this study was approved by The University of British Columbia Animal Care Committee. This thesis was conducted under the supervision of Dr. Jayachandran N. Kizhakkedathu at the Centre for Blood Research, University of British Columbia, Vancouver.

A modified version of Chapter 2 has been published. **Yan Mei**, Kai Yu, Joey C. Y. Lo, Lily E. Takeuchi, Narges Hadjesfandiari, Hossein Yazdani-Ahmadabadi, Donald E. Brooks, Dirk Lange, Jayachandran N. Kizhakkedathu. Polymer-nanoparticle interaction as a design principle in the development of a durable ultrathin universal binary antibiofilm coating with long-term Activity. *ACS Nano*, 2018, 12, 11881-11891. I am the first author and was responsible for concept designing, polymer synthesis, surface modification, surface characterization, *in vitro* evaluation of protein adsorption, platelet adhesion, bacterial adhesion and biofilm formation, data analysis, and manuscript writing. Kai Yu examined the surface morphology and performed formed force measurements using atomic force microscopy. Joey C. Y. Lo performed animal studies to prove the efficacy of the coating. Lily E. Takeuchi helped with cell studies to demonstrate the biocompatibility of the coating.

A modified version of Chapter 3 is under submission for publication. **Yan Mei**, Kai Yu, Dirk Lange, Jayachandran N. Kizhakkedathu. Mechanism of polymer guided polycatecholamine assembly and deposition. I was responsible for concept designing, polymer synthesis, surface modification, surface characterization, *in vitro* evaluation of bacterial adhesion, data analysis,

and manuscript writing. Kai Yu examined the surface morphology and performed force measurements using atomic force microscopy.

Chapter 4 generates a new type of antibiofilm coating for preventing biofilm formation. I was responsible for all the experiments and data analysis. The experimental work includes polymer synthesis, surface modification, surface characterization and *in vitro* evaluation of bacterial adhesion.

# Table of Contents

## List of Tables

## List of Figures

## List of Symbols

| | |
|---|---|
| °C | Degree Celsius |
| s | Second |
| h | Hour |
| g | Gram |
| mg | Milligram |
| mL | Milliliter |
| M | Molar |
| mM | Millimolar |
| µg | Microgram |
| nm | Nanometer |

## List of Abbreviations

| | |
|---|---|
| 4-VP | 4-Vinylpyridine |
| AAEGal | 2′-acrylamidoethyl-β-D-galactopyranoside |
| AGE | Allyl glycidyl ether |
| AM | Acrylamide |
| AMP | Antimicrobial peptide |
| APEG | Allyloxy polyethylene glycol |
| APMA | *N*-(3-Aminopropyl) methacrylamide hydrochloride |
| ATR-FTIR | Attenuated total reflectance Fourier transform infrared |
| ATRP | Atom transfer radical polymerization |
| BPEI | Branched polyethyleneimine |
| BSA | Bovine serum albumin |
| CAB | Catheter-associated bacteriuria |
| CAUTI | Catheter-associated urinary tract infection |
| CFU | Colony-forming unit |
| CHX | Chlorhexidine |
| CTL | Cateslytin |
| DAPI | 4′,6-Diamidino-2-phenylindole |
| DLS | Dynamic light scattering |
| DMA | *N,N*-dimethylacrylamide |
| DMA | Dopamine methacrylamide |

| | |
|---|---|
| DMAEMA | 2-(Dimethylamino)-ethyl methacrylate |
| ePTFE | Expanded poly(tetrafluoroethylene) |
| EDTA | Ethylenediaminetetraacetic acid |
| EMEM | Eagle's modified essential media |
| Fib | Fibrinogen |
| fPEG | Perfluoroalkyl polyethylene glycol |
| FITC | Fluorescein isothiocyanate |
| GPC | Gel permeation chromatography |
| HA | Hyaluronic acid |
| HEA | *N*-Hydroxyethyl acrylamide |
| HEMA | 2-Hydroxyethyl methacrylate |
| Hgb | Hemoglobin |
| HMA | *N*-Hydroxymethyl acrylamide |
| HMTETA | 1, 1, 4, 7, 10, 10-hexamethyl triethylene tetramine |
| HPG | Hyperbranched polyglycerol |
| HPG-SH | Hyperbranched polyglycerol bearing terminal thiol moieties |
| HPMA | *N*-(2-Hydroxypropyl) methacrylamide |
| LbL | Layer-by-layer |
| LB | Lysogeny broth |
| Lys | Lysozyme |
| MPDSAH | 3-((Methacryloyl)amido)propyl)dimethyl(3-sulfopropyl)ammonium hydroxide |

| | |
|---|---|
| MPC | 2-Methacryloyloxyethyl phosphorylcholine |
| MPN | Metal-phenolic network |
| MW | Molecular weights |
| nHA | *n*-Heptylamine |
| NF | Nitrofurazone |
| NO | Nitric oxide |
| pPVC | Plasticized PVC |
| PAA | Poly(acrylic acid) |
| PAA-Alk | Poly(acrylic acid) with alkyne functionality |
| PAA-Az | Poly(acrylic acid) with azide functionality |
| PAAEGal | Poly(2′-acrylamidoethyl-β-D-galactopyranoside) |
| PAM | Polyacrylamide |
| PANI | Polyaniline |
| PAH | Poly(allylamine hydrochloride) |
| PBS | Phosphate-buffered saline |
| PDA | Polydopamine |
| PDI | Polydispersity index |
| PDLLA | Poly(D,L-lactide) |
| PDMA | Poly(*N*,*N*-dimethylacrylamide) |
| PE | Polyethylene |
| PEI | Polyethyleneimine |
| PEG | Polyethylene glycol |

| | |
|---|---|
| PEGMA | Polyethylene glycol methacrylate |
| PEO | Polyethylene oxide |
| PEOX | Poly(2-ethyl-2-oxazoline) |
| PES | Poly(ether sulfone) |
| PET | Poly(ethylene terephthalate) |
| PG | Pyrogallol |
| PGA | Poly(L-glutamic acid) |
| PHEA | Poly(*N*-hydroxyethyl acrylamide) |
| PHEMA | Poly(2-hydroxyethyl methacrylate) |
| PHPMA | Poly(*N*-(2-hydroxypropyl) methacrylamide) |
| PHMA | Poly(*N*-hydroxymethyl acrylamide) |
| PHMB | Polyhexamethylene biguanide |
| PI | Polyimide |
| PLL | Poly(L-lysine) |
| PMAA | Poly(methacrylic acid) |
| PMOX | Poly(2-methyl-2-oxazoline) |
| PMPC | Poly(2-methacryloyloxyethyl phosphorylcholine) |
| PMPDSAH | Poly((3-(methacryloylamino)propyl)dimethyl(3-sulfopropyl)ammonium hydroxide) |
| PNE | Polynorepinephrine |
| PNIPAAM | Poly(*N*-isopropylacrylamide) |
| PP | Polypropylene |

| | |
|---|---|
| PPEGMA | Poly(polyethylene glycol methyl ether methacrylate) |
| PPROPOX | Poly(2-n-propyl-2-oxazoline) |
| PRP | Platelet-rich plasma |
| PSBMA | Poly(sulfobetaine methacrylate) |
| PSU | Polysulfone |
| PTHMAM | Poly(*N*-(tris(hydroxymethyl)methyl) acrylamide |
| PU | Polyurethane |
| PVDF-HFP | Poly(vinylidene fluoride-*co*-hexafluoropropylene) |
| PVA | Polyvinyl alcohol |
| PVC | Polyvinyl chloride |
| PVCL | Poly(*N*-vinylcaprolactam) |
| PVP | Polyvinylpyrrolidone |
| QCM-D | Quartz crystal microbalance with dissipation monitoring |
| SEM | Scanning electron microscope |
| Si-ATRP | Surface-initiated atom transfer radical polymerization |
| TDMAC | Tridodecylmethylammonium chloride |
| TEM | Transmission electron microscopy |
| THMAM | *N*-(tris(hydroxymethyl)methyl) acrylamide |
| Tris | Tris(hydroxymethyl)aminomethane |
| TSB | Tryptic soy broth |
| uHMW | Ultrahigh molecular weight |
| uPVC | Unplasticized polyvinyl chloride |

| | |
|---|---|
| UTI | Urinary tract infection |
| UV-Vis | Ultraviolet–visible spectroscopy |
| WCA | Water contact angle |
| XPS | X-ray photoelectron spectroscopy |
| MRSA | methicillin-resistant *Staphylococcus aureus* |
| UPEC | uropathogenic *Escherichia coli* |
| *A. coffeaeformis* | *Amphora coffeaeformis* |
| *A. baumannii* | *Acinetobacter baumannii* |
| *B. subtilis* | *Bacillus subtilis* |
| *C. albicans* | *Candida albicans* |
| *E. faecalis* | *Enterococcus faecalis* |
| *K. pneumoniae* | *Klebsiella pneumoniae* |
| *P. aeruginosa* | *Pseudomonas aeruginosa* |
| *P. mirabilis* | *Proteus mirabilis* |
| *S. aureus* | *Staphylococcus aureus* |
| *S. epidermidis* | *Staphylococcus epidermidis* |
| *S. mutans* | *Streptococcus mutans* |
| *S. saprophyticus* | *staphylococcus saprophyticus* |

## Acknowledgements

My journey as a PhD student was filled with both joy and frustration, but nonetheless, it has been a good learning experience for me. Through this program, I learned to appreciate the amount of time and effort involved in discovering new findings.

First and foremost, I would like to thank my supervisor Dr. Jayachandran Kizhakkedathu for providing guidance and direction throughout the PhD studies. Thank you for being approachable, helping me at difficult times, challenging me when necessary and encouraging my professional development. I am wholeheartedly grateful to him for all the support and I appreciate the opportunity to work in his lab. Many thanks to my committee members, Dr. Edward Pryzdial, Dr. Donald Brooks and Dr. Dirk Lange, for their guidance and scientific input.

Special thanks to Dr. Kai Yu for being my mentor in the lab and sharing your knowledge. Thank you for supporting me in stressful situations. I would like to thank Joey Lo, Irina Chafeeva, Iren Constantinescu and Derrick Horne, for providing me with excellent training on various techniques used for this project.

My gratitude to Dr. Manu Kalathottukaren, Dr. Narges Hadjesfandiari, Sreeparna Vappala, Haisle Moon, Lily Takeuchi, Dr. Jasmine Hamilton, Youping Li, Dr. Srinivas Abbina, Dr. Prashant Kumar, Dr. Anilkumar Parambath, Dr. David Yang, Vincent Leung, Dr. Erika Siren, Usama Abbasi, Chanel La, Daniel Luo, Arsh Gill, Hossein Ahmadabadi and all former lab members of Brooks and Kizhakkedathu laboratories, for creating a fun work environment.

Lastly, a big thanks to my mom and dad for their unconditional love and support.

**Dedication**

To my parents

To those doctors who saved my live

# Chapter 1: Introduction

## 1.1 Catheter-associated urinary tract infection

Nosocomial infections are the 4$^{th}$ largest cause of death in developed countries. Due to the increased number of surgical procedures and the increase in antibiotic resistant bacteria, the hospital infection events have increased by 36% in the past two decades. There are more than 2,000,000 nosocomial infections per year in the United States alone, leading to more than 100,000 related deaths [1-2]. In Canada, it is estimated that each year 220,000 to 250,000 incidents result in 8,000 to 12,000 deaths. According to United States Centers for Disease Control and Prevention, Catheter-associated urinary tract infection (CAUTI) is the most common type of nosocomial infection, accounting for more than 40% of such infections. The treatment of CAUTI is incredibly difficult whilst the catheter remains in place.

### 1.1.1 Urological catheters

Urinary catheters (**Figure 1.1**) are medical devices that help to drain urine from the bladder. The most common reasons for their use include urinary incontinence, urinary retention, urine monitoring, and post-surgery of the prostate or genitals. There are three major types of catheter design: condom catheter, intermittent catheter and Foley catheter [3]. The Foley catheters are usually used for long-term by patients with urinary retention problems thus associated with high infection risk. The original Foley catheter was made from natural rubber latex, a low-cost material that is easily processed and has decent mechanical properties. However, the recent studies demonstrated that the latex surface promoted biofilm formation as well as encrustation. Hence, polyurethane (PU), polyvinyl chloride (PVC), silicone have been developed as the base catheter materials over the years. Silicone is more commonly used since it circumvents many of the drawbacks faced by other materials [4].

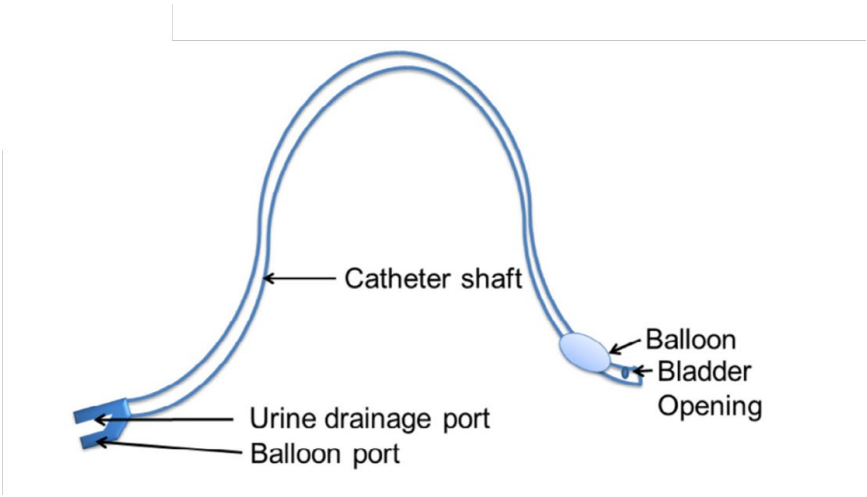


**Figure 1.1 A Foley catheter for long-term use.**

**The figure was retrieved with permission from Reference [3].**

### 1.1.2 CAUTI: clinical and economic consequences

The definition of catheter-associated bacteriuria (CAB) in publications varies, but most would agree that concentration of more than 100 colony-forming unit (CFU)/mL indicates significant growth of bacteria. CAB is universal in patient who have been catheterized for more than one week. Fortunately, most patients with CAB are asymptomatic, with only 24% of those patients develop symptomatic urinary tract infection (UTI). The symptoms of symptomatic UTI include lower abdominal pain, fever and vomiting. UTI is also associated with an increased risk of death, though someone argued that the higher risk of dying was result of patient's intrinsic factors. The clinical consequences of UTI undoubtedly add significant financial burden to the healthcare systems around the world. UTI increases average hospital stays vary between 1-2 days. The extra increase in cost for symptomatic UTI depends on individual situation, but the minimum cost would be $676 based on the reports from University of Michigan Health System. Annual treatment cost for UTI exceeds $350 million in the United States alone [1].

### 1.1.3 Major problems associated with CAUTI

Two major problems associated with urinary catheters and make physicians hard to treat CAUTI are biofilm formation and encrustation. Although these two problems are caused by different factors, they can supplement each other and make the clinical situation more complicated.

#### 1.1.3.1 Biofilm formation

Biofilm formation is the biggest problem associated with CAUTI. The planktonic bacteria interact with catheter surface immersed in the fluid and within minutes become adhered. Hydrophobic interaction and van der Waals force are responsible for the initial adhesion. The adhered bacteria multiply, aggregate and then produce extracellular polymeric substances that colonize the surface and form a conditioning film along with adsorbed proteins and organic molecules. A conditional film on the catheter consisting of peptides, protein fragments and organic molecules, allowing the emerging biofilm to develop a mature, three-dimensional structure (**Figure 1.2**). The rate of biofilm development depends on the bacterial types and concentration in the urine, the flow rate of liquid through the catheter and the surface properties of the catheter. Biofilms have been reported to be about 200 μm in thickness and can even reach a layer of 500 μm. [3] The bacteria in a mature biofilm can be detached due to depletion in nutrients and spread infections. Bacteria embedded in the biofilm have high tolerance to systemic antibiotic treatments. Three factors can explain the phenomenon: (1) slow penetration of antibiotics due to the matrix formation; (2) formation of a resistant phenotype that alter their metabolism to a low energy state; (3) expression of antibiotic resistance genes.

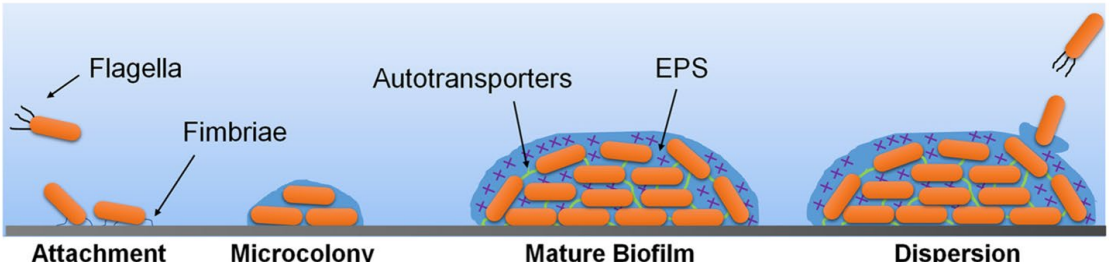


**Figure 1.2 The process of biofilm formation.**

**From left to right: (1) Planktonic bacteria attachment. (2) Aggregation of bacteria. (3) Extracellular polymeric substance production and mature biofilm formation. (4) Bacteria dispersed from mature biofilm. The figure was retrieved with permission from Reference [5].**

The bacteriology of CAUTI is quite predictable: the majority of UTIs are caused by the Gram-negative uropathogenic *Escherichia coli* (UPEC). UPEC are better adapted to surviving in the urine conditions and evading the host's immune response. The analysis of biofilms on the catheter surface also demonstrated other important Gram-positive and Gram-negative bacterial species, including *Pseudomonas aeruginosa* (*P. aeruginosa*), *Proteus mirabilis* (*P. mirabilis*), *Enterococcus faecalis* (*E. faecalis*), *Klebsiella pneumoniae* (*K. pneumoniae*), *Staphylococcus aureus* (*S. aureus*), and *Staphylococcus saprophyticus* (*S. saprophyticus*) [6]. Nowadays, UTIs are increasingly caused by the multidrug-resistant bacteria including the bacteria strains that resist all the available drugs.

### 1.1.3.2 Encrustation

Catheter encrustation is another critical complication associated with the UTI. Encrustation begins with the colonization of the urease-positive bacterial species, including *P. mirabilis*, *P. aeruginosa*, *E. faecalis*, and *P. vulgaris*. These urease-positive pathogens trigger the conversion of urea into ammonia and carbamate, leading to an increase in pH and subsequent crystallization of urinary components. The most common bacteria that causes catheter

encrustation is *P. mirabilis*. Encrustation not only increases the patient discomfort but also increases the potential risk of developing UTI. However, none of the currently available catheters are resistant to mineral crystal deposition and subsequent encrustation.

## 1.2 Prevention of CAUTI: the role of coating

Many strategies have been developed to prevent the CAUTI as it is a significant clinical problem. The direct strategy for preventing the catheter-associated infection is to limit their use, as approximately 20-50% of urinary catheters are placed unnecessarily [7]. Once an indwelling catheter is deemed necessary, improving hygiene procedures during catheterization can also help to decrease the incidence of CAUTI. Unfortunately, the CAUTI incidence could not be totally prevented using these strategies. Many patients who received professional care still develop CAUTI. Systemic antibiotic administration has not been adopted as front-line therapy to prevent CAUTI due to the high risk of selecting the resistant bacteria.

Extensive efforts have been made to develop the coatings to reduce the incidence of CAUTI [8]. In this section, the antibiofilm coatings for urinary catheters have been categorized based on their chemical basis. **Table 1.1** shows the examples of urinary catheter coatings that are clinically applied or undergoing investigation.

| Chemical basis | Developed since | Current status | Pros | Cons |
|---|---|---|---|---|
| Silver | 1949 | Clinical applied | Effectiveness | Toxicity<br>High cost |
| Antibiotic | 1993 | Clinical applied | Effectiveness | Microbial resistance |
| Organic antiseptic | 2003 | *In vivo* | Low cost | High toxicity |
| Antimicrobial peptide | 2014 | *In vivo* | Low toxicity | High cost<br>Poor stability |
| Bacteriophage | 2006 | *In vitro* | Specific target | Narrow activity<br>Poor Stability |
| Nitric oxide | 2009 | *In vivo* | Low toxicity | Short-term storage |
| Hydrophilic polymer | 2002 | *In vivo* | Low toxicity | Uncertain stability |

**Table 1.1 Different types of catheter coatings used to prevent initial bacterial adhesion and subsequent biofilm formation.**

### 1.2.1 Silver coatings

Silver coating is one of the few coatings for urinary catheters that has been approved by the FDA and marketed in the US since 2008. Silver ions exert various antibacterial actions, including inactivating crucial enzymes by interacting with thiol groups, enhancing pyrimidine dimerization by photodynamic reaction, and causing cell wall changes induced by electron dense granules. Silver is an effective antimicrobial agent killing multiple bacterial species even at low

concentrations. As early as 1986, Lundeberg launched a prospective, randomized study in 102 patients to find out if urinary catheters coated with silver can delay the UTI [9]. Fifty-one patients were inserted with a standard latex Foley catheter and fifty-one patients received a silver-coated Foley catheter inserted. There was a significant difference in incidence rates of CAB between two groups: 12% for the silver-coated catheter *versus* 34% for the standard catheter at three days after catheterization. The three following silver hydrogel catheter trials launched by the same group between 1990-1993 also demonstrated the efficacy of the silver coatings in preventing CAB [10]. In 2014, a detailed study was conducted by Ritter's group to determine the effect of a silver-alloy hydrogel catheter on symptomatic CAUTI. They observed a 58% relative reduction occurred in the silver-alloy hydrogel group when National Healthcare Safety Network-defined CAUTIs were considered [11]. However, the effectiveness of silver coating was found to be controversial. A nonrandomized crossover study in 2016 demonstrated no benefit of silver-coated catheter in reducing the incidence of CAUTI in seriously ill patients [12]. Of note, silver-resistant bacteria are common in environment where silver is widely administrated, and resistance to silver is very likely to become a problem in the future. Another drawback of the current silver coating is the high cost. These limitations may hinder the market for silver coating in the future.

### 1.2.2 Antibiotic coatings

Antibiotics are low molecular weight compounds that inhibit the growth of bacteria. Many antibiotics including nitrofurazone (NF), ciprofloxacin, gentamicin, norfloxacin, vancomycin, minocycline and rifampin have been incorporated into the urinary catheters and proven to be more efficient than the silver coatings. NF-coated urinary catheters are one of the most studied and currently marketed in the United States. Kuskowski's group compared two

commercially available antimicrobial-coated Foley catheters for inhibition of eleven urinary tract infection-associated microorganisms *in vitro*. Their results showed that NF-coated catheters outperformed the silver alloy-coated catheters in terms of their inhibitory activity, both in planktonic solution and on catheter surface [13]. Yoon's group evaluated the efficacy of NF-coated urinary catheter in inhibitory activity of CAUTI. NF-coated group showed slightly lower CAUTI incidence rate of 15.2% compared to the incidence rate of 24.2% reported in the control group. Especially in patients who were inserted for 5-7 days, the incidence rate of CAUTI was significantly lower in the NF-coated group [14]. Other antibiotics studied in the prevention of CAUTI are minocycline and rifampin. Raad's group examined the efficacy of urinary catheters impregnated with minocycline and rifampin in reducing CAB in a clinical trial. They found that the patients who received the antibiotic-impregnated catheters had significantly lower rates of Gram-positive bacteriuria than the control group (7.1% *versus* 38.2%) but similar rates of Gram-negative bacteriuria (46.4% *versus* 47.1%) and candiduria (3.6% *versus* 2.9%) [15]. The use of antibiotics to modify the surface is fraught with the potential risk of developing antibiotic resistance when the drug concentration becomes sub-inhibitory. This potential risk is more likely to happen on urinary catheters as a result of high bacterial concentration in urine than other parts of the body. It also has been noted that NF-coated catheters can cause discomfort in patients.

### 1.2.3 Organic antiseptic coatings

Antiseptics are antimicrobial agents that are applied to living tissue to reduce the infection rate. Urinary catheters incorporated with antiseptic coatings have been studied for several decades as they are less likely to develop microbial resistance compared to the antibiotics. Chlorhexidine (CHX) is a cationic biguanide commonly used as mouthwash to prevent oral plaque. CHX can act on cells very rapidly and is biocidal. CHX interacts with

bacterial cell membranes to destabilize and ultimately lyse bacterial cells at low concentrations, while CHX enters the cells directly and causes coagulation of intracellular constituents at high concentrations. Lavy's group assessed the efficacy of urinary catheters coated with sustained-release varnish of CHX in decreasing catheter-associated biofilm formation in dogs. They found that the number of bacteria at all portions of the urinary catheter was significantly lower in the CHX-coated group compared with the uncoated group [16]. CHX has also been studied in combination with other antiseptics. Raad's group developed a technique to prevent CAUTI *via* impregnating urinary catheters with Gendine, a combination of Gentian violet and CHX [17]. Gendine-coated urinary catheters reduced the CFU in all organisms tested for biofilm adherence compared with uncoated and silver hydrogel-coated catheters *in vitro*. In an animal model, CAB was present in 60% of rabbits with uncoated catheters and 71% of those with silver hydrogel-coated catheters but not in those with Gendine-coated catheters. Although with high efficacy, the killing mechanisms of the antiseptics do not include target specificity, as a result, it targets not only the bacterial cells but also the surrounding healthy cells. Hence, the toxicities towards the healthy cells have significantly decreased their development and outlook.

### 1.2.4 Antimicrobial peptide coatings

Antimicrobial peptides (AMPs) have gained significant attention in recent years due to their broad range of antimicrobial activities. These cationic peptides are made of 10 to 50 residues of amino acids. Their mechanism of action is achieved by disrupting the bacterial cell wall, inhibiting DNA, RNA and protein synthesis, altering gene expressions and enhancing immunomodulation. The diverse antimicrobial mechanisms of AMPs make them potential candidates for urinary catheter coatings. Leong's group initially demonstrated a feasible way of immobilizing two AMPs (RK1 and RK2) on catheters *via* the allyl glycidyl ether (AGE) polymer

brush linker [18]. The peptide-immobilized surface conferred good antimicrobial and antibiofilm activities toward *E. coli*, *S. aureus* and *Candida albicans* (*C. albicans*) in artificial urine and demonstrated no toxicity towards smooth muscle cells. They further introduced a more convenient two-step surface immobilization strategy for conjugating a synthetic AMP (CWR11) onto the commercial Foley catheter [19]. The AMP-immobilized catheter displayed potent antimicrobial properties against both Gram-positive and Gram-negative bacteria *in vitro* and retained its antimicrobial activity for more than three weeks. Our group developed an anti-adhesive antimicrobial peptide coating on clinically used PU catheters and demonstrated the antimicrobial efficacy, both *in vitro* and in *vivo* [20]. The use of AMP E6 in combination with antiadhesive polymer brush coating conferred excellent antimicrobial activities toward *P. aeruginosa*, *S. aureus*, and *S. saprophyticus*. In addition, this newly developed AMP-based coating showed more than 4 log10 reduction in bacterial adhesion on PU catheters in a mouse CAUTI model. Some of the issues associated with AMP-coated catheters are the high cost of peptide synthesis, stability and relatively low efficacy.

### 1.2.5 Bacteriophage coatings

A bacteriophage is a type of virus that can enter bacteria and replicate. They are selective and can disrupt various metabolic pathways in bacteria. Bacteriophages cause less bacterial resistance and toxicity towards mammalian cells thus were applied to urinary catheters. The initial work in this field was done by Dolan's group in 2006 [21]. They found the silicone catheters pretreated with a *Staphylococcus epidermidis* (*S. epidermidis*) bacteriophage significantly reduced viable biofilm formation by *S. epidermidis* over one day *in vitro*, suggesting the potential ability to prevent CAUTI by using the bacteriophages coatings. They further pretreated silicone catheters with a mixture of two bacteriophages, *P. aeruginosa* and *P.*

*mirabilis*, to reduce the biofilm formation [22]. Phage pretreatment reduced *P. aeruginosa* biomass by 4 log10 and *P. mirabilis* biomass by more than 2 log10 over two days. Despite the considerable research done in bacteriophage-based antimicrobial coatings, more research towards the development of multi-pathogenic resistant coatings by using phage cocktail containing coatings are anticipated.

### 1.2.6 Nitric oxide coatings

Nitric oxide (NO) has been known as an antimicrobial agent since the 1980s. The mechanism of action includes nitrosation of amines and thiols, lipid peroxidation, tyrosine nitration and DNA cleavage. Av-Gay's group developed a novel approach to create antibiofilm coatings on urinary catheters by impregnating the catheters with gaseous NO using a proprietary technology [23]. The modified catheters slowly released the NO over a 14-day period. The NO-impregnated catheters were able to inhibit the growth of surrounding *E. coli*, demonstrating the ability to eradicate a bacterial concentration of up to $10^4$ CFU/ml. Their following studies assessed the antimicrobial activities of NO-coated catheters, silver alloy-coated catheters, NF-coated catheters and uncoated catheters [24]. NF-coated and NO-coated catheters showed superior antimicrobial activities compared to silver-coated catheters and uncoated catheters. These positive findings highlight the need for further studies to address potential clinical considerations, such as the release of NO during the storage period.

### 1.2.7 Hydrophilic polymer coatings

Attachment of bacteria on the surface is also affected by the surface chemistry. Antifouling polymer coatings have been applied on urinary catheters to reduced bacterial adhesion and encrustation. Gorman's group investigated the surface properties of a polyvinylpyrrolidone (PVP) coating applied to PU and determined its suitability as a urinary

catheter [25]. They found that the application of a hydrophilic PVP coating to biomaterials was able to prevent bacterial adherence and encrustation. In another study, the suitability of polyethylene oxide (PEO)-based multiblock copolymer/segmented PU blends as coating materials for the commercial urinary catheters was assessed by Bae's group [26]. The bacterial adhesion tests demonstrated that the blend surfaces effectively suppressed the adhesion of *E. coli*, *S. epidermidis*, and *P. mirabilis*. It was also observed that the catheters coated with blends showed good resistance to encrustation. Tzanov's group functionalized urinary catheters with zwitterionic moieties in a novel enzymatic approach [27]. Reduced biofilm formation by about 80% was observed on zwitterionic polymer coated catheters compared to unmodified urinary catheters.

Heparin is a highly sulfated glycosaminoglycan and has a long history of medical use in human. It is often used as an anticoagulant agent but also investigated for the purpose of preventing CAUTI. Levin's group coated urinary catheters using a heparin tridodecylmethylammonium chloride (TDMAC) complex [28]. Coating the catheter with TDMAC alone resulted in 3.6-fold higher adherence whereas coating with the TDMAC-heparin complex reduced more than 90% of bacteria adhesion compared to the control. Their results indicated that TDMAC-heparin binary coating of urinary catheters reduced bacterial adherence and thereby may delay the acquisition of CAUTI. Of note, the hydration layer of these polymer coating may become breached and bacteria can still adhere on the surface of the catheter, thus lacking long-term efficacy.

## 1.3 Antibiofilm strategies

There are four major strategies for designing antibiofilm coatings based on their mechanism of prevention: antifouling strategy, contact killing strategy, release killing strategy, and multifunctional strategy [29-31]. These four strategies will be briefly reviewed in this section (**Figure 1.3**).

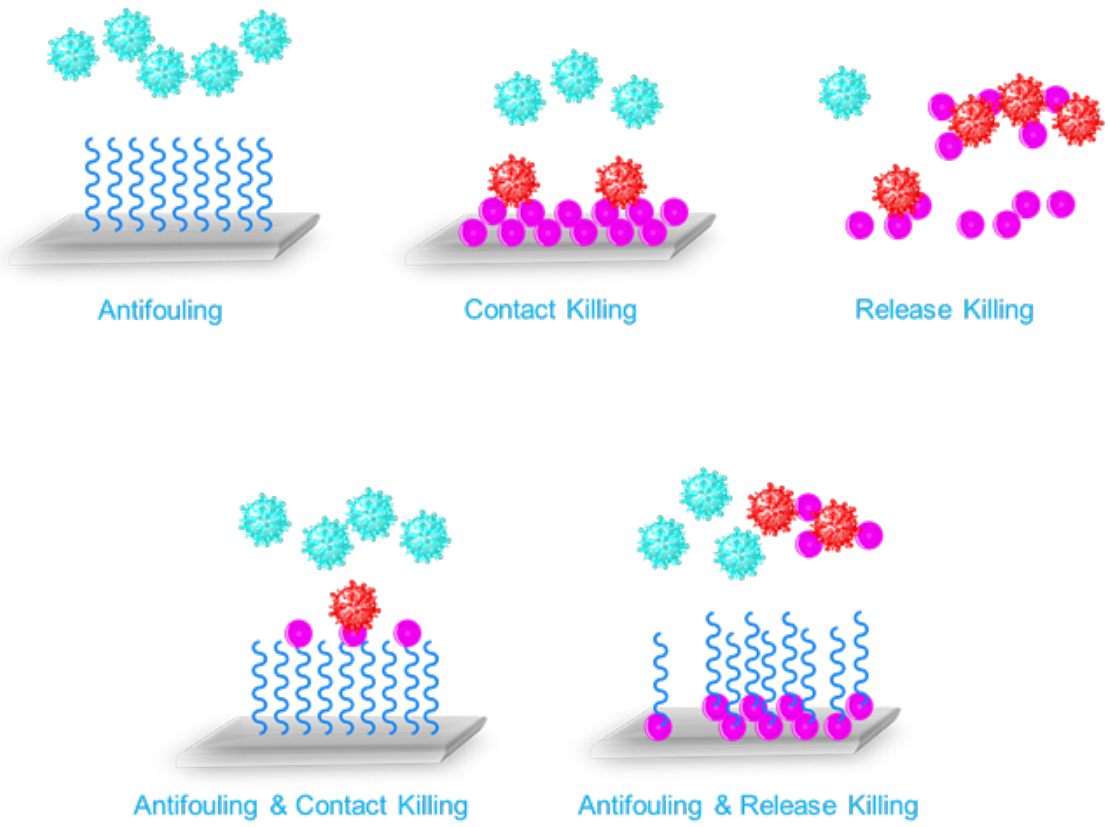


**Figure 1.3 Different strategies to combat surface biofouling.**

| Strategy | Effective component | Pros | Cons |
|---|---|---|---|
| Antifouling | Hydrophilic polymer<br>Amphiphilic polymer<br>Topography | No toxicity | Lack of long-term efficacy |
| Contact killing | Organic antiseptic<br>Antibiotic<br>Antimicrobial peptide<br>Enzyme | Long-term stability | Reduced activity after tethering<br>Accumulation of dead cells on surface |
| Release killing | Metal<br>Organic antiseptic<br>Antibiotic<br>Antimicrobial peptide<br>Enzyme<br>Nitric oxide | Flexible drug loading amount<br>Remaining of the drug activity | Development of bacteria resistance<br>Toxicity |
| Multifunctional | Antifouling & Contact killing<br>Antifouling & Release killing | Combined killing mechanisms | Complicated modification process |

**Table 1.2 Summary of the pros and cons of the different antibiofilm strategies.**

### 1.3.1 Antifouling coatings

Antifouling coatings seek to prevent the initial bacterial adhesion using nontoxic agents [32-34]. Bacterial adhesion at the interface composed of two stages: a rapid and reversible stage followed by a secondary locking stage. Chemical surface modification and physical surface modification approaches have been developed to delay the initial adhesion. Immobilization hydrophilic or amphiphilic polymers is the most common chemical modification approach to impart bacterial resistance to a surface. Apart from the chemistry, the morphology of a surface also can be structured and directed to reduce biofilm formation. The most representative examples are superhydrophobic surface and liquid-infused surface [35]. However, the use of physical surface modification approach to modulate bacterial adhesion is more challenging than initially anticipated. Short-term success of coating on prevention of bacterial adhesion does not guarantee it long-term efficacy.

### 1.3.2 Contact killing coatings

Contact killing coatings have been developed to generate continuous killing surface without leaching bioactive agents. In this strategy, antimicrobial agents are covalently anchored to the substrate by chemical grafting. Attached bacteria are believed to be killed as a result of disruption of their cell membrane. Because the killing efficacy is based on the membrane interactions, the most common methods for generating the contact killing coatings are introducing cationic compounds onto the substrates. Cationic antiseptics, antibiotics, antimicrobial peptides and enzymes have been covalently introduced to the substrates to generate contact killing surfaces [36-37]. The mechanisms behind the surface-induced killing might be different from the solution-based approaches for killing bacteria. The key challenge of this strategy is to prove these tethered biocidal maintain their antimicrobial activities. Another

concern is these tethered surfaces might be buried under a layer of dead bacterial cells, leading to their deactivation.

### 1.3.3 Release killing coatings

Release killing coatings exert their activities by leaching antimicrobial agents over the course of time, which allows killing both the planktonic and attached bacteria. The drugs need to be preloaded onto the surface. Compared to the systemic drug delivery, direct releasing from the coating offers a high local concentration of the drug, thus reaching high efficiency with less toxicity to adjunct fluids and tissues. There are two typical release profiles: controlled release [38-39] and on-demand release [40]. The controlled release profile usually combines an initial burst release with a long-term tail release with gradually decreasing concentration. An initially short-term, high-dose release of antimicrobial agents protect the implanted medical devices during the initial phase of the implantation when they are most susceptible to bacterial growth. The long-term tail release of antimicrobial agents maintains the medical devices' antibiofilm activities until it is being taken out or being integrated with the surrounding tissues. While for coatings with controlled release profiles, sustained release of biocides may result in development of bacteria resistance and toxic effects on surrounding environment. Therefore, the on-demand release platform, which only delivers antimicrobial agents when in contact with bacteria is a more promising approach. It has been demonstrated that bacteria colonization usually leads to local pH decrease and enzyme release. So, the on-demand release profiles are normally created by pH-responsive or enzyme-responsive self-defensive coatings. To date, designing antibiofilm coatings with release profiles that exactly aligns with the therapeutic window is still challenging.

### 1.3.4 Multifunctional coatings

Multifunctional coatings do not rely solely on a single strategy but rather relays on a combination of more than one strategy against biofilm formation. Combining strategies that are complementary to each other in tackling biofilm formation may open a promising pathway to overcome the inherent drawbacks encountered within each strategy. Multifunctional coatings that include dual antifouling and contact killing capabilities or dual antifouling and release killing properties have been reported [41]. A key challenge of the multifunctional coatings is optimizing the antibiofilm properties without losing the activities of individual antibiofilm mechanisms used.

## 1.4 Universal antibiofilm coatings

### 1.4.1 Universal coating systems

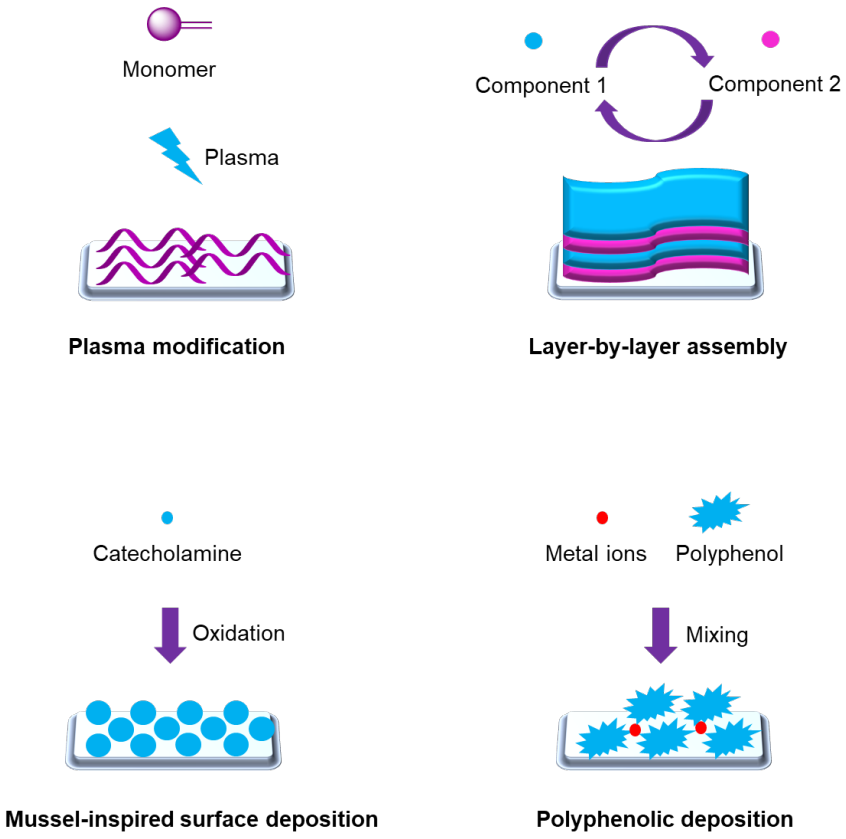


**Figure 1.4 A schematic representation of diverse universal coating technology.**

Universal coatings are systems that can be generated on a wide range of substrates and have great potential for medical device applications. Direct and specific chemical interactions between the coating and the substrate are avoided in order to meet the universal concept. To design a universal coating, multiple noncovalent interactions, such as electrostatic interaction, hydrogen bonding, hydrophobic attraction or van der Waals interaction are used as the driving force for surface anchoring. Additional physical or chemical crosslinkings are further applied to stabilize the coating [42]. In this section, the most common universal coating systems, which

include plasma modification, layer-by-layer (LbL) assembly, mussel-inspired deposition and polyphenolic deposition are summarized (**Figure 1.4, Table 1.3**). Some less commonly used coating systems, such as chemical vapor deposition and laser deposition, are also considered but will not be discussed here.

| Coating system | Developed | Anchoring | Crosslinking | Pros | Cons |
|---|---|---|---|---|---|
| Plasma modification | 1929 | Covalent bonding | Covalent bonding | Stable | Specific equipment |
| LbL assembly | 1991 | Electrostatic interaction | Electrostatic interaction<br>Hydrogen bonding<br>Covalent interaction<br>Coordination bonding | Variable thickness | Time consuming |
| Mussel-inspired deposition | 2007 | Multiple interactions | Multiple interactions | Simple | Rough morphology |
| polyphenolic deposition | 2013 | Multiple interactions | Multiple interactions | Quick reaction | Rough morphology |

**Table 1.3 Summary of the universal coating systems.**

### 1.4.2 Plasma modification

Plasma, also referred as the fourth state of matter, was named by Langmuir in 1929. Plasma can be divided into thermal plasma and non-thermal plasma. Non-thermal plasma is a very reactive environment. Several different interactions between the plasma and substrates are possible, including plasma treatment, plasma post-irradiation grafting, plasma syn-irradiation,

and plasma polymerization. Plasma treatment does not involve monomers but gas. Chemical functionalities or free radicals are introduced onto the substrates when treated with the plasma. Typically employed gases include air, Ar, He, $O_2$, $N_2$, $NH_3$, and $CF_4$ [43].

Plasma treatment is mainly used to increase the surface energy or improve the surface hydrophilicity. It should be noted the introduced functionalities are not permanent since the surfaces tend to recover from the initial modification [44]. Hence, plasma post-irradiation grafting, plasma syn-irradiation, and plasma polymerization are more common methods to confer stable functionalities on substrates.

Plasma post-irradiation grafting is a two-step modification process and generates stable coatings compared to the plasma treatment. The initial step is to generate specific groups which can initialize further polymerization under plasma treatment. Ar and He plasma is known to introduce radicals on the surface, while oxygen and atmosphere plasma can generate peroxide and hydroperoxides groups. The plasma-treated substrates can be then transferred to a monomer solution to graft polymer chains on the surface *via* the graft-from approach. Plasma syn-irradiation combines adsorption of monomers on surface and subsequent exposure to a non-thermal plasma. The plasma will create radicals on surfaces in the absorbed monomer layer, thus forming a crosslinked polymer layer on the top. In simple terms, plasma polymerization is the polymerization took place during the plasma state. In a plasma, monomers in vapor phase are converted into reactive fragments, which can recombine to form polymers and deposit onto substrates. As a result, the deposited polymer layer is highly crosslinked and will not necessarily form structures that are comparable to those of polymers generated using the conventional polymerization methods. Diverse functional groups, such as anhydride groups, amino groups,

epoxide groups, and perfluoroalkyl groups have been introduced by employing monomers with vinyl groups using plasma polymerization [45-46].

#### 1.4.2.1 Universal antifouling coatings based on plasma modification

Plasma modification, specifically plasma post-irradiation grafting can be used to introduce antifouling polymer brushes on diverse substrates. Chang's group modified expanded poly(tetrafluoroethylene) (ePTFE) membranes with either zwitterionic poly(sulfobetaine methacrylate) (PSBMA) or neutral polyethylene glycol methacrylate (PEGMA) *via* atmospheric plasma-induced surface polymerization [47]. They found that the unmodified ePTFE membranes presented a favorable surface to *S. epidermidis* and *E. coli* attachment. In contrast, no visible bacteria cells were found on the PSBMA grafted membranes, while only a few bacterial cells remained on PEGMA coated membranes. Neoh's group covalently grafted a crosslinked agarose polymer layer onto a silicone surface *via* oxygen plasma treatment followed by a subsequent polymerization [48]. The developed coating reduced *S. aureus*, *E. coli*, and *P. aeruginosa* biofilm formation by more than two orders of magnitude.

#### 1.4.2.2 Universal contact killing coatings based on plasma modification

Plasma modification was used to functionalize the substrate with a layer containing biocide components. Li's group developed universal antimicrobial coatings using a process involving plasma treatment, UV-induced graft copolymerization of 4-vinylpyridine (4-VP), and quaternization of the grafted pyridine groups with hexylbromide. They applied the coating technologies on diverse substrates, including PU [49], poly(vinylidene fluoride-co-hexafluoropropylene) (PVDF-HFP) [50], and poly(D,L-lactide) (PDLLA) [51] nanofibrous membranes. All the modified nanofibrous membranes possessed highly effective antibacterial activities against Gram-positive and Gram-negative bacterial species. Vreuls' group reported a

robust and straightforward two-step modification procedures for anchoring the AMPs onto stainless steel *via* a plasma polymerized epoxy interlayer [52]. In comparison to unmodified stainless-steel pieces, 3-6 log10 reduction of Gram-positive or Gram-negative populations was observed on the AMP immobilized surfaces.

#### 1.4.2.3 Universal release killing coatings based on plasma modification

The plasma polymer can also act as a reservoir for the controlled release of antimicrobial agents that combat biofilm formation. Plasma polymers can be used to control the release rate, either *via* their crosslink density or *via* a plasma polymer covered layer. Griesser's group generated amine-rich surface by plasma polymerization of *n*-heptylamine (nHA) and amine groups were further used for the complexation of in-diffusing silver ions [53]. The *n*-HA plasma polymer coating provided a suitable matrix for the diffusive release of silver ions from embedded silver nanoparticles. The rate of release was also shown to be controllable by the application of a second plasma polymer layer. This newly developed coating completely inhibited bacterial colonization by *S. epidermidis* and allowed normal adhesion and spreading of osteoblastic cells. In another study, Bose's group have incorporated $Ag_2O$ into plasma sprayed hydroxyapatite coatings for improved antimicrobial activity [54]. By incorporating $Ag_2O$ into the coating, they were able to effectively enhance the coating with sustainable long-term antimicrobial properties while minimizing negative cytoplasmic effects on osteoblast cells.

#### 1.4.2.4 Universal multifunctional coatings based on plasma modification

Plasma modification has been used to fabricate dual-functional surfaces: antifouling and contact killing. Plasma post-irradiation grafting is the most used method to fabricate dual functional coatings. Li's group conjugated allyloxy polyethylene glycol (APEG) with polyhexamethylene biguanide (PHMB) and grafted the conjugates onto a silicone rubber surface

as a bottle brush-like coating *via* plasma-induced and UV-assisted surface-initiated polymerization [55]. The APEG-PHMB coating displayed improved antifouling and antibiofilm properties as a result of its abundant PEG blocks and cationic guanidine groups. The coating showed more than 5 log10 reduction of *E. coli* adhesion in a rodent subcutaneous infection model. They further rationally designed and synthesized a monomer containing dual functional groups, i.e., PEG and AMP. Using a similar strategy, copolymers were further grafted onto the surface of silicone rubber [56]. The dual functional coating demonstrated antifouling and antimicrobial activities both *in vitro* and *in vivo*.

### 1.4.3 Layer-by-layer assembly

One of the most rapidly growing methods for developing universal thin coatings has been the alternating adsorption of charged macromolecules based on layer-by-layer (LbL) assembly. The original idea was carried out by Iler in 1966, which involved the assembly of negatively charged silica particles and positively charged alumina fibrils. However, this method has not been studied in detail until 1991 when Decher, as a pioneer researcher in this field, achieved full characterization of LbL multilayer films [57]. Considering the simplicity and versatility of the technique, the LbL assembly has been widely applied to create functional coatings during the past two decades. There are four major driving forces including electrostatic interaction, hydrogen bonding, covalent interaction, and coordination bonding to develop multilayer coatings.

Electrostatic interaction serves as the predominant driving force for achieving the film assembly *via* surface charge inversion after Decher's discovery in 1991. The structures of LbL multilayers using polyelectrolytes could be affected by many parameters such as pH, temperature, ionic strength, solvent, as well as chemistry and molecular weight of

polyelectrolytes [58-59]. It is worthwhile to note that strong polyelectrolytes are fully charged independent of pH, while weak polyelectrolytes with carboxylic acid or amine groups are highly responsive to the pH change in the solution. Therefore, a tiny change in the solution pH for the weak polyelectrolytes could induce dramatic changes of the coating's structure and composition. Rubner's group used two typical weak polyelectrolytes poly(acrylic acid) (PAA) and poly(allylamine hydrochloride) (PAH) and demonstrated that dramatic changes in the thickness of a bilayer can be achieved with very minor changes in the solution pH [60]. By changing the solution pH, it is possible to systematically vary the thickness of an adsorbed polymer layer from 0.5 nm to 8 nm. Ionic strength is another critical parameter which remarkedly affects the properties of LbL multilayer coatings. Ji's group investigated the effect of ionic strength on the construction of the poly-L-lysine (PLL)/DNA films [61]. They discovered that the salt concentration of the deposition solution had a huge effect on the film construction. The growth of the multilayer films was sustained when the salt concentration increased from 0 M to 0.5 M, while further increase of the salt concentration from 0.5 M to 1.5 M decreased the incorporation of DNA.

Hydrogen bonding has been established to be the second most investigated driving forces for generating LBL multilayers. It allows neutral polymers to be incorporated into the multilayers if they can serve as hydrogen donors or acceptors. The initial work was performed by Rubner's group, in which polyaniline (PANI) was served as the hydrogen donor and other hydrophilic polymers were served as the hydrogen acceptors [62]. They found that the use of hydrogen bonding forces to assemble these multilayers resulted in relatively thick and high PANI content bilayers due to the tendency of the hydrogen bonding polymers to adsorb with a high segmental density of loops and tails. The use of environmentally friendly aqueous solutions

for hydrogen bonding assembly is more promising for biomedical applications. The self-assembly of hydrogen bonding is usually achieved by combining a weak polyelectrolyte such as PAA or poly(methacrylic acid) (PMAA) with a neutral polymer (e.g. PEO, PVP) [63-64]. However, these depositions could only be achieved at acid pH when the polyacid is fully protonated. More recently, a polyphenol tannic acid (TA) has been introduced into LbL multilayers with abundant neutral polymers (e.g. PEO, PVP, poly(*N*-isopropylacrylamide) (PNIPAM), poly(*N*-vinylcaprolactam) (PVCL)) [65]. The pH value for the film deposition is close to physiological conditions and this makes TA based LbL multilayer films one of the promising candidates for biomedical applications.

The LbL multilayer coatings generated *via* electrostatic interaction or hydrogen bonding have poor stability in high ionic strength or pH change. Covalent interaction offers an additional route to construct multilayer films with exceptional stability as the energy of covalent interaction is higher than other non-covalent interactions. In general, two strategies have been reported based on the covalent interaction system: post covalent conversion and consecutive covalent assembly. Post covalent conversion strategy generates multilayer coating *via* non-covalent pathways initially followed by the one-step covalent crosslinking [66]. Messersmith's group coupled catechol groups to the polyethyleneimine (PEI) and hyaluronic acid (HA) backbones and assembly them on substrates LbL using the electrostatic interaction [67]. Subsequent covalent crosslinking was achieved by changing the solution pH to 8.5. For the consecutive covalent assembly strategy, the multilayer coatings are built using covalent reaction in each assembly process. Click chemistry refers to a set of covalent reactions with high yields that can be performed under mild conditions. The combination of click chemistry and LbL assembly requires less building time and labor work. Caruso's group synthesized poly(acrylic acid) with

azide functionality (PAA-Az) or with alkyne functionality (PAA-Alk) using living radical polymerization, and generated LbL multilayer coatings by sequentially exposing the substrates to PAA-Az and PAA-Alk solutions containing copper sulfate and sodium ascorbate [68]. This combination was shown to be convenient and efficient for preparing stable multilayer coatings.

Coordination bonding is a strong interaction between metal ions and organic ligands, which has been used as the driving force to construct multilayers coatings. Recently, Caruso's group reported the assembly of stable multilayer films *via* sequential deposition of TA and $Fe^{3+}$ through metal-ligand coordination [69]. Kang's group also discovered the controlled deposition could be achieved by sequential immersion of the substrates into TA solution and $Fe^{3+}$ solution, with a bilayer thickness about 2 nm [70]. However, reversible construction and deconstruction of LBL films was observed by the addition of ethylenediaminetetraacetic acid (EDTA).

#### 1.4.3.1 Universal antifouling coatings based on LbL assembly

Universal antifouling coatings could also be achieved by introducing LbL multilayers with the terminal layer (ending layer) with cell-resistant properties. Most of the anti-adhesive multilayer coatings contain a negatively charged or uncharged ending. Egles's group showed that PLL/poly(L-glutamic acid) (PGA) multilayers ending by several PLL/PGA-g-PEG bilayers demonstrated antifouling properties [71]. The *E. coli* adhesion was reduced by 72% on films ending by one PLL/PGA-g-PEG bilayer and by 92% on films ending by three PLL/PGA-g-PEG bilayers compared to the bare silica. The anti-adhesive properties of polysulfone (PSU) microfiltration membranes coated with poly(allylamine hydrochloride) (PAH)/PAA multilayers were investigated by Chen's group [72]. The bacterial deposition kinetics on the multilayers coated membranes were slower than the deposition kinetics on the uncoated membranes. In addition, the bacterial removal efficiency was significantly enhanced from <10% to as high as

99% after introducing the LbL multilayers. A novel polyanion, grafted with amphiphilic perfluoroalkyl polyethylene glycol (fPEG) side chains, was synthesized by Vancso's group and subsequently LbL assembled with PEI on a silicon wafer [73]. The LbL multilayer films effectively prevented the adhesion of a marine bacterium. More recently, Caruso's group have reported the formation of LbL TA/$Fe^{3+}$ MPN films and have quantified bacterial adhesion on the surface as a function of the composition of the terminal layer [74]. The presence of PEOX alone was enough to reduce *E. coli* adhesion regardless of its orientation as both functionalized with galloyl-modified PEOX and hydroxy-terminated PEOX showed 66% reduction in bacterial adhesion. Most of the non-covalent interactions are relatively strong, which has created a set of versatile coatings. However, these coatings could be decomposed under harsh conditions, compromising their antifouling activity.

#### 1.4.3.2 Universal contact killing coatings based on LbL assembly

The LbL assembly can be used as a universal method for fabricating contact killing coatings by tethering the antimicrobial agent as the outermost layer. Worley's group synthesized two *N*-halamine copolymer precursors, poly(2,2,6,6-tetramethyl-4-piperidyl methacrylate-*co*-acrylic acid potassium salt) and poly(2,2,6,6-tetramethyl-4-piperidyl methacrylate-*co*-trimethyl-2-methacryloxy-ethylammonium chloride) and successfully coated them onto cotton fabric *via* LbL assembly [75]. They found that the chlorinated samples inactivated both *S. aureus* and *E. coli* within 15 minutes. Tang's group reported a novel antibacterial coating on 3D fibrous tissue scaffolds prepared by the LbL assembly, which allowed easy control of antimicrobial polyhexamethylene biguanide (PHMB) loading on the fiber surface [76]. The antimicrobial-terminated coating with seven bilayers was not only effective in killing bacteria but also nontoxic to fibroblast cells.

#### 1.4.3.3 Universal release killing coatings based on LbL assembly

Antimicrobial agents could be incorporated in LbL multilayer films and released to kill bacteria in a controlled or smart manner. For the controlled release, the incorporated dosage of antimicrobial agents could be easily changed by the number of deposited layers, while release rate could be modified by polymer chemistry and film architecture. Hammond's group generated a multilayer coating *via* directly layering the antibiotic gentamicin with negatively charged HA in an alternating LbL tetralayer with a hydrolytically degradable poly(β-amino ester) and polyanion HA [77]. The multilayer films released gentamicin through a combination of hydrolytic degradation, film deconstruction, and gentamicin diffusion. The gentamicin gradually released from the LbL coatings providing promising antimicrobial efficacy against *S. aureus*. By changing the polyanion layer from HA to PAA [78], the multilayer films generated the release profile combining a burst-release of the cargo over first several days and the four weeks of continuous zero-order release. The LbL films were effective in inhibiting the *in vitro* and *in vivo* growth of *S. aureus*.

Smart coatings that deliver antimicrobial agents only when in contact with bacteria also have been developed using LbL assembly. According to the triggers, these coatings can be categorized into two types: pH-responsive self-defensive coatings and enzyme-responsive self-defensive coatings. The driving force behind the pH-defensive release is the charge balance within the multilayer films. Sukhishvili's group developed highly efficient, pH-responsive, controlled-release antibacterial coatings constructed by direct assembly of TA with one of several cationic antibiotics using the LbL assembly [79]. All the developed coatings did not release antibiotics in physiological conditions, while they released antibiotics in acidic conditions. Using similar design principles, their group loaded gentamicin and antibacterial

cationic peptide L5 on chemically crosslinked poly(methacrylic acid) (PMAA) hydrogel-like films generated by LbL assembly to achieve pH-triggered release capabilities [80]. They also added the negatively charged clay-platelets to the hydrogel matrix to provided pH-independent binding sites for gentamicin, thus ensuring that a fraction of the antibiotic remained bound within the coating [81]. The coatings released PAA-bound gentamicin as a result of environmental acidification, whereas gentamicin adsorbed to clay nanoplatelets remained bound within the coating, affording sustained antibacterial protection. In addition, a series of LbL multilayer coatings with enzyme-triggered release killing capability have been developed. The common approach for constructing such coatings is to include enzyme-sensitive components, such as HA and PLL in the multilayered films. Biocompatible and biodegradable LbL multilayer films based on hyaluronic acid-cateslytin (HA-CTL) conjugate and chitosan were deposited on a planar surface by Boulmedais's group, to design an enzyme-responsive release killing coating [82]. The multilayer coating fully inhibited the development of Gram-positive *S. aureus* and *C. albicans* yeasts by releasing CTL, the endogenous host-defensive AMP.

#### 1.4.3.4 Universal multifunctional coatings based on LbL assembly

Generation of multifunctional coatings with anti-adhesive and contact killing functions have been achieved by LbL assembly. Chitosan as antimicrobial agent and heparin as an anti-adhesive agent were alternatively deposited onto treated poly(ethylene terephthalate) (PET) films *via* electrostatic interaction by Ji's group [83]. The constructed multilayer films were able to prevent the initial bacterial adhesion and kill the planktonic bacteria efficiently. Antifouling azido-functionalized poly(ethylene glycol) methyl ether methacrylate -based polymer chains and antimicrobial alkynyl-functionalized 2-(methacryloyloxy)ethyl trimethyl ammonium chloride-based polymer chains were assembled LbL and crosslinked *via* click-chemistry by Rittschof's

group [84]. The generated multilayer coatings were resistant to bacterial adhesion and were bactericidal to marine Gram-negative bacteria.

### 1.4.4 Mussel-inspired deposition

Polydopamine (PDA) technology is a simple and easily adaptable surface modification method, and it is the first one-step universal surface chemistry first reported by Messersmith's group in 2007 (**Figure 1.5**) [85]. PDA technology became one of the most powerful tools for surface modification nowadays, for its simplicity, versatility, low cost and many other potential advantages. The PDA coating begins with spontaneous oxidation of dopamine, with a final deposited thickness less than 50 nm using a typical procedure. The choice of dopamine concentration and buffer, the use of oxidants and external stimuli all can affect the coating structure and thickness. Ball's group clearly demonstrated that dopamine concentration influences the kinetics of PDA deposition, thickness and roughness [86]. They observed a constant increase in the maximal film thickness and surface roughness with an increase in the dopamine solution with the range of 0.1 and 5 mg/mL. d'Ischia's group changed the buffer type for the PDA aggregation and discovered that tris(hydroxymethyl)aminomethane (Tris) buffer is an efficient modulator for PDA buildup and aggregation [87]. Water soluble chemical oxidants such as sodium periodate, ammonium persulfate, potassium permanganate, copper sulfate have been used to accelerate the process of PDA coating deposition. For instance, the use of sodium periodate can obtain ultrafast and thick PDA coating at room temperature [88]. In addition, the generation of radical species by providing external energy such as ultraviolet light and microwave can also facilitate the thick PDA coating formation. Levkin's group demonstrated that UV irradiation at 260 nm triggered the dopamine oxidation and formed a coating in a few hours [89]. Lee's group showed that microwaves efficiently shortened the coating time from 6 h

to 15 min [90]. Although the mechanism of PDA chemistry is still being debated, it is widely accepted that the initial driving force for the PDA formation is the oxidation of dopamine by the oxygen. The quinone groups oxidized from catechol groups then undergo further reactions to generate oligomers. These oligomers then aggregate to form PDA particles *via* multiple interactions [91].

Norepinephrine was another catecholamine derivative used for material-independent coating since the development of PDA coating. In 2009, Lee's group developed a facile and universal approach for surface modification using norepinephrine [92]. The coating can serve as a platform for further protein conjugation and ring-opening polymerization of biodegradable polymers. Further investigation revealed polynorepinephrine (PNE) coating was ultra-smooth and a newly found early intermediate, 3,4-dihydroxybenzaldehyde, played an important role in the generation of such ultra-smooth coatings. PNE coating can be used as a NO-loading scaffold and is potentially useful for biomedical applications [93].

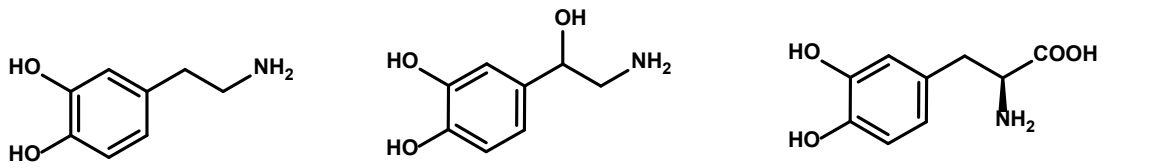


**Figure 1.5 Chemical structure of dopamine and its derivatives.**

In 2012, a one-step surface functionalization method dopamine-assisted co-deposited was first proposed by Lee's group *via* mixing solutions of dopamine and other chemicals of interested including polymerization initiators, antimicrobial agents, tertiary amines, growth factors, and polysaccharides [94]. This work stated researchers' interest in developing universal coatings *via*

dopamine-assisted co-deposition strategy. The dopamine-assisted co-deposition includes a second component during the deposition process, which makes the system more complicated than PDA deposition alone. Based on the chemical nature of the second component, the dopamine-assisted co-deposition system could be classified as: covalent co-deposition and non-covalent deposition [95]. Since dopamine can interact with amino groups *via* Schiff-based and Michael addition reactions, PEI can be co-deposited with PDA to form a robust coating. Xu's group co-deposited PDA with 600 Da PEI on to the polypropylene (PP) membrane surface, and the incorporation of PEI significantly improve the membrane's hydrophilic and water permeability [96]. Their further investigation revealed that low molecular weight PEI at low concentration accelerated the co-deposition process, while high molecular weight PEI or high PEI concentration were detrimental to the co-deposition efficiency [97]. The surface chemistry and morphology of the binary coatings can be altered by changing the solution conditions. Dopamine can also react with thiol groups *via* Michael addition reaction. Lee's group co-deposited dopamine with 2-dimethylaminoethanethiol on polyethylene (PE) separators, followed by a silicification reaction to improve the power and safety of Li-ion batteries [98]. As mentioned earlier, it has been widely accepted that non-covalent interaction plays a critic role during the PDA assembly and deposition. This indicates PDA may interact and deposit with functional components *via* non-covalent pathway. The first report based on non-covalent co-deposition was reported by Stadler's group [99]. They investigated the deposition of dopamine when mixing with a neutral polymer on standard substrates. They found that polyethylene glycol (PEG) and polyvinyl alcohol (PVA) were successfully incorporated into the PDA coating without the need for the covalent bonding. PVP suppressed the coating formation as it acted as a strong hydrogen acceptor. Though Ball's group pointed out that polycations and polyanions could inhibit PDA

aggregation and further deposition [100], negatively charged heparin was also successfully incorporated into the PDA coating by Huang's group [101].

Since catechol groups play a crucial role in the robust surface adhesion, many functional polymers have been conjugated with catechol groups to confer anchoring abilities. The simplest method is to graft the catechol groups to natural molecules. Reported by Lee's group, a new adhesive heparin derivative named hepamine which was prepared by conjugating heparin with dopamine, showed excellent surface coating capability on diverse substrates [102]. Nam's group found that dextran containing about 6.7% catechol moieties strongly bound to the titanium substrate at a neutral pH *via* multivalent interactions [103]. Lee's group demonstrated that HA-catechol conjugates containing 5.1% catechol moieties can adhere on various substrates [104]. Synthetic polymers also have been modified with catechol groups. Cho's group designed a simple coating method for generating superhydrophobic, self-cleaning surfaces by using a perfluorinated dopamine derivative as a polymerization precursor. The static water contact angles larger than 150° and the low water sliding angles less than 7° confirmed the formation of superhydrophobic, self-cleaning surfaces [105]. Catechol-grafted PEGs with 4-5 catechol groups per polymer were successfully synthesized and anchored on diverse substrates by Lee's group. They confirmed that PEG-catechol exhibited superior modification capabilities compared to other existing PEGylation strategies [106]. Kohane's group further presented a one-step method to form a thick and stable surface coating based on the aggregation of a short amphiphilic four-armed PEG-dopamine polymer into particles and subsequent surface binding by catechol chemistry [107]. Hyperbranched polyglycerol (HPG) conjugates with different ratios of catechol groups were synthesized in Haag's lab. Their results revealed that multivalent catechol anchoring and cross-linking were critical for sufficient surface coverage; polymer with greater than 5%

catechol groups showed better surface coverage on the titanium substrate [108]. However, these conjugates were not very effective on covering polymeric substrates. They further presented a new bioinert multilayer architecture which was hierarchically constructed [109]. Based on a crosslinked chemical active foundation layer combined with a crosslinked bioinert connection layer, and terminated with a monofunctional bioinert top layer, the chemical activity gradually decreases and the bioinert property gradually increases from bottom to top. With these characteristics, this new architecture can be used to form a highly stable material-independent surface coating. Jiang's group developed zwitterionic polymers with a catechol chain end and applied them to a variety of hydrophobic polymer substrates [110-111]. Although catechol is a powerful group for surface anchoring, some catechol-based polymers show limited surface coverage on polymeric substrates. Catechol is helpful for surface anchoring and intralayer crosslinking but does not guarantee the achievement of coatings that are truly universal. Further investigations on other interactions are required.

#### 1.4.4.1 Universal antifouling coatings based on mussel-inspired deposition

Mussel-inspired surface deposition strategy has been widely used to construct antifouling coatings during the past decade. PDA coating could be deposited on all the substrates, and the anchored catechol/quinone groups could be further conjugated with molecules having either amino or thiol groups. The first example of post-modification of PDA has been demonstrated by Messersmith' group [112]. Since then, a variety of hydrophilic polymers with amino/thiol groups have been immobilized onto diverse substrates in a similar manner to achieve antifouling activities. Chung's group designed antifouling pressure retarded osmosis membranes by synthesizing HPG with one thiol site and subsequently grafting them onto the PES hollow fiber membranes [113]. The introduction of hydrophilic HPG branches to PES membrane surfaces

reduced approximately 90% of *E. coli* and *S. aureus* adhesion without changing the morphology and bulk properties of the membranes. Caruso's group reported a versatile approach for the design of low-fouling surfaces *via* the mussel-inspired immobilization of zwitterionic peptides [114]. The peptide functionalized surfaces effectively prevented the adhesion of Gram-negative and Gram-positive bacteria. Matsuyama's group modified the reverse osmosis membrane initially with PDA coating as a precursor layer, followed by PMPC copolymer conjugation [115]. Dynamic bacterial suspension filtration showed that surface modification with PMPC clearly enhanced the biofouling resistance of the reverse osmosis membranes. However, all these coatings' antifouling activities were observed in the short-term biofouling tests. Vrouwenvelder's group functionalized the ultrafiltration membranes with a PDA layer, followed by the PEG conjugation [116]. The modified membranes showed significantly reduced adhesion of *P. aeruginosa* in the short-term adhesion tests, but no reduction of biofouling was observed from the long-term biofouling experiments. The universal coating approach consisting PDA anchoring, spin-coating-assisted deposition of catechol-containing polymers, and their crosslinking *via* catechol-$Fe^{3+}$ interactions was developed by Kang's group. Their initial studies conjugated alginate with catechol groups and the molecules was deposited onto PDA-coated substrate *via* spin coating [117]. The generated stable alginate coatings of varying thickness were constructed and showed excellent resistance to bacterial adhesion. Using the same concept, multilayered PEG coatings highly resistant to marine diatom adhesion were successfully constructed on various substrates [118]. PDA could also be served as a respective anchor site for immobilizing the atom transfer radical polymerization (ATRP) initiator. Chang's group demonstrated the use of respective biomimetic catecholic initiator for surface-initiated atom transfer radical polymerization (Si-ATRP) from 316L type stainless-steel surfaces to graft

antifouling PSBMA brushes [119]. Their results showed that PSBMA grafted from PDA interfacial layers achieved better bacterial biofouling resistance than from commonly used silane-based assembly layer.

The dopamine-assisted co-deposition strategy has been used to incorporate a series of antifouling agents, thus generating universal coatings to prevent biofilm formation. Schiffman's group described a simple and universal surface modification strategy that generated an antibiofilm coating by a simultaneous deposition of PDA with poly(2-methacryloyloxyethyl phosphorylcholine) (PMPC) [120]. The resultant binary coating demonstrated a nearly 10-fold reduction in *E. coli* adhesion relative to unmodified glass. They further expanded the coating method to other substrates, including cellulose nanofiber mats [121], PEG and agar hydrogels, and PSU ultrafiltration membranes [122-123]. Approximately an order-of-magnitude reduction in bacterial adherence was observed on all these coated substrates. Xu's group developed a universal and efficient method to construct antibiofouling membrane surfaces *via* the rapid co-deposition of PDA and PSBMA triggered by $CuSO_4/H_2O_2$. The binary PDA/PSBMA coatings exhibited durable resistance to bacterial fouling [124].

To provide antibiofouling properties, catechol groups have been introduced to various fouling resistant materials to prevent bacterial biofouling on the surface. Brooks lab synthesized a copolymer of *N*,*N*-dimethylacrylamide (DMA) and *N*-(3-aminopropyl) methacrylamide hydrochloride (APMA) and coupled with catechol groups [125]. A dual layer coating consisting of a bottom PDA layer and an antifouling poly(*N*,*N*-dimethylacrylamide) (PDMA) component introduced an antifouling character to platelet storage bag material, which reduced bacterial adhesion up to 93%. Several polyacrylic acid based functional copolymers were synthesized and conjugated with dopamine *via* the facile carbodiimide chemistry by Zhao's group [126]. The

poly(polyethylene glycol methyl ether methacrylate) (PPEGMA) and PSBMA based coatings owned better anti-adhesion activity towards *E. coli* and *S. aureus*. Elimelech's group demonstrated a highly antifouling thin-film composite membrane by grafting PSBMA brushes *via* a catholic initiator [127]. They found that the membrane coated with the zwitterionic polymer brush layer exhibited higher resistance against bacteria adhesion, reaching nearly 90% bacterial adhesion reduction compared to the unmodified membrane.

#### 1.4.4.2 Universal contact killing coatings based on mussel-inspired deposition

PDA coating can function as an anchor to graft secondary antimicrobial agents containing thiols or amines, thus establishing universal contact killing coatings. From a study by Wei's group, titanium substrate was coated by one-step self-assembly of dopamine followed by immobilization of the antibiotic cefotaxime sodium through catechol chemistry [128]. The antibiotic-immobilized titanium effectively prevented adhesion and proliferation of *E. coli* and *Streptococcus mutans* (*S. mutans*) for the long-term. Rahimipour's group demonstrated a similar method to fabricate antimicrobial surfaces with antibacterial quaternary ammonium salts or novel ultrashort antimicrobial lipopeptides [129]. They showed that the antibacterial activity of the new analogs was not adversely affected by their immobilization onto various surfaces, and the developed surfaces effectively killed airborne *E. coli* and *S. aureus* when in contact.

In addition, catecholic polymers with antimicrobial segments have been used to construct contact killing coatings. Kuroda's group synthesized amphiphilic polycations with different mole ratios of monomers containing dodecyl quaternary ammonium, methoxyethyl, and catechol groups *via* free-radical polymerization and prepared the polymer coating by immersing glass slides into a polymer solution and subsequent drying and heating [130]. They anticipated that the quaternary ammonium side chains endowed the coatings with antibacterial activity, as the

methoxyethyl side chains balanced the hydrophobic/hydrophilic property of the coating, and the catechol groups promoted polymer anchoring. The coated surfaces displayed antimicrobial activity towards *E. coli* and *S. aureus* in a 1 h short-term assay and prevented the accumulation of viable *E. coli*, *S. aureus*, and *Acinetobacter baumannii* (*A. baumannii*) for up to 96 h.

#### 1.4.4.3 Universal release killing coatings based on mussel-inspired deposition

The one-step assembly of dopamine and metal ions can produce a release killing metal-PDA binary coating layer on various substrates *via* the oxidative polymerization of dopamine and simultaneous reduction of metal ions. Nam's group employed PDA with simultaneous reduction of $Ag^{+}$ to prepare PVA nanofibrous membranes functionalized with silver nanoparticles [131]. The PDA-mediated metal coatings on PVA nanofibers exhibited dramatic suppression of *E. coli* growth. Zhou's group reported a one-step method to chelate $Cu^{2+}$ onto filtration membrane surfaces by simply soaking the filtration membranes in a dopamine solution containing $Cu^{2+}$ [132]. The incorporated $Cu^{2+}$ from the membrane surface delivered superior antimicrobial activities against *S. aureus*. Tang's group developed a facile and universal method for generating release killing coating on a thin-film composite polyamide reverse osmosis membrane *via* post-modification of PDA [133]. The surface was initially modified with PDA, whose reducing catechol groups subsequently immobilized $Ag^{+}$ in situ to form uniformly dispersed silver nanoparticles inside the PDA layer. Both diffusion inhibition zone and CFU tests demonstrated clear antimicrobial activities of the silver loaded membranes on *Bacillus subtilis* (*B. subtilis*) and *E. coli*.

#### 1.4.4.4 Universal multifunctional coatings based on mussel-inspired deposition

Several universal coatings with both antifouling and contact killing functionalities have been demonstrated based on mussel-inspired deposition. PDA coatings form a thin layer on

virtually all kinds of material surfaces by a simple immersion technique and provide anchoring sites for immobilizing of antifouling and antimicrobial polymers. Yang's group synthesized a series of diblock copolymers of PEG and cationic polycarbonates *via* metal-free organocatalytic ring-opening polymerization and successfully grafted them onto silicone rubber using an active PDA layer [134]. The polymer coatings with a hydrophobic component eradicated *S. aureus* and methicillin-resistant *Staphylococcus aureus* (MRSA) in solution, and efficiently prevented surface fouling. In particular, the coated surfaces with the optimal polymer composition exhibited significantly higher antifouling activity than the PEG-coated surfaces. To impart the antiadhesion and bactericidal properties, Kang's group grafted poly(2-hydroxyethyl methacrylate) (PHEMA) brushes from the PDA-modified stainless-steel surface *via* Si-ATRP of 2-hydroxyethyl methacrylate (HEMA) and coupled with chitosan [135]. The surface-functionalized stainless-steel reduced bacterial adhesion and exhibited antibacterial efficacy against *E. coli*.

Catechol-containing polymers with antifouling and antimicrobial properties have been synthesized and coated onto substrates. Yang's group synthesized new brush-like polycarbonates with three important components, i.e., pendent PEG for antifouling, catechol for adhesive, and cations for antibacterial and coated the synthetic polymer onto the substrates by one-step immersion [136]. The optimized coating structure was able to kill both Gram-positive and Gram-negative bacteria in solution and prevent bacterial fouling on the surface. Additionally, this new coating was stable under a simulated blood flow. Chen's group successfully synthesized a novel bio-inspired P(DMA-*co*-MPC-*co*-DMAEMA) terpolymer with three important components, i.e., MPC for antifouling, dopamine methacrylamide (DMA) for anchoring, and 2-(dimethylamino)-ethyl methacrylate (DMAEMA) for the potential contact killing [137]. The terpolymer was

coated onto the substrate surface by a one-step immersion. After quaternization, the coating was able to kill both Gram-positive and Gram-negative bacteria and effectively released bacteria corpse from the surface.

Universal antifouling and release killing coatings have been developed based on mussel-inspired surface chemistry. Messersmith's group demonstrated a simple immersion strategy for substrate coatings that inhibited bacterial adhesion and actively killed bacteria *via* silver release [138]. The strategy was enabled by a PDA primer, which acted as an anchoring site for antifouling polymers to graft onto as well as an incorporation site in which silver nanoparticles were nucleated from a silver salt solution. The group finally confirmed the antifouling and antimicrobial performance of the developed surfaces against both Gram-positive and Gram-negative bacterial strains. Boyer's group utilized the versatile anchoring property of PDA to design an antibiofilm coating that possessed low-fouling and NO releasing capabilities [139]. To achieve this, substrates were functionalized with PDA *via* simple immersion, followed by the grafting of PEG *via* Michael addition, and subsequent formation of NO precursors by purging with NO gas. The NO releasing PEGylated film inhibited biofilm attachment by 96% and 70% after exposure to Gram-negative *P. aeruginosa* culture solution for 24 and 36 h, respectively.

### 1.4.5 Polyphenolic material deposition

It is well known that the presentation of polyphenols in red wine or tea leads to a coating on the surface of containers. Polyphenols contain high density of catechol and gallol functional groups. Due to their structural resemblance to catecholamine, polyphenols are expected to exhibit superior solid-liquid interfacial properties. Messersmith's group initially described a novel bioinspired approach to the form phenolic coatings on diverse substrates using TA or pyrogallol (PG) as the precursors [140]. Subsequently, they screened a library of twenty phenolic

and polyphenolic compounds for surface anchoring [141]. Besides TA and PG, six additional precursors including catechin, epigallocatechin, epigallocatechin gallate, morin, catechol, and hydroxyhydroquinone were identified as suitable precursors to deposit on substrates (**Figure 1.6**). However, most of these precursors only showed coating ability under high salt conditions. Lee's group proposed a new approach for surface modification *via* using 5-pyrogallol 2-aminoethane and pointed out that the presence of amine groups with the pyrogallol moiety was critical for generating stable coatings [142]. Like catecholamine aggregation and deposition, the presence of oxidants and UV irradiation can also trigger oxidative polymerization and deposition of phenolic compounds [143].

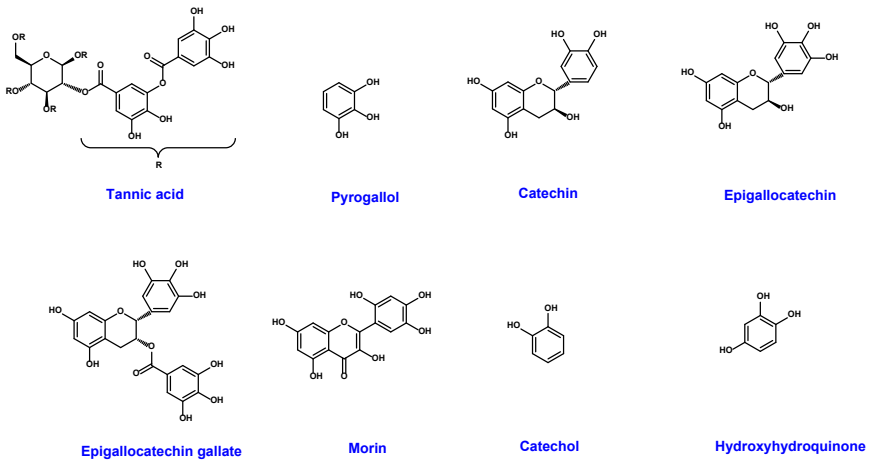


**Figure 1.6 Chemical structures of the phenolic and polyphenolic compounds that were able to achieve surface anchoring.**

Besides unitary phenolic coatings, another surface anchoring strategy based on metal-phenolic network (MPN) has been developed. Caruso's group first reported a simple, versatile and rapid method for surface coating [144]. Film formation is initiated by the adsorption of the polyphenol and directed by multivalent TA-$Fe^{3+}$ coordination bonding. The coordination

between TA and $Fe^{3+}$ is pH-dependent: at low pH, the hydroxyl groups are protonated, which causes the disassembly of the crosslinking. Only mono-complex formed at pH<2.0, resulted in the coating disassembly. When pH increased to 3.0-6.0, the coating was still unstable although bis-complex formed. Only with tris-complex formation at pH>7.0, the coating exhibited long-term stability. The metal-phenolic network has been expanded to a broad library of metals including $Cu^{2+}$, $Al^{3+}$ and $Zr^{4+}$ [145]. The disassembly kinetics of MPN depends on the type of the metals used, as each metal has a different affinity towards TA. The same metal can also be coordinated with multidentate phenolic ligands, such as gallic acid, pyrogallol, and pyrocatechol [146].

#### 1.4.5.1 Universal antifouling coatings based on polyphenolic deposition

It is well-known that TA can anchor on almost all the substrates. Kang's group synthesized HPG bearing terminal thiol moieties (HPG-SH) and immobilized HPG-SH on TA deposited stainless-steel substrates [147]. This post-modification strategy confered low biofouling characteristics of the stainless-steel substrates. They also functionalized several other molecules with TA to confer the conjugates with universal anchoring ability. TA was modified with alkyl bromide groups *via* esterification [148]. The brominated TA was anchored on the stainless-steel substrates for Si-ATRP of hydrophilic monomers. The zwitterionic PMPC and PSBMA immobilized surfaces exhibited good resistance against *S. aureus* and *Amphora coffeaeformis* (*A. coffeaeformis*) attachment and barnacle cyprids settlement. TA was functionalized with maleimido groups *via* etherification of TA with *N*-3-bromopropylmaleimide [149]. The trihydroxyphenyl groups in the conjugates can be used for the bioinspired surface anchoring on stainless-steel substrates, while the maleimido groups are ready for the subsequent Michael addition with thiolated carboxymethyl chitosan. The thiolated carboxymethyl chitosan

coatings generated by solution immersion and spin coatings significantly reduced *E. coli* adhesion by 85.5% and 95.5%, respectively. They further functionalized polysaccharide agarose with alkyl bromo moieties, followed by etherification with TA *via* Williamson ether synthesis [150]. The bifunctional conjugates could be deposited onto a variety of substrates *via* direct adsorption and intermolecular crosslinking. The polysaccharide agarose-containing coatings on the stainless-steel substrates were effective in reducing *E. coli* adhesion by 80.5%.

The discovery of MPN has prompted the applications of TA-$Fe^{3+}$ complexes in functional surface coatings. Lee's group generated a functional coating on PES membrane *via* a rapid one-step assembly coating of TA and $Fe^{3+}$ [151]. The surface density of live *P. aeruginosa* on the TA-$Fe^{3+}$ coated membrane was much smaller than that on the bare PES membrane after 4h of filtration; only 0.17% of live *P. aeruginosa* was observed on the TA-$Fe^{3+}$ coated membrane compared to that on the bare membrane. MPN can also serve as the bioinspired anchors for immobilizing the antifouling agents. TA coating of a PDA-coated surface was carried out using $Fe^{3+}$ coordination chemistry by Kang's group, PEG [152] and PVP [153] were immobilized on the TA-coated surfaces *via* hydrogen bonding. The diatom densities on the final PEG-coated and PVP-coated substrates were 83.4% and 80% lower than on the unmodified stainless-steel substrates. Using a covalent conjugation strategy, the zwitterionic PEI was grafted onto a TA-$Fe^{3+}$ complexes deposited PES membranes *via* Michael addition or Schiff base reaction by Zhao's group [154]. The modified PES membranes exhibited excellent resistance against Gram-positive *S. aureus* and Gram-negative *E. coli* adhesion.

#### 1.4.5.2 Universal release killing coatings based on polyphenolic deposition

Antimicrobial metal ions have been incorporated with polyphenolic to construct universal release killing coatings. Zan's group developed a one-step method to fabricate a universal release

killing coating which can be achieved in minutes [155]. The coating was formed in just a few minutes at room temperature after mixing PEI, $Ag^+$, and TA in water. The formed coating not only exhibited strong antimicrobial activities against both Gram-positive *S. aureus* and Gram-negative *E. coli*, but also supported the proliferation of dental pulp stem cells.

## 1.5 Goal and outline of the project

In the previous sections, various universal coating approaches imparting surfaces with antibiofilm properties have been reviewed. Antifouling strategy, contact killing strategy, and release killing strategy are the three major approaches that were extensively studied on surface to create biofilm resistance. One major concern related to contact killing coatings is the fact that cationic surfaces with bacterial killing abilities accumulate unnecessary biological components (e.g. dead bacterial debris) compromising coating's long-term performance. Development of antibiotic resistance is still unavoidable when releasing coatings are applied to medical devices. Based on this understanding, antifouling coatings are the most promising coatings for medical devices since they have less potential to cause side effects and toxicities.

Unfortunately, current antifouling approaches can barely meet the requirements needed as an antibiofilm coating on urinary catheters. The requirements include inhibition of bacterial colonization, adaptation to diverse materials, easy application to urinary catheters, stability of the coating and long-term efficacy. This thesis aims to provide new antifouling technologies for prevention of CAUTI that fulfill these requirements. The final goal is to offer novel approaches to prevent infections, save lives and improve the quality of live in patients who need catheterization.

Inspired by the composition of adhesive proteins in mussels, Messersmith's group reported a method to form multifunctional polymer coatings through simple dip-coating of

objects in an aqueous solution of dopamine [85]. Based on this concept, we designed a simple and universal antibiofilm coating method by combing mussel-inspired surface chemistry with polymer-nanoparticle interaction. In Chapter 2 and Chapter 3, we screened for the optimal composition and evaluated the universality of the approach, stability and biocompatibility of the coating both *in vitro* and *in vivo* to achieve the optimal coating composition. In addition, we analyzed the mechanism of coating formation and investigated how molecular weight and polymer chemistry of the co-assembled hydrophilic polymers as well as the catecholamine type influence the coating structure.

Optimized coating developed in Chapter 2 and Chapter 3 has a characteristic thickness of 19 nm. Although very efficient in preventing biofilm formation, the coating itself is too thin to incorporate enough antimicrobial drugs. Thus, by using the hydrogen bonding interaction between the TA and hydrophilic polymers in combination with LbL assembly technique mentioned in Chapter 4, we proposed a universal antibiofilm coating with variable thickness. This thickness-variable coating could be used as a platform for generating multifunctional coatings.

Overall, the focus of this thesis is to develop effective strategies to generate antifouling coatings on medical devices using co-assembly approaches utilizing polycatecholoamine and diverse hydrophilic polymers and study their antibiofilm activities against both Gram-positive and Gram-negative bacteria *in vitro* and *in vivo*.

# Chapter 2: Design and development of a novel universal antibiofilm coating

In this chapter, we develop a novel ultrathin coating with long-term antibiofilm activity based on mussel-inspired surface chemistry and polymer-nanoparticle interaction. This chapter introduces the screening to find the best coating, followed by characterizing the surface chemistry and morphology, validating the universality and stability, demonstrating the biocompatibility, and evaluating the antibiofilm activity *in vitro* and *in vivo*.

## 2.1 Introduction

One of the key challenges associated with device/ implant associated infection is the formation of bacterial biofilms within ~7 days of implantation which impede device/implant functions [31, 156-160]. Despite advancements in the development of antimicrobial and antibiofilm coating in recent years, current coating technologies to prevent biofilm formation fail to address all factors, including the prevention of biological deposition (proteins and organic molecules) [161], inhibition of bacterial colonization, adaptation to diverse materials [162], easy application to devices of various sizes and shapes, and stability of the coating.

Mussel-inspired surface chemistry is one of the most widespread strategies and has the potential to overcome most of the challenging issues in antibiofilm coating development [85, 163-167]. The strategies utilized to endow substrates with antibiofilm functions include *via* post-modification of polydopamine (PDA) and the utilization of polymer-catechol conjugates [109, 112, 134, 136, 168-172]. Although these strategies are versatile and universally applicable, none of these methods reported today showed promising long-term outcomes as a result of the formation of incomplete antifouling layer or limited surface coverage [110, 114, 120, 173-175].

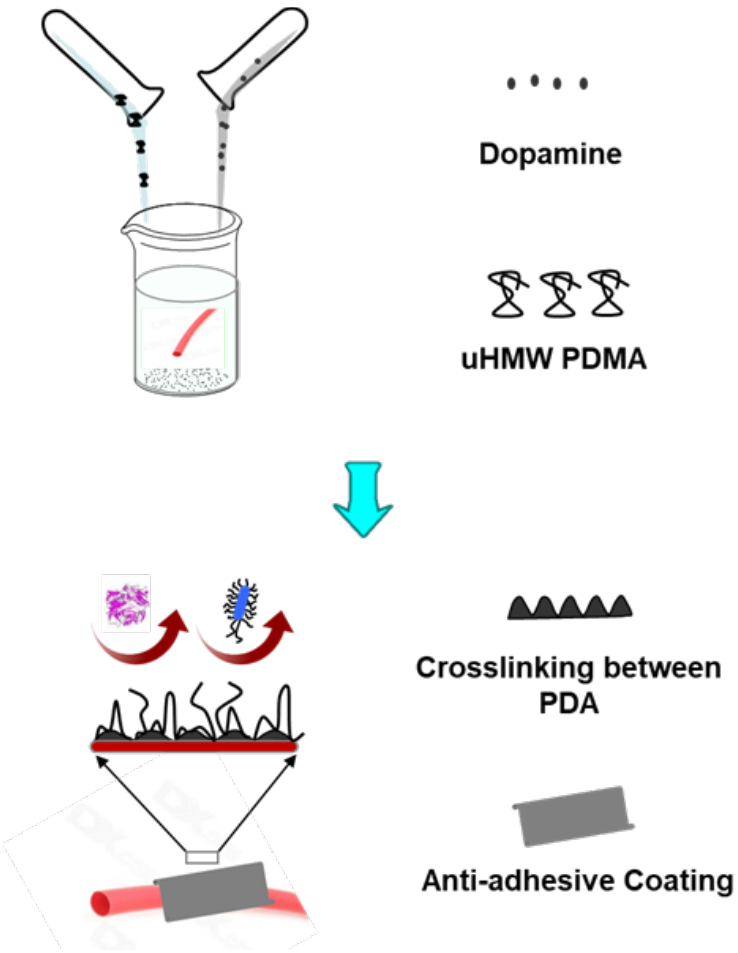


**Figure 2.1 Design of universal binary coating with antifouling performance.**

**Schematic of binary PDA/PDMA antibiofilm coating deposition in aqueous conditions. Dopamine and PDMA-795K were mixed in aqueous buffer, and coating was applied *via* a simple dip coating process. The average thickness of the binary coating was around 19 nm.**

The long-term antibiofilm activity is the key bottle neck in the advancement of mussel-inspired coating technologies. Most of the current antibiofilm coatings are short-lived, the short-term protein and bacterial adhesion on freshly coated substrates are not predictive of their long-term antibiofilm behavior. As shown previously, in certain situations, some short-lived antibiofilm coatings may function as bacterial reservoirs over the longer term, and this will have important implications for their use in healthcare [116, 176]. Thus, further methods are needed to

prevent biofilm formation which can be easily applied to diverse substrates to generate long-term activity.

Here, we report on a one-step dip coating surface modification method (**Figure 2.1**) that makes use of polymer-polydopamine interaction to form an ultrathin (∼19 nm) and durable layer. We utilized a screening process to identify the composition of the coating that generates broad spectrum antibiofilm activity and durability. We show that a nano coating composed of ultra-high molecular weight (uHMW) poly(*N*,*N*-dimethylacrylamide) (PDMA) in combination with PDA is highly effective in preventing the deposition of fouling proteins and biofilm formation in the presence of $>10^8$ CFU/mL bacteria for prolonged periods of time (>4 weeks) in the absence of antimicrobial agents. The coating was approved its efficacy in a mouse urinary infection model.

## 2.2 Materials and methods

### 2.2.1 Materials

Reagents were purchased from Sigma-Aldrich and used as received unless otherwise noted. Water was purified using a Milli-Q Plus water purification system (Milipore Corp., Bedford, MA) and used in all experiments. Monomers including *N*,*N*-dimethylacrylamide (DMA, 99%), acrylamide (AM), *N*-hydroxymethylacrylamide (HMA, 48% in water), *N*-hydroxyethylacrylamide (HEA, 97%), *N*-[tris(hydroxymethyl) methyl]acrylamide (THMAM, 93%), [3-[(methacryloyl)amido]propyl]dimethyl(3-sulfopropyl)ammonium hydroxide inner salt (MPDSAH, 96%), 2-methacryloyloxyethyl phosphorylcholine (MPC, 97%) were purchased from Sigma-Aldrich, and *N*-(2-hydroxypropyl)methacrylamide (HPMA) was purchased from Polysciences. *N*,*N*-Dimethylacrylamide was distilled under reduced pressure before use. Monomer 2′-acrylamidoethyl-β-D-galactopyranoside (AAEGal) was synthesized according to

our previous protocol [177]. The single-side-polished silicon wafers were bought from University Wafer (Boston, MA). Titanium (~250 nm) deposited silicon wafer was prepared by e-beam evaporation of titanium (physical vapor deposition). The process was progressed in a home-assembled Evaporator 2000 system equipped with a quartz crystal microbalance to monitor the film thickness and a cryo pump to reach high-vacuum ($10^{-7}$-$10^{-6}$ Torr) conditions. After deposition, the substrates were washed with Milli-Q water, dried *via* a $N_2$ gun, and stored for further usage. Polyurethane (PU) sheet with a thickness of 0.78 mm and Polypropylene (PP) sheets with a thickness of 0.30 mm were purchased from Professional Plastics (CA, USA). Unplasticized polyvinyl chloride (uPVC) was purchased from Goodfellow Cambridge Limited (U.K.) with 0.2 mm thickness. Platelet bag material (Solmed EH-222) mainly composed of PVC and TEHTM was generously provided by the American Renolit Corporation and denoted here as plasticized PVC (pPVC). Polyimide (PI) was provided by the previous lab member without appropriate labeling. 14 Gauge and 24 Gauge SurFlash I.V. Catheters made of PU, were purchased from Terumo.

### 2.2.2 Polymer synthesis

The high and ultra-high molecular weight polymers were synthesized by aqueous ATRP [178, 179]. In a typical experiment, copper(II) chloride ($CuCl_2$; 2 mg), copper(I) chloride (CuCl; 15.9 mg), and 1, 1, 4, 7, 10, 10-hexamethyl triethylene tetramine (HMTETA, 96.2 μL) were added successively into a glass tube, followed by the addition of 20 mL of Milli-Q water. The solution was degassed with three freeze-pump-thaw cycles and then transferred into the glovebox. The catalyst solution (20 mL) was thoroughly mixed before the addition of monomers (2 g). The amount of methyl 2-chloropropionate in methanol added to the reaction mixture was controlled to change the molecular weight of the polymers, and the polymerization could proceed

at room temperature (22 °C) for 24 h. The soluble polymer was finally collected by dialysis (molecular weight cutoff: 1000) against water for 1 week. uHMW hyperbranched polyglycerol (HPG) was synthesized according to our previous protocol [180]. Other high and ultrahigh molecular weight polymers including polyvinyl pyrrolidone (PVP), polyethylene oxide (PEO), Poly(2-ethyl-2-oxazoline) (PEOX) and dextran were purchased from Sigma-Aldrich, ON.

### 2.2.3 PDA particle synthesis

The 2 mg/ml dopamine was dissolved in 10 mM Tris-HCl buffer and kept for 24 h without stirring at room temperature. The PDA particles were separated by centrifugation (5000 rpm) and washing multiple times with deionized water.

### 2.2.4 Gel permeation chromatography

The molecular weight and polydispersity index (PDI) of polymers were determined by gel permeation chromatography (GPC) on a Waters 2690 separation module fitted with a DAWN EOS multiangle laser light scattering detector from Wyatt Technology Corp. with 18 detectors placed at different angles and a refractive index detector (Optilab DSP from Wyatt Technology Corp.). An Ultrahydrogel linear column with a bead size of 6-13 μm (elution range $10^3$ to $5\times10^6$ Da) and an Ultrahydrogel 120 with a bead size of 6 μm (elution range 150 to $5\times10^3$ Da) from Waters were used. The dn/dc value of high and ultrahigh molecular weight polymers in the mobile phase was determined at $\lambda$= 620 nm and was used for determining molecular weight parameters. The number average mean square radius moments were taken as the radius of gyration of the polymer. The detailed information about high molecular weight polymers was provided in **Appendix A1**.

### 2.2.5 Coating process

Unless stated otherwise, substrates were coated according to the protocol described here. The titanium deposited silicon wafers were exposed to oxygen plasma for 2 min to remove adventitious contamination. Other polymer substrates were cleaned by ultrasonication in deionized water for 10 min and dried under a steam of nitrogen. For a typical coating preparation process, a mixture of 2 mg/mL catecholamine and 10 mg/mL polymer was prepared in 10 mM Tris-HCl buffer (pH= 8.5) [85]. For the PDA/PMPDSAH coating, polymer was dissolved in Tris-HCl buffer together with 5 mg/mL sodium chloride to promote the polymer dissolution. The substrates were then immersed in either catecholamine alone or catecholamine-polymer solution and were kept for 24 h without stirring. Afterward, the modified samples were rinsed with Tris-HCl buffer and deionized water and dried in a steam of nitrogen. The modified substrates were used for further characterization. The 2 mg/mL preformed PDA particles and 10 mg/mL PDMA-795 K combination were also used to coat the silicon wafer as a control.

### 2.2.6 Ellipsometry analysis

The variable-angle spectroscopic ellipsometry (VASE) spectra were collected on an M-2000 V spectroscopic ellipsometer (J.A. Woollam, Lincoln, NE) at 50°, 60°, and 70° at wavelengths from 480 to 700 nm with an M-2000 50W quartz tungsten halogen light source. The VASE spectra were then fitted with a multilayer model utilizing WVASE32 analysis software based on the optical properties of a generalized Cauchy layer to obtain the dry thickness of the deposited layers. Silicon wafer was used as the substrate.

### 2.2.7 Attenuated total reflectance Fourier transform infrared analysis

Attenuated total reflectance Fourier transform infrared (ATR-FTIR) spectra were recorded using a Thermo-Nicolet Nexus FTIR spectrometer (Nicolet Instrument, Waltham, MA)

with a MCT/A liquid nitrogen cooled detector, KBr beam splitter and MKII Golden Gate Single Refection ATR accessory (Specac Inc. Woodstock, GA). Spectra were recorded at 4 $cm^{-1}$ resolution and 64 scans were collected for each sample. PP film was used as the substrate and used for background subtraction.

### 2.2.8 X-ray photoelectron analysis

X-ray photoelectron (XPS) was performed using a Leybold LH Max 200 surface analysis system (Leybold, Cologne, Germany) equipped with a Mg Kα source at a power of 200 W. Elements were identified from survey spectra. High-resolution spectra were collected at 48 eV pass energy. Silicon wafer was used as the substrate.

### 2.2.9 Water contact angle measurements

For water contact angle (WCA) measurements, digital images of a 10 µL water droplet on the surface were taken using a digital camera (Retiga 1300, Q-imaging Co.), and analyzed using Northern Eclipse software. Six different spots on the PP film and PDA/PDMA coated samples were tested for each sample and the average value was reported.

### 2.2.10 Stability of the coating

The stability of the coatings in physiological conditions was monitored measuring the thickness of the coating by ellipsometry measurements. The coated samples on silicon wafers were incubated in PBS buffer for different periods (3 days to 3 weeks), ultrasonicated in Phosphate-buffered saline (PBS) buffer for 10 min or autoclaved at 121 °C for 30 min before measuring the thickness change. The coated samples on titanium were also challenged with above-mentioned procedures and evaluated for early stage biofilm formation protocol.

### 2.2.11 Protein adsorption by QCM-D measurements

Quartz crystal microbalance with dissipation monitoring (QCM-D) was used for evaluation of bovine serum albumin (BSA) adsorption on coatings. The coated gold sensors (PDA/PDMA-795 K at ratio 1:5) were placed into the titanium flow chamber. PBS buffer was pumped over the sensor surface for 10 min, and baseline equilibrium was reached. Then, the BSA solution in PBS (50 μg/mL) was pumped into the flow chamber for additional 15 min, followed by a PBS rinse for 10 min. The flow rate used for all steps was 0.05 mL/min, and the temperature was set to 22 °C.

### 2.2.12 Protein adsorption by fluorescence measurements

To determine the extent of absorbed protein on the PP film, the samples were incubated with fluorescent labelled BSA (BSA-FITC conjugate) and fibrinogen (Fib-Alex-fluor 594 conjugate). BSA conjugate (1 mg/mL) and 0.25 mg/mL Fib conjugate was prepared in PBS buffer. Before incubation with protein solutions, the samples were equilibrated with PBS for 10 min. Afterwards, the uncoated and coated (PDA/PDMA-795K at ratio 1:5) PP films were incubated with 0.3 mL stock solutions for 2 h, thoroughly washed with PBS buffer for 3 times and dried in a steam of nitrogen. The images of non-absorbed and protein-absorbed samples were taken using a fluorescence microscope (NikonEclipse TE 2000-U with an X-Cite 120 fluorescence illumination system, fluorescein isothiocyanate (FITC) and rhodamine filters, and a DS-U1 suit digital camera). The obtained images were switched to the gray scale by Adobe Photoshop, and the intensity was recorded. Detailed information for calculation is shown in **Appendix A2**.

### 2.2.13 Platelet adhesion

Blood from healthy consented healthy donors was collected into 3.8% sodium citrated tubes at Centre for Blood Research. The protocol was approved by the University of British Columbia's clinical ethics board. Platelet-rich plasma (PRP) was prepared by centrifuging the whole blood at 150 x g for 10 min in an Allegra X-22R Centrifuge (Beckman Coulter, Canada). The uncoated and PDA/PDMA-795K coated PP films were pre-incubated in PBS buffer for 10 min and then incubated with 0.3 ml PRP for 4 h at 37 °C in a 1.5 mL polystyrene Eppendorf tube without shaking. After incubation, the samples were removed, washed with PBS and incubated with 2.5% glutaraldehyde for 2 h at 4°C to fix the adhered platelets. The samples were then gradient dried with 50%, 60%, 70%, 80%, 90%, and 100% (v/v) ethanol in water for 10 min in each step and air dried. Finally, each sample was sputter coated with gold prior to observation with SEM.

### 2.2.14 Cell adhesion

Human BJ fibroblasts purchased from Cedarlane Corporation (Burlington Ontario) were cultured in tissue polystyrene flasks within Eagle's Modified Essential Media (EMEM) (Thermofisher) in a humidified incubator (37 °C and 5% $CO_2$) until they were sub confluent. Cells were then serially passaged using a solution of 0.25 % Trypsin-0.03% EDTA (Trypsin/EDTA). During culture, the media was changed every second day. Cells were then seeded at a density of $3*10^4$ cells/$cm^2$ onto the uncoated and PDA/PDMA-795K coated 8-well tissue culture chamber slides for 48 h. After 48 h cultures, the substrates were washed with PBS and the adhered fibroblasts were stained with 4′,6-diamidino-2-phenylindole (DAPI) (Invitrogen). Finally, 8-well tissue culture chamber was mounted on glass slides and imaged

using a fluorescence microscope (NikonEclipse TE 2000-U with an X-Cite 120 fluorescence illumination system, DAPI filter, and a DS-U1 suit digital camera).

### 2.2.15 Cell viability

Human BJ fibroblasts were seeded onto 48 well plates at a density of $3*10^4$ cells/well. Cells could adhere for 24 h before incubation with samples. PDA/PDMA-795K solutions (24 h after mixing) of varying concentrations were prepared in EMEM and incubated with the cells for 48 hours in duplicate. After incubation, cells were washed three times with PBS and trypsinized using 0.25% Trypsin-EDTA (Millipore Sigma). Cells were stained using 7-Aminoactinomycin D (Biolegend) and discrimination of dead cells was conducted via flow cytometry on a CytoFlex Flow Cytometer (Beckman Coulter). Mean (%) viability and standard deviations are reported.

### 2.2.16 Screening of initial bacterial adhesion

For initial bacterial adhesion screening assay, a V-shaped 96-well PP plate format was used. The coating was prepared using different polymers on a 96-well plate with a composition of 1:5 dopamine and polymer in buffer. After the coating preparation, the 96-well plate was sterilized with 75% ethanol. An overnight culture of *Staphylococcus aureus* (*S. aureus*) lux strain (Xen36 Lux) was first adjusted to $10^6$ CFU/mL in Lysogeny broth (LB) medium. Each well was equilibrated with LB for 10 min and then covered with 0.2 mL bacterial suspension. The inoculated plate was incubated for 4 h at 37 °C. After the bacterial adhesion process, the wells were filled with PBS and washed twice to remove nonadherent bacteria. The wells with adhered bacteria were ultrasonicated for 10 min to release bacteria cells into PBS buffer (0.2 mL). The bacterial suspension was serially diluted and spread on an agar plate. After culturing overnight, the number of viable bacterial cells was quantified by counting the number of colonies on the agar plate.

### 2.2.17 Screening of early stage biofilm formation

For early stage biofilm formation screening assay, a 96-well black PP plate format was used. The coating was prepared using different combinations of polymers and catecholamines on a 96-well plate with a composition of 1:5 catecholamine and polymer in Tris-HCl buffer. After the coating preparation, the 96-well plate was sterilized with 75% ethanol. An overnight culture of *S. aureus* lux strain was first adjusted to $10^6$ CFU/mL in LB medium. Each well was equilibrated with LB for 10 min and then covered with 0.2 mL bacterial suspension. The inoculated plate was incubated for 24 h at 37 °C shaking at 50 rpm. After the bacterial adhesion process, the wells were filled with PBS and washed twice to remove nonadherent bacteria. For the assessment of surface adhered bacteria, SYTO 9, a green-fluorescent nucleic acid staining agent, was used to label all the bacterial cells by penetrating cells membranes. The washed 96-well plates were soaked in a dye solution at room temperature in the dark for 15 min. The stained 96-well plated were read under a fluorescent read to determine the bacterial density.

### 2.2.18 Evaluation of early stage of biofilm formation

Five different bacteria [*S. aureus* lux strain (Xen36 Lux); methicillin-resistant *S. aureus* lux strain (USA300); *E. coli* lux strain (DH5-α, plasmid pUC 19); *P. aeruginosa* lux strain (PAO1 Tn7::Plac-lux); *S. saprophyticus* strain (ATCC 15305)] were tested on diverse substrates to determine early stage biofilm formation. The coatings were applied to different substrates. The sterilized samples were cut into pieces and transferred into a 24-well plate. Overnight culture of bacteria was first adjusted to $10^6$ cells/mL in LB. Each sample was equilibrated with LB for 10 min and then immersed in 1 mL bacterial culture. The 24-well plate was incubated at 37 °C with shaking at 50 rpm. After 24 h incubation, suspension was removed, and the samples were thoroughly washed with PBS to remove loosely adhered bacteria. For the assessment of surface

adhered bacteria, SYTO 9, a green-fluorescent nucleic acid staining agent, was used to label all the bacterial cells by penetrating cells membranes. The washed samples were soaked in a dye solution at room temperature in the dark for 15 min. The stained bacterial cells were viewed under a fluorescent microscope using the FITC filter. For SEM analysis, the samples were taken out and fixed with 2.5% glutaraldehyde for 2 h at 4 °C. After serial dehydration with 50%, 60%, 70%, 80%, 90%, and 100% ethanol for 10 min each, the samples were dried, coated with a thin layer of Au, and observed under scanning electron microscope (SEM). The number of bacteria on the samples was quantified by counting the total number adhered bacteria from at least six representative images at the sample magnification. The results obtained from the coated samples were normalized using the adhered number from original uncoated samples.

### 2.2.19 Long-term biofilm formation studies under shaking condition

Uncoated and coated titanium pieces were placed into 24-well plates for generating biofilm formation. A total volume of 1 mL tryptic soy broth (TSB) culture containing $5*10^4$ cells/mL *S. aureus* lux was added to each well. After every 24 h, suspension was removed, the samples were slightly washed under shaking condition (50 RPM) for 5 min before new TSB culture with $5*10^4$ cells/mL *S. aureus* was added. At day 1, day 3, day 7, day 14, and day 21, the samples were thoroughly washed, and the fluorescent stain Syto-9 was used to microscopically assess the surface-attached biomass. The samples were analyzed using a confocal laser scanning microscope using the FITC 488 channel (Nikon Instruments Inc.). All images were acquired using identical acquisition settings.

### 2.2.20 Long-term biofilm formation studies under flow condition

For the flow condition, the uncoated and coated titanium pieces were inserted into the circulating tubes of a formally established flow model (**Appendix A3**) at 37 °C [181]. A flow

rate of 114 mL/min was chosen based on the rotary pump RPM settings. A total volume of 500 mL LB culture containing $10^6$ cells/mL *S. aureus* lux was added on day 0. The bacterial culture was totally replaced every day and circulated for 1 day, 3 days, 7 days, 14 days, and 28 days before being drained from the loop. The bacterial concentration reached $>10^8$ cells/mL during the circulation. Finally, the substrates were removed, thoroughly washed, stained with Syto-9, and assessed using a confocal laser scanning microscope (FITC 488 channel, Nikon Instruments Inc.). All images were acquired using identical acquisition settings. The samples were also fixed and serially dehydrated for SEM analysis.

### 2.2.21 Evaluation of initial bacterial adhesion of the coated catheters *in vitro*

For *in vitro* studies, 14 Gauge catheters were used with a longitudinal slit made to better expose the inner surface of the catheter for coating purposes. The optimized coating solution, dopamine 2 mg/mL with 10 mg/mL PDMA-795K, were applied on 14 Gauge catheters. After sterilization in 70% ethanol for 5 min. the uncoated and coated catheters were rinsed with LB medium and transferred to Eppendorf tubes. An overnight culture of *S. aureus* lux strain (Xen36 Lux) was first adjusted to $10^6$ CFU/mL in LB medium. Each Eppendorf tube was covered with 1 mL bacterial suspension. The inoculated Eppendorf tube was incubated for 6 h at 37 °C shaking at 50 rpm. After the bacterial adhesion process, the catheters were filled with PBS and washed three times to remove nonadherent bacteria. The catheters with adhered bacteria were ultrasonicated for 10 min to release bacteria cells into PBS buffer (1 mL). The bacterial suspension was serially diluted and spread on an agar plate. After culturing overnight, the number of viable bacterial cells was quantified by counting the number of colonies on the agar plate.

### 2.2.22 Evaluation of biofilm formation of the coated catheters *in vivo*

All the protocols for the animal experiments were approved by the University Animal Care Committee (A17-0297). Prior to animal procedures, 24 Gauge catheters were coated with the optimal solution as previously described. Briefly, the needle portion of the catheter was temporarily removed, and a 4 mm section from the tip of the 24 Gauge catheter was cut off for coating. For both uncoated and coated samples, the 4 mm piece and the remaining catheter portion were sterilized with 70% ethanol, washed three times with sterile PBS, and reassembled back onto the original needle [20].

A total of 20 male C57BL/6 mice (Harlan®) at 10 weeks of age were included in experiments. 10 mice were included in the uncoated group and 10 mice were included in the coated group. All mice were administered inhalational anesthesia with 3% isoflurane for initial induction. Once anaesthetized, isoflurane was set to 2.5%, and animals were positioned dorsally. The abdominal area was shaved, and the area around the mouse bladder was secured by using a plastic belt in a heating pad set at 38 °C. Sterile ultrasound gel was applied, and a Vevo 770® High Resolution Imaging System was used to locate and visualize the bladder. The modified 24 Gauge catheter, mounted on the original needle, was positioned at a 30° just above the pubic bone with the bevel directed to the anterior. Once the needle had been properly aligned and visualized on the ultrasound machine, it was carefully inserted towards the bladder. As soon as the 4 mm catheter segment was confirmed to be entirely inside the bladder *via* ultrasound imaging, the needle was removed while the "pusher" was pushed slightly inward. This dislodged the short 24 Gauge catheter segment into the lumen of the bladder, such that once the "pusher" was removed, the only thing that remained inside the mouse bladder was the implanted 4 mm catheter piece. One day after catheter implantation, all mice were anaesthetized and $5*10^5$

CFU/mL *S. aureus* lux (Xen36 Lux) in 50 µL PBS was percutaneously injected into the bladder lumen using a 30 Gauge needle under ultrasound guidance, utilizing separate needles for each mouse. Once successfully injected, mice were kept anaesthetized with 1% isoflurane for 1 h on a heating pad to allow time for bacteria to adhere onto the implanted catheter.

At 7 days post-instillation, all mice were sacrificed by $CO_2$ asphyxiation. Urine samples were collected from the bladder, and the bacteria concentration in the urine was quantified *via* serial dilutions and CFU counts. Inserted catheters were collected, rinsed with sterile PBS and transferred to 200 µL of fresh PBS prior to sonication for 10 min to aid biofilm dispersal. Samples were then vortexed at high speed for 10 s, and bacterial numbers were determined by serial dilutions and CFU counts.

## 2.3 Results and discussion

### 2.3.1 Screening of binary antibiofilm coating

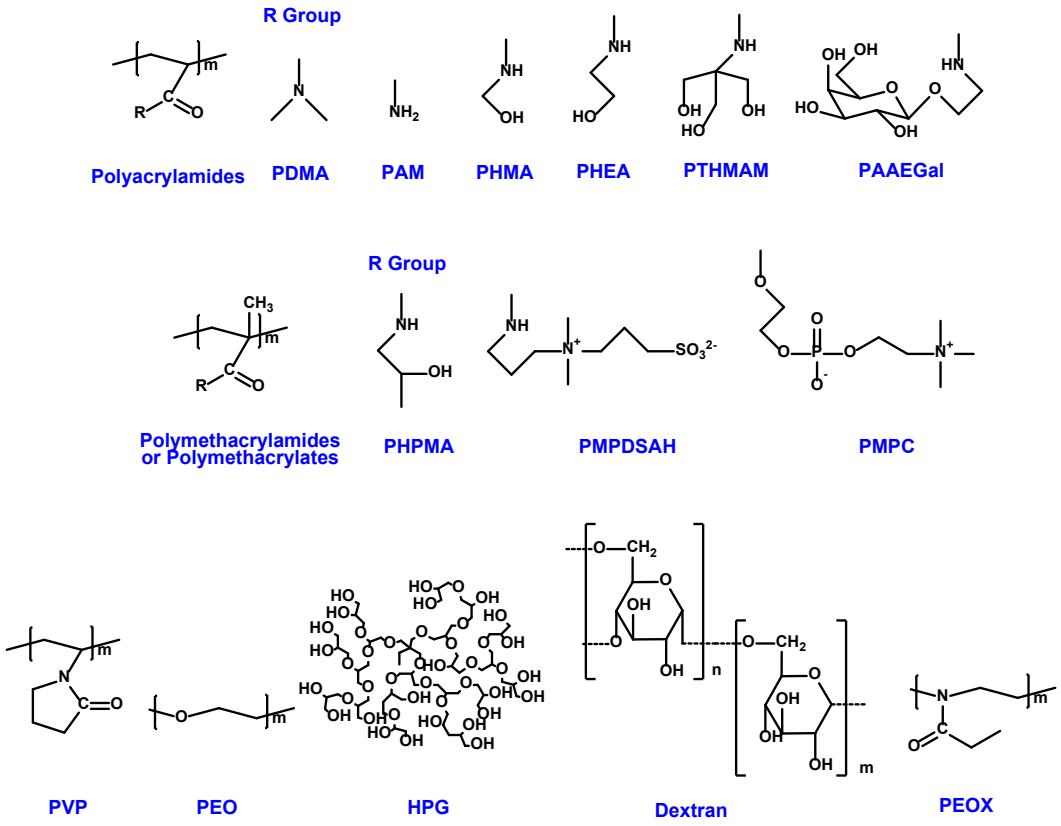


**Figure 2.2 Chemical structures of the hydrophilic polymers screened for the development of universal binary coatings.**

**PDMA: Poly(*N*,*N*-dimethylacrylamide), PAM: Polyacrylamide, PHMA: Poly(*N*-hydroxymethylacrylamide), PHEA: Poly(*N*-hydroxyethylacrylamide), PTHMAM: Poly(*N*-(tris(hydroxymethyl)methyl)acrylamide), PAAEGal: Poly(2′-acrylamidoethyl-β-D-galactopyranoside), PHPMA: Poly(*N*-(2-hydroxypropyl)methacrylamide), PMPDSAH: Poly(*N*-(3-(methacryloylamino) propyl)-*N*,*N*-dimethyl-*N*-(3-sulfopropyl)ammonium hydroxide), PMPC: Poly(2-methacryloyloxyethyl phosphorylcholine), PVP: Polyvinylpyrrolidone, PEO: Polyethylene oxide, HPG: Hyperbranched polyglycerol, PEOX: Poly(2-ethyl-2-oxazoline).**

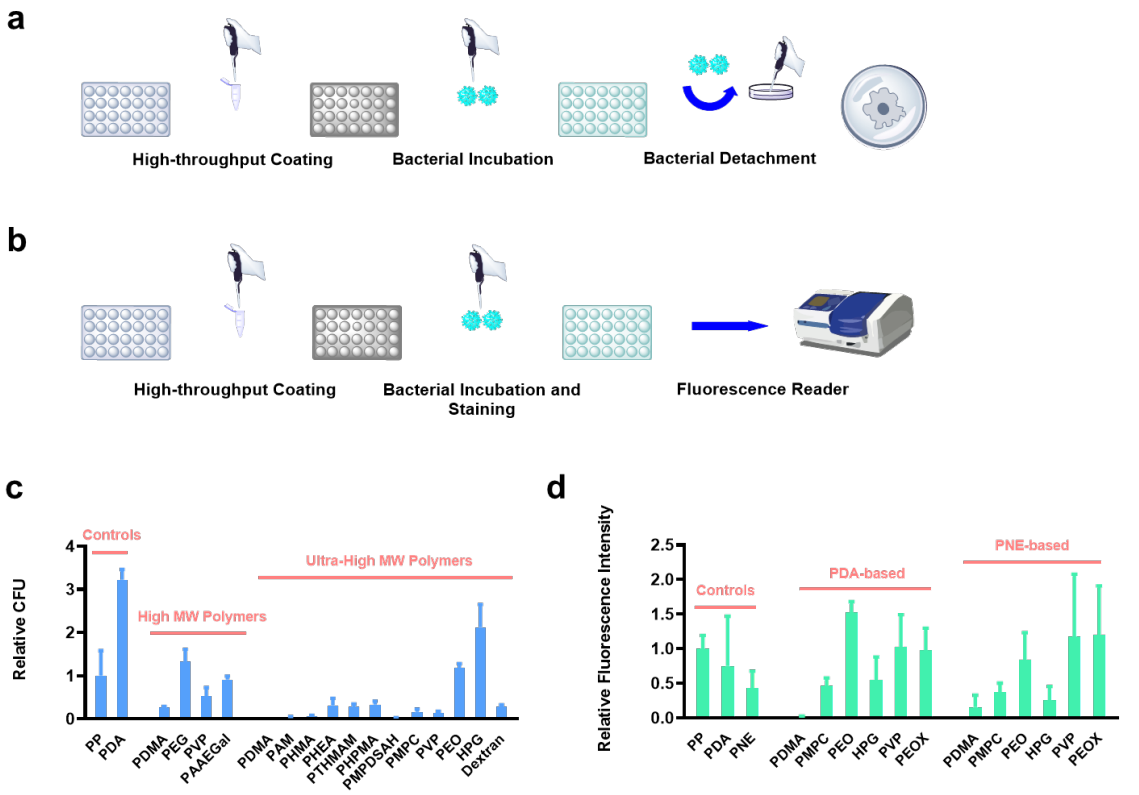


**Figure 2.3 Screening of *S. aureus* bacterial adhesion and early stage biofilm formation on different coatings.**

**(a) Schematic of high-throughput surface functionalization and bacterial adhesion assay for diverse coatings. (b) Schematic of high-throughput surface functionalization and early stage biofilm formation assay for diverse coatings. (c) Quantification of initial *S. aureus* adhesion on different polymers deposited 96-well PP plates after incubation in LB containing $10^6$ cells/mL (initial concentration) for 4 h by CFU method. (d) Quantification of early stage *S. aureus* biofilm formation on different binary coatings deposited 96-well PP plates after incubation in LB containing $10^6$ cells/mL for 24 h by fluorescence reader.**

Our coating composition consists of two components: a surface anchoring agent polycatecholamine and an antifouling hydrophilic polymer. We initially screened a small library of hydrophilic polymers **(Figure 2.2**) with different molecular weights (MWs), chemistries, and architectures in combination with dopamine/norepinephrine in the binary coating to study their potential ability to prevent biofilm formation. For this, we utilized a high-throughput 96-well PP plate model (**Figure 2.3a**) and quantified initial *S. aureus* adhesion on the surface at 4 h time

point, which is a crucial time point in the initiation of biofilm formation. Only select polymers with uHMW were found to prevent >99% of initial bacterial adhesion (**Figure 2.3c**). Another high-throughput assay was also used for evaluating coatings' ability to prevent early stage biofilm formation (**Figure 2.3b**). The results given in **Figure 2.3d** demonstrate that polymer chemistry plays a more important role than catecholamine type in preventing early stage biofilm formation.

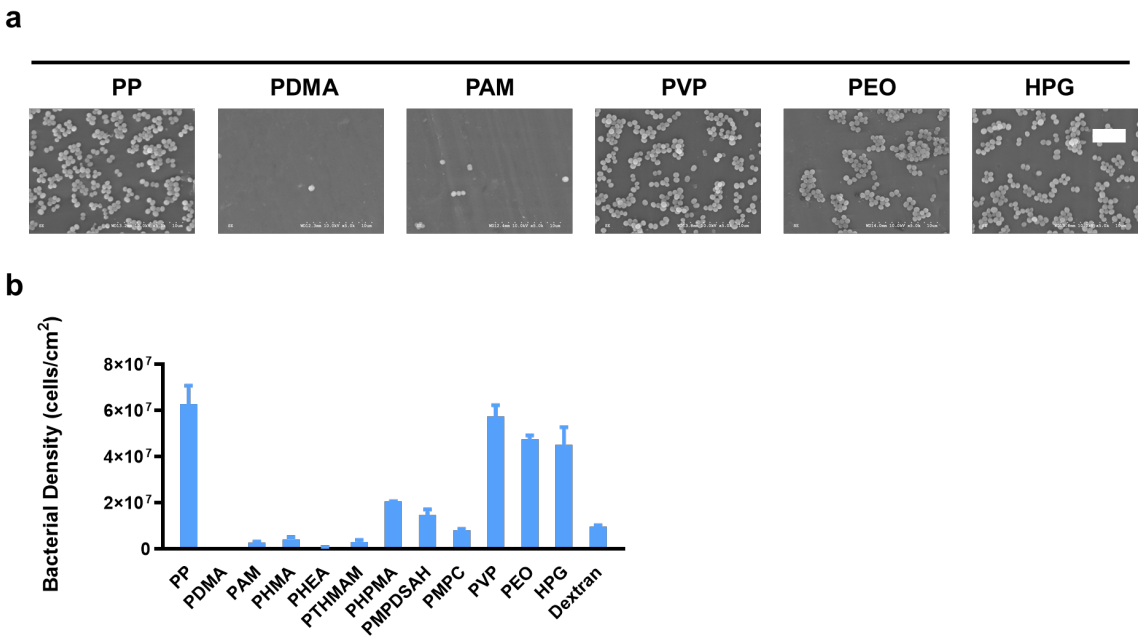


**Figure 2.4 Influence of polymer chemistry on early stage biofilm formation.**

**(a) Representative SEM images of early stage biofilm formation of *S. aureus* on coatings composed of uHMW polymer and PDA deposited on PP films after incubation in LB containing $10^6$ cells/mL (initial concentration) for 24 h. Scale bar is 5 µm. (b) Quantification of early stage *S. aureus* biofilm formation on different coatings composed of uHMW polymers and PDA deposited on PP films after incubation in LB containing $10^6$ cells/mL (initial concentration) for 24 h.**

We then systematically investigated the effect of polymer chemistry on early stage biofilm formation on PP film at 24 h utilizing SEM. Overall, the results (**Figure 2.4**) showed

early stage biofilm formation differs significantly with different uHMW polymers used, suggesting that the characteristics of the polymers present in the initial coating solution are crucial for the effective antifouling activity. Among the diverse uHMW polymers tested, PDMA was found to be the most efficacious, demonstrating >99.3% prevention of early stage biofilm formation.

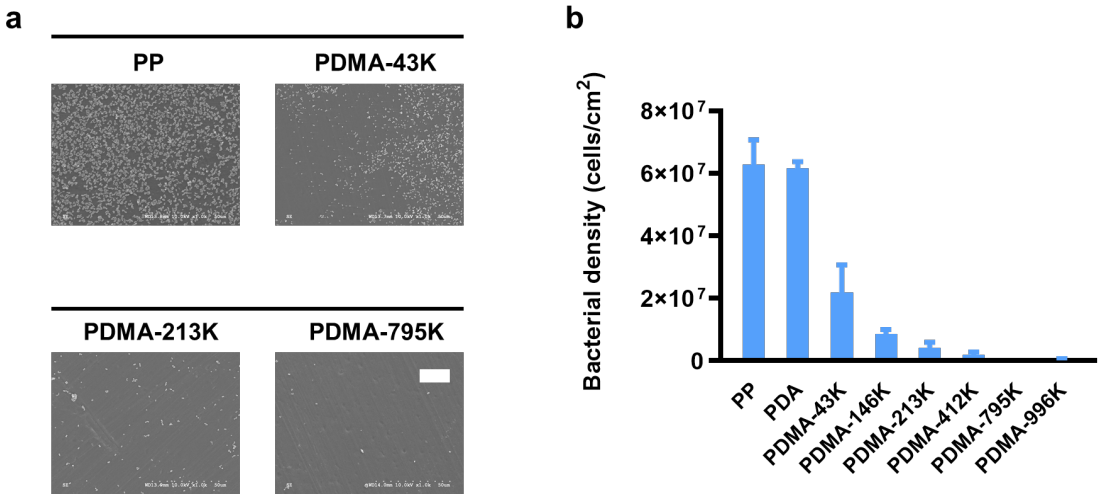


**Figure 2.5 Influence of molecular weight on the early stage biofilm formation.**

**(a) Representative SEM images of early stage of biofilm formation of *S. aureus* on uncoated PP, PDA, PDMA-43K, PDMA-146K, PDMA-213K, PDMA-412K, PDMA-795K and PDMA-996 K coated PP films after 24 h incubation in LB medium. Scale bar is 20 µm. (b) Quantification of early stage *S. aureus* biofilm formation on coatings composed of different molecular weight PDMA and PDA on PP films. The result shows a reduction of >99.3% by use of the PDMA-795K.**

Based on this observation, we investigated the influence of MW of PDMA on biofilm formation by SEM imaging. The PDMAs with MWs≥795 kDa provided the highest resistance against early stage biofilm formation; only very few bacterial cells were observed on the PDA/PDMA-795K binary coating (**Figure 2.5**).

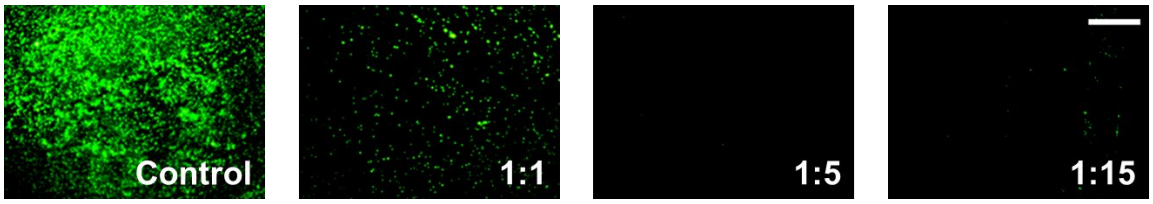


**Figure 2.6 Influence of polymer concentration on early stage biofilm formation.**

**Representative fluorescence microscopy images of early stage *S. aureus* biofilm formation on uncoated PP film, PDA: PDMA-795 K (1:1) coated PP film, PDA: PDMA-795 K (1:5) coated PP film, and PDA: PDMA-795 K (1:15) coated PP film after 24 h incubation in LB medium. Scale bar is 100 µm. Green fluorescence represents all bacteria cells attached to the surface visualized using Syto-9 stain.**

Using this most efficacious polymer, we further investigated the influence of dopamine/PDMA ratio on antifouling performance of the coating. Overall, 1:5 dopamine/PDMA-795K ratio was found to provide the greatest resistance to *S. aureus* colonization (**Figure 2.6**).

### 2.3.2 Characterization of the optimal binary coating

To further characterize the coating, we determined the thickness by ellipsometry, chemical composition by XPS and ATR-FTIR spectroscopy as well as wettability by water contact angle measurements. The dry thickness of the coating was found to decrease with increasing MW of the PDMA, reaching 18.9 nm for PDMA-795 K (**Table 2.1**).

| Coatings | [1]Thickness (nm) | [2]Si (At%) | [2]C (At%) | [2]N (At%) | [2]O (At%) | N/C |
|---|---|---|---|---|---|---|
| Silicon | NA | 50.06 | 9.27 | 1.16 | 39.51 | 0.125 |
| PDA | 32.2 ± 0.1 | 3.38 | 59.28 | 6.38 | 30.96 | 0.108 |
| PDMA-43K | 33.8 ± 0.4 | 1.19 | 72.50 | 8.20 | 18.11 | 0.113 |
| PDMA-146K | 21.9 ± 0.4 | NA | NA | NA | NA | NA |
| PDMA-213K | 20.8 ± 0.1 | 0.82 | 71.16 | 10.21 | 17.81 | 0.143 |
| PDMA-412K | 18.3 ± 0.6 | NA | NA | NA | NA | NA |
| PDMA-795K | 18.9 ± 1.3 | 0.45 | 71.67 | 10.67 | 17.21 | 0.149 |
| PDMA-996K | 17.7 ± 0.4 | NA | NA | NA | NA | NA |
| [3]Control | 0.7 ± 0.2 | NA | NA | NA | NA | NA |

**Table 2.1 Thickness and composition of binary coatings prepared on silicon wafer generated with different molecular weight PDMAs.**

**1- from ellipsometry measurements; 2- from XPS analysis; 3- The control coating was generated by mixing 2 mg/ml preformed PDA particles with 10 mg/ml PDMA-795K.**

The surface composition showed that the coating became increasingly enriched with PDMA with increasing MW, as indicated by the increased ratio of nitrogen (N 1s)/carbon (C 1s) and C=O/C−OH (**Figure 2.7**).

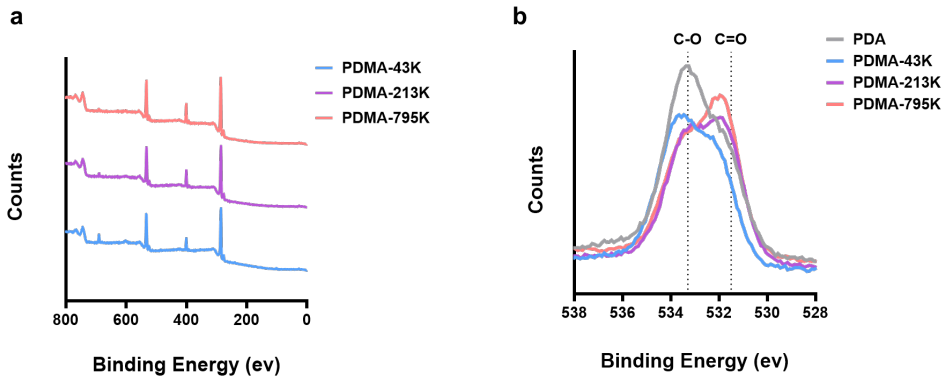


**Figure 2.7 XPS analysis of PDA and PDA/PDMA coatings with different molecular weight.**

**(a) Wide scan of binary PDA/PDMA coatings with different molecular weight PDMAs coated silicon wafers obtained using XPS. (b) Detail O1s scan of PDA, PDMA-43K, PDMA-213K, PDMA-795K coated silicon wafers obtained using XPS. Higher N content and C=O/C-OH ratio were found in the presence of high molecular weight polymer coatings, indicating more PDMA was incorporated.**

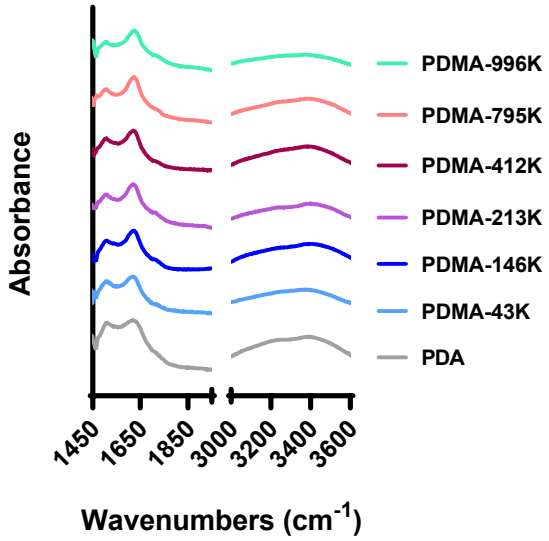


**Figure 2.8 ATR-FTIR spectra of binary PDA/PDMA coatings with different molecular weight PDMAs on PP films.**

**Uncoated PP film was selected as the background. The increased peak at 1623 $cm^{-1}$ of the coating indicates the incorporation of PDMA. The peak intensity increases with increase in molecular weight of PDMA.**

ATR-FTIR spectroscopy analysis supported the findings that uHMW PDMA was incorporated into the coating to a greater extent (**Figure 2.8**). As a consequence of hydrophilic polymer enrichment, the wettability of the surface is greatly improved with the use of uHMW PDMAs compared to the uncoated PP films (**Figure 2.9**).

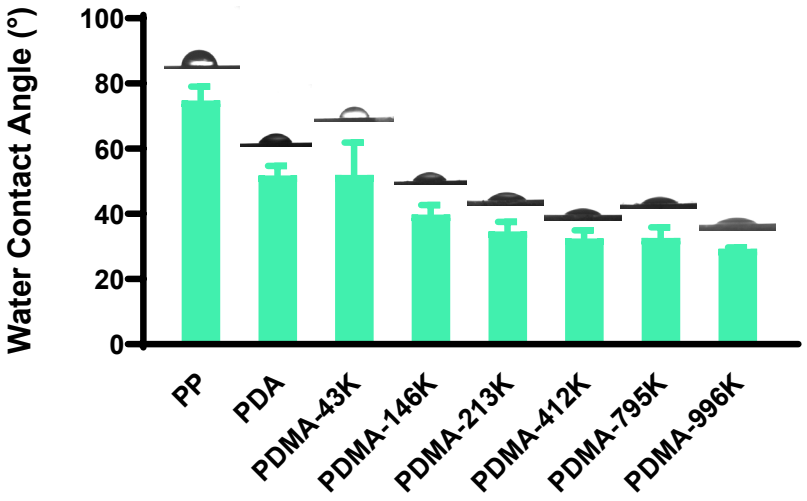


**Figure 2.9 Static water contact angles of binary PDA/PDMA coatings prepared using different molecular weight PDMAs on PP films.**

### 2.3.3 Universality and long-term stability of the coating

Next, we investigated the universality of the coating method and its application to diverse materials used in biomedical devices including titanium, polypropylene (PP), polyurethane (PU), polyethylene (PE), unplasticized polyvinyl chloride (uPVC), plasticized polyvinyl chloride (pPVC), and polyimide (PI). The application of the optimized coating (dopamine: PDMA-795 K (1:5)) was evaluated using static water contact angle measurements (**Figure 2.10a**). Results show that all coated surfaces gave ~30° water contact angle irrespective of the substrate used. We analyzed early stage biofilm formation at 24 h on these diverse substrates modified with the

optimized coating composition and demonstrated the prevention of bacterial adhesion (**Figure 2.10b**).

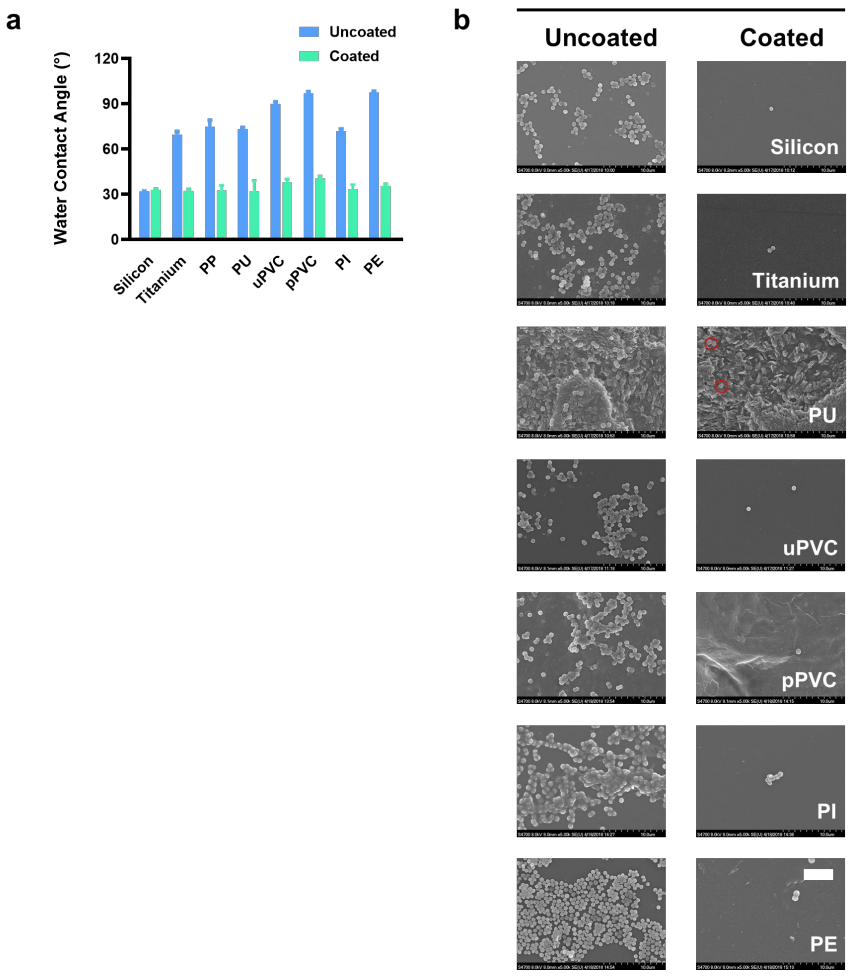


**Figure 2.10 Universality of the binary PDA/PDMA-795K coating.**

**(a) Water contact angles of uncoated and PDA/PDMA-795 K coated substrates. Substrates include silicon, titanium, PP, PU, uPVC, pPVC, PI, and PE. (b) Representative SEM images showing early stage biofilm formation on diverse uncoated and coated substrates after incubating in LB medium with *S. aureus* (initial concentration: $10^6$ cells/mL) for 24 h. Scale bar is 5 µm.**

Using titanium as the base material, we also analyzed the early stage biofilm resistance by multiple bacterial strains. The fluorescent microscopic images show that the optimized

coating is able to prevent early biofilm formation by both Gram-positive and Gram-negative bacterial species including *S. saprophyticus*, *MRSA*, *E. coli*, and *P. aeruginosa* (**Figure 2.11**).

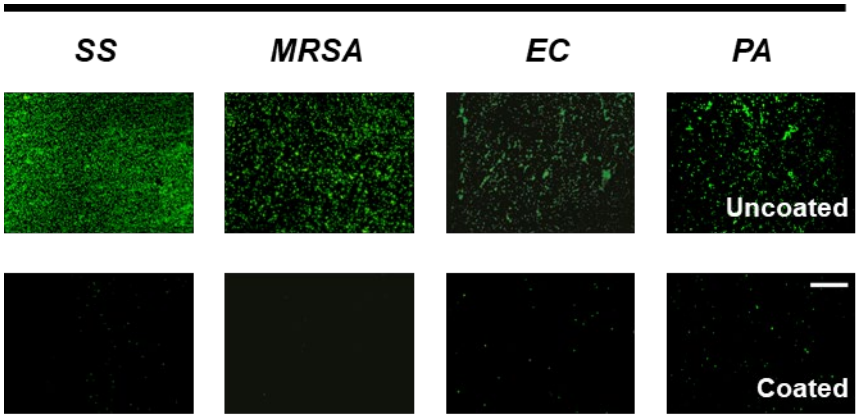


**Figure 2.11 Antibiofilm activity of the binary PDA/PDMA-795K coating against multiple bacterial strains.**

**Representative fluorescence microscopy images of early stage biofilm formation on uncoated and coated $TiO_2$ after incubating in LB medium with *S. saprophyticus* (*SS*), *MRSA*, *E. coli* (*EC*), and *P. aeruginosa* (*PA*) for 24 h (initial concentration: $10^6$ cells/mL). Scale bar is 100 µm. Green fluorescence represents all live bacterial cells attached to the surface visualized using Syto-9 stain.**

Finally, the stability of the coating was investigated by measuring coating thickness after being stored in wet conditions for 3 weeks. No significant difference in coating thickness was noted (**Figure 2.12a**). The optimized coating also showed negligible thickness change after being exposed to 10 min ultrasonication or 30 min autoclaving process (**Figure 2.12a**). Subsequent biofilm studies verified that the coating maintained the antifouling properties following dry and wet storage, ultrasonication, and autoclaving (**Figure 2.12b**).

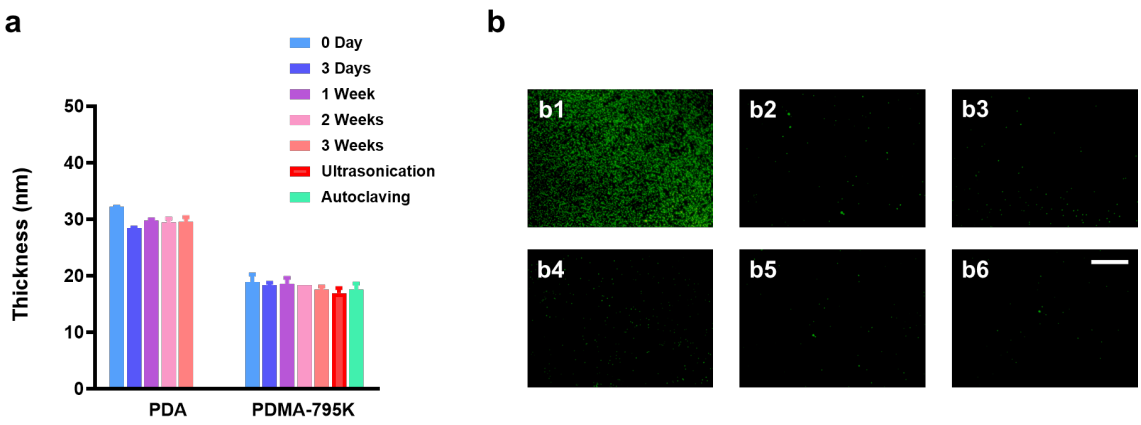


**Figure 2.12 Long-term stability of the binary PDA/PDMA-795K coating.**

**(a) Thickness evaluation of PDA/PDMA-795 K deposited coatings on silicon wafer after 0 day, 3 days, 1 week, 2 weeks, and 3 weeks of incubation in PBS buffer as well as 10 min ultrasonication and 20 min autoclaving process, as determined by ellipsometry. (b) Representative fluorescence microscopy images of early stage *S. aureus* biofilm formation on (b1) uncoated titanium, (b2) fresh PDA/PDMA-795K coated titanium, (b3) PDA/PDMA-795K coated titanium after 2 weeks of storage in air, (b4) PDA/PDMA-795K coated titanium after 2 weeks of storage in PBS buffer, (b5) PDA/PDMA-795K coated titanium after 10 mins ultrasonication in PBS buffer, (b6) PDA/PDMA-795K coated titanium after 30 mins autoclaving at 121°C. The scale bar is 100 µm. These data show that the storage, ultrasonication and autoclaving are not influencing the anti-biofilm activity of the coating.**

### 2.3.4 The antifouling activity and biocompatibility

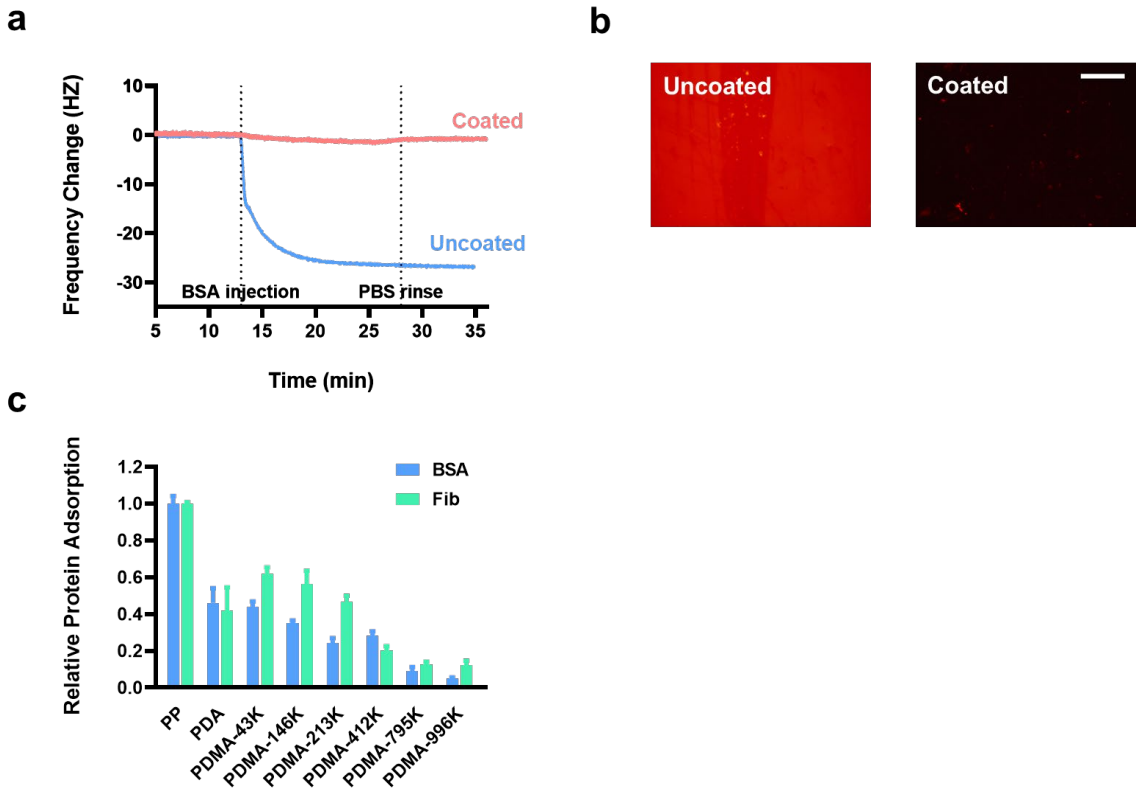


**Figure 2.13 The protein adsorption on the binary PDA/PDMA coatings.**

**(a) QCM-D frequency shift upon the adsorption of BSA on bare gold surface and PDA/PDMA-795 K coated gold surface. After obtaining a stable PBS baseline for 10 min, the BSA solution (50 µg/mL) was injected for 15 min, followed by a 10 min PBS wash. (b) Representative fluorescence images of uncoated and PDA/PDMA-795 K coated PP films after fibrinogen adsorption. Uncoated and coated PP films were incubated with 0.25 mg/mL fibrinogen (Alex Fluor-594 conjugate) for 2 h and washed. Scale bar is 100 µm. (c) Quantification of BSA and Fib adsorption of different PDA/PDMA coatings prepared on PP films using different molecular weight PDMAs. The results show a reduction of 91% for BSA adsorption and 87.5% for Fib adsorption by use of the PDMA-795K.**

One of the key elements driving indwelling device-associated infection and the failure of previously developed coatings is the deposition of a conditioning film on the material surface [182]. Given this, future antifouling coatings need to be able to resist protein and bacterial

deposition on the material surface. To address this important characteristic, we analyzed the deposition of BSA adsorption on the optimized coating using the QCM-D method and by fluorescence microscopy using fluorescently labeled BSA and fibrinogen [173], two of the most commonly found components of urinary conditioning film [183]. Overall, results from QCM-D analysis clearly showed our coating has superior antifouling activity; the amount of adsorbed BSA on the bare QCM chip was calculated to be 563.2 ± 0.1 ng/cm$^2$, while the coated chip resulted in a 17-fold decrease (38.1 ± 0.2 ng/cm$^2$) in BSA adsorption compared to the bare gold chip (**Figure 2.13a**). This superior antifouling activity also translated to polymeric substrates, as coating of unpolished PP films also resulted in a significantly lower levels of BSA and fibrinogen adsorption (91% and 88% decrease respectively) to the uncoated surface (**Figure 2.13b&c**).

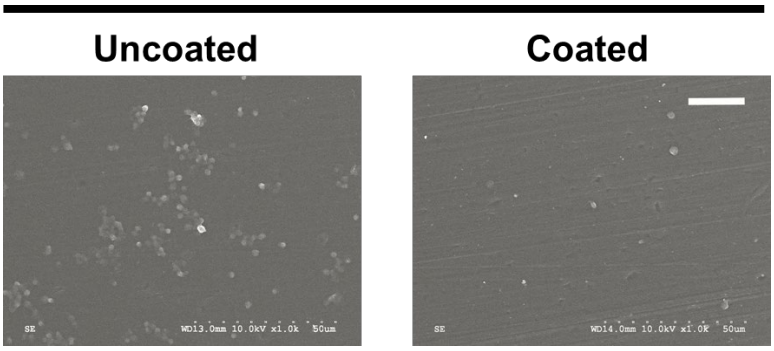


**Figure 2.14 Platelet adhesion on the binary PDA/PDMA-795K coating.**

**Representative SEM images of platelet adhesion on uncoated and PDA/PDMA-795K coated PP films. The samples were incubated with platelet-rich plasma for 4 h before SEM imaging. The scale bar is 20 µm.**

The anti-adhesion activity toward blood platelets was also further demonstrated (**Figure 2.14**), which indicated that the coating might be suitable for blood-containing devices including central venous catheters.

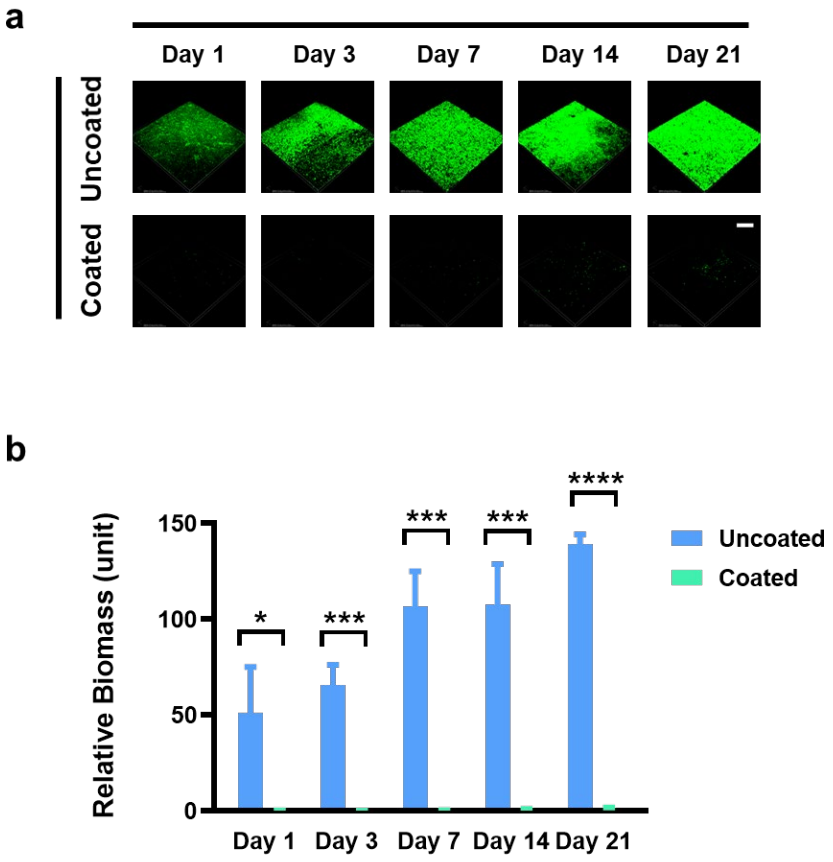


**Figure 2.15 Biofilm formation under shaking condition.**

**(a) Representative confocal fluorescence microscopy images of *S. aureus* biofilm formation on uncoated $TiO_2$ and PDA/PDMA-795K coated $TiO_2$ after 1 day, 3 days, 7 days, 14 days, and 21 days incubation in TSB medium under shaking condition. Scale bar is 200 µm. Green fluorescence represents all bacterial cells attached to the surface visualized using Syto-9 stain. (b) Calculated biomass accumulated on the surface under shaking condition. Statistical analysis: Student's two-tailed unpaired t-test. *: p<0.05; **: p<0.005; ***: p<0.0005; ****: p<0.0001.**

One of the most significant challenges faced by the previously developed surface coating techniques is their ability to resist bacterial biofilm formation over the long-term [116]. Considering that many indwelling devices need to remain biofilm free for long periods of time, being able resist these detrimental bacterial layers from forming is vital. To investigate the ability of our PDA/PDMA-795K coating to resist bacterial biofilm formation, we exposed

uncoated and coated surfaces to high concentration of *S. aureus* (>$10^8$ CFU/mL), a strong biofilm former associated with indwelling device-associated infections, in both shaking and flow conditions over a 3- and 4-week period, respectively. Bacteria were allowed to adhere and colonize the materials for 24 h, after which time the culture was replenished daily to allow for efficient biofilm conditions. The level of biofilm formation was visualized over time using confocal and SEM microscopy. Using these analyses, we found biofilm formation to be reduced >99% on the ~19 nm-thick PDA/PDMA-795K coated surfaces after 3 weeks of growth (**Figure 2.15**).

Similarly, using a flow model developed in our laboratory (**Appendix A3**), we observed a very low number of single bacteria on the coated samples compared to the uncoated controls at the end of the 4-week incubation period, corresponding to a > 97% reduction in bacterial biomass (**Figure 2.16a&b**). SEM analysis confirmed that the coated substrate resisted biofilm formation on the surface unlike the uncoated substrate which showed the development of microcolonies encased in EPS matrix on day 14 and a more mature biofilm by day 28 (**Figure 2.16c**).

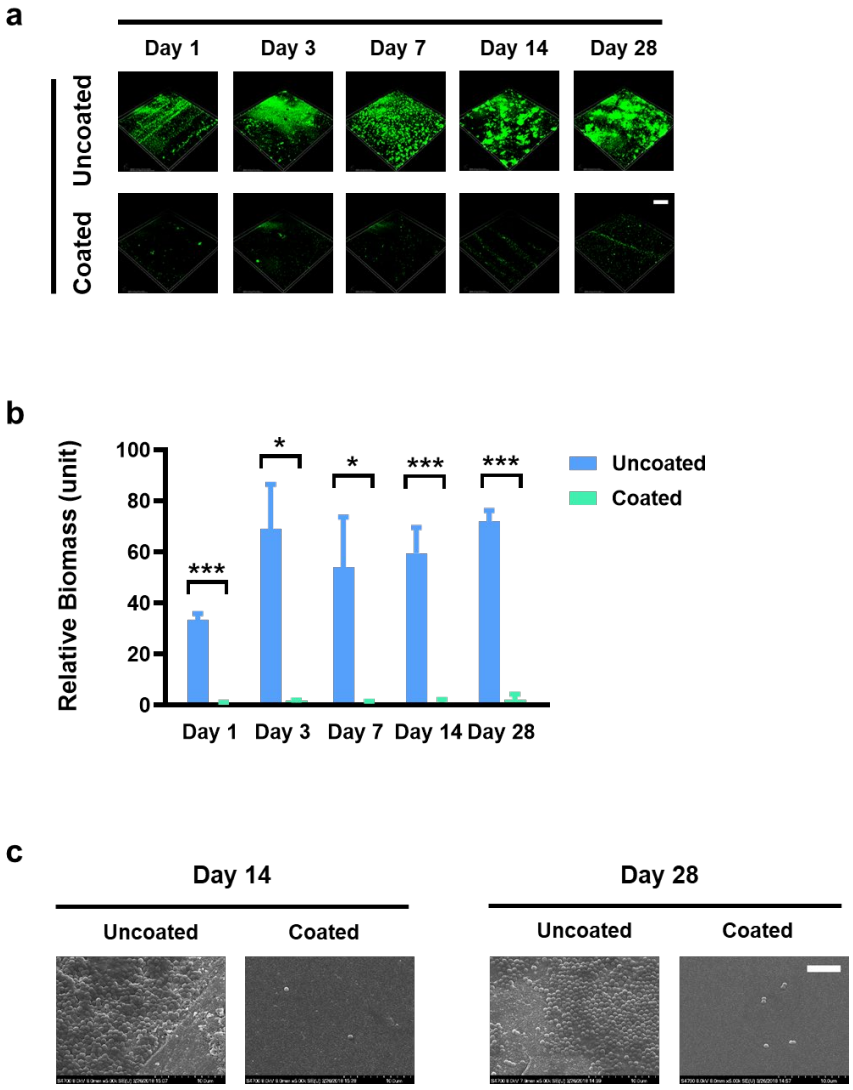


**Figure 2.16 Biofilm formation under flow condition.**

**(a) Representative confocal fluorescence microscopy images of *S. aureus* biofilm formation on uncoated $TiO^2$ and PDA/PDMA-795 K coated $TiO_2$ after 1 day, 3 days, 7 days, 14 days, and 28 days incubation in LB medium under flow condition. Scale bar is 200 µm. (b) Calculated biomass accumulated on the surface under flow condition. (c) Representative SEM images of *S. aureus* biofilm formation on uncoated $TiO_2$ and PDA/PDMA-795 K coated TiO2 after 14 days and 28 days incubation in LB medium under flow condition. Scale bar is 5 µm. Statistical analysis: Student's two-tailed unpaired t-test. *: p<0.05; **: p<0.005; ***: p<0.0005; ****: p<0.0001.**

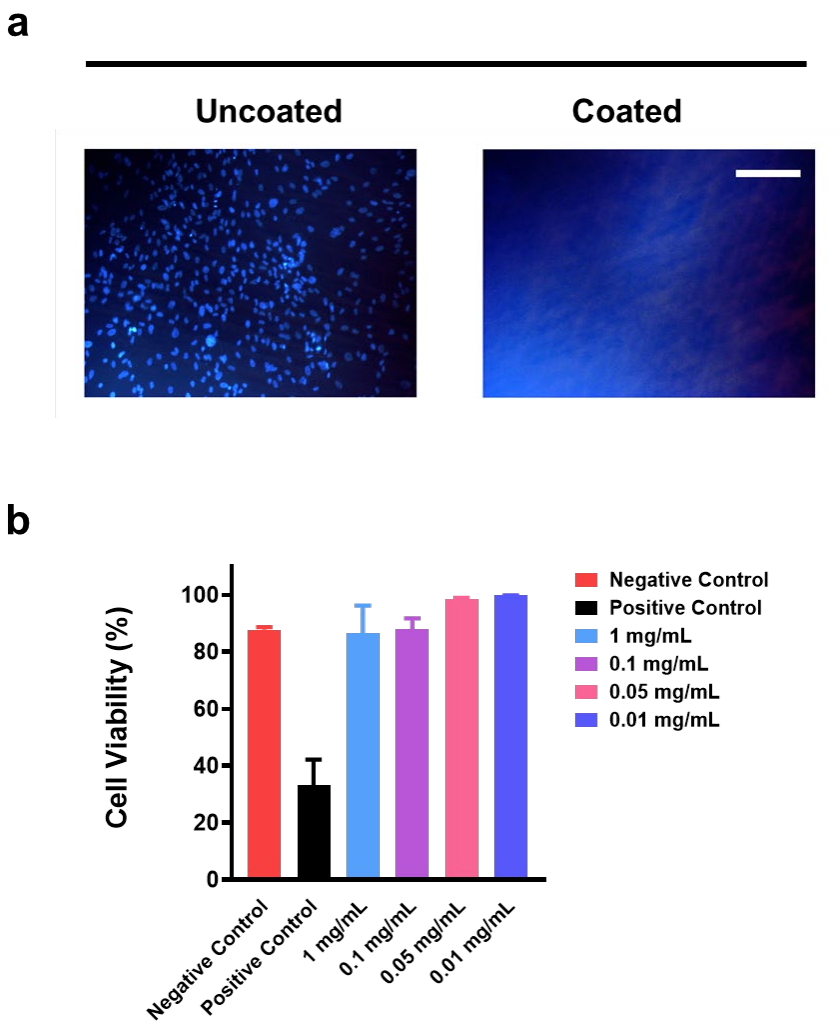


**Figure 2.17 Biocompatibility of the binary PDA/PDMA-795K coating.**

**(a) Representative fluorescence microscopy images of fibroblast adhesion on uncoated and PDA/PDMA-795K coated PS tissue culture chambers. The samples were incubated with fibroblasts for 48 h before imaging. Nuclear stain DAPI was used to visualize the cells on the surface. The scale bar is 200 µm. (b) Cell viability of fibroblasts in the presence of PDA/PDMA-795K solutions at difference concentrations. 2 mg/ml dopamine and 10 mg/ml PDMA-795K were mixed for 24 h and diluted to the desired concentrations for cell viability studies. The culture media group was set as a negative control and the DMSO group was set as a positive control.**

The interaction between the coating and mammalian cells (fibroblasts) was further evaluated to determine the safety of the coating. The cells were spread nicely on the uncoated PS

surface after 48 h of incubation, however, almost no cells were adhered on the PDA/PDMA-795K coated PS substrate (**Figure 2.17a**). Furthermore, the cell viability studies did not show any toxicity toward PDA/PDMA-795 K solution even at considerably high concentration (1 mg/mL); all solutions showed cell viability in the range of 86-99% (**Figure 2.17b**).

### 2.3.5 Application of the binary coating on indwelling catheters

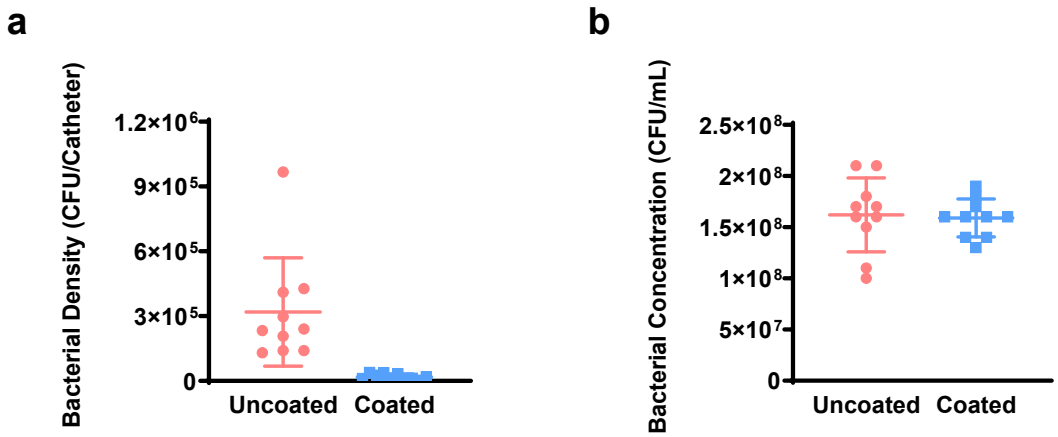


**Figure 2.18 Antibiofilm activity of PDA/PDMA-795K coated PU catheter in LB medium.**

**(a) Reduction of bacterial adhesion on catheter surface of *S. aureus* on PDA/PDMA-795K coated catheter surface. (b) Reduction of planktonic growth of S. aureus in PDA/PDMA-795K coated catheter involved medium. 1 mL bacterial culture with initial count of $5*10^4$ CFU/mL was added to each sample in Eppendorf tubes and incubated at 37 °C at 50 rpm for 6 h. The adhered bacteria were then detached from the catheter by sonication and spot plated for CFU counts. The concentration of planktonic growth of bacteria was measured by CFUs as well.**

The antibiofilm activity of coated catheter surfaces was tested in LB medium against Gram-positive bacteria *S. aureus*. Uncoated and PDA/PDMA-795K coated catheter surfaces were tested by assessing the number of adhered bacteria on catheter surface and planktonic bacteria in LB medium following 6 h of incubation. **Figure 2.18a** shows the adhesion of *S.*

*aureus* on differently coated surfaces, while **Figure 2.18b** shows the number of planktonic bacteria left in solution. These results demonstrated that the binary PDA/PDMA coating was able to reduce the adhesion of *S. aureus* by about 94.2%, compared to the uncoated catheter, while the reduction in planktonic growth of *S. aureus* was not observed in the case of PDA/PDMA coating.

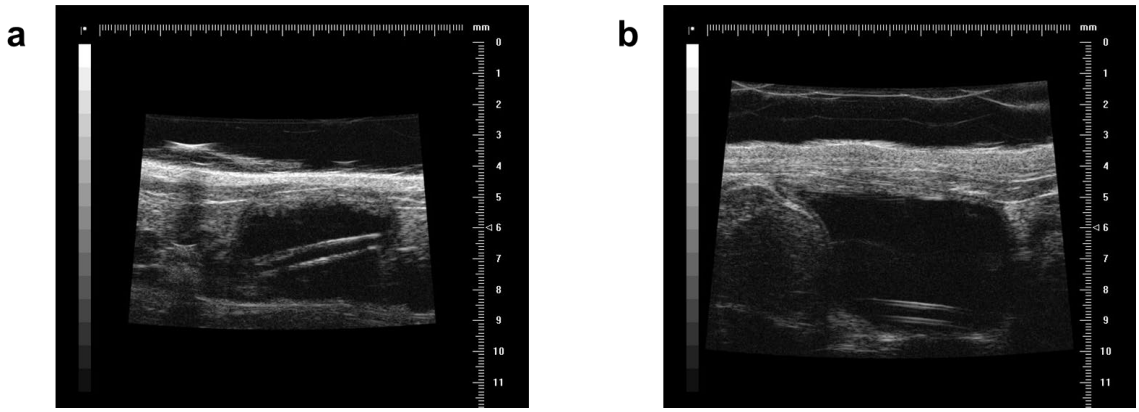


**Figure 2.19 Successful catheterization of PU catheter pieces.**

**Ultrasound images of bladders of mice with (a) uncoated implant pieces and (b) PDA/PDMA-795K coated implant pieces at 7 days post-bacterial instillation.**

To show efficacy of the PDA/PDMA-795K coating *in vivo*, we utilized an ultrasound-guided percutaneous model of CAUTI developed in Lange's group. This model has proven to be very efficient with a 100% catheter implantation rate and retention of catheters [184]. Given that we have observed a consistent antibiofilm activity towards *S. aureus* in different tests, we opted to test our novel coating against this pathogen. PU implants of 24 Gauge and 4mm in length were successfully catheterized *via* ultrasound-guided percutaneous implantation for a total of 20 mice (**Figure 2.19**).

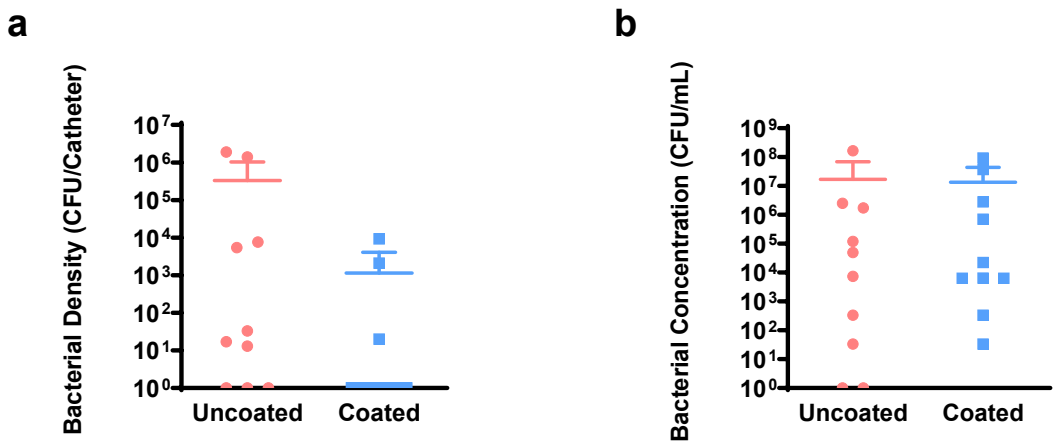


**Figure 2.20 Antibiofilm activity of PDA/PDMA-795K coated PU catheter *in vivo* in urinary infection model.**

**Number of survived *S. aureus* recovered from the PU catheter surface (a) and in the urine (b) after 7 days in the mice percutaneous model. N=10 for the uncoated catheter and N=10 for the coated catheter.**

In terms of bacterial growth in the urine on day 7, the average CFU counts for mice bearing untreated control catheters was $1.7*10^7$ CFU/mL while those implanted with catheters bearing PDA/PDMA-795K was $1.3*10^7$ CFU/mL indicating no reduction in the number of planktonic bacteria in the bladders of animals from the two different groups (**Figure 2.20**). The reduction in bacterial numbers on the catheter sample was confirmed by CFU counts on day 7. Specifically, the number of adherent bacteria on uncoated control catheters was $3.3*10^5$ CFU/catheter, whereas that for catheters coated with the PDA/PDMA-795K was $1.1*10^3$ CFU/catheter, demonstrating a greater than 2-log decrease in bacterial adherence on coated catheters. Although the reduction rate of the coated catheters was high, the bacterial adhesion on uncoated catheters and coated did not show a significant difference (P=0.12). This is due to the fact that *S. aureus* may not be an ideal candidate for the CAUTI model, bacterial adhesion was even not observed on some of the uncoated catheters. Since the submission of the thesis, members of our research group further experimented the antibiofilm activity of these coating

using different bacterial strains. Towards this, a reliable model of CAUTI with different bacterial strains were developed and the antibiofilm activity of the PDA/PDMA-795K coating was investigated. Our results show that PDA/PDMA-795K coating significantly reduced biofilm formation in mouse infection models. Currently these results are in preparation for publication.

## 2.4 Conclusions

We developed a novel ultrathin coating with long-term antibiofilm activity based on mussel-inspired surface chemistry. We utilized the interaction between catecholamine and uHMW hydrophilic polymers to generate stable coatings with broad spectrum antibiofilm activity. We used bacterial adhesion assays as an initial screening method to identify coating compositions that give superior performance and found that only selected polymers, catecholamine and molecular weights gave promising antifouling activity. The optimized 19 nm coating demonstrated excellent antifouling and antibiofilm properties (>4 weeks) against diverse bacteria ($\sim 10^8$ CFU/mL) in shaking and flow conditions. The ultrathin coating is effective on diverse substrates including metals and polymeric substrates. The coating was successfully adapted to commercial catheters and demonstrated efficacy both *in vitro* and *in vivo*.

# Chapter 3: The mechanism of the binary coating formation

In Chapter 2, we developed a novel binary antibiofilm coating and demonstrated its application to diverse materials, stability, biocompatibility, *in vitro* and *in vivo* antibiofilm activity. In Chapter 3, we started with investigation of the binary coating structure, and then studied how molecular weight and chemistry of the hydrophilic polymer as well as the type of catecholamine affect the coating structure.

## 3.1 Introduction

Surface modification is one of the focused areas in developing advanced materials for diverse applications including biomedical devices, automobile parts, smart fabrics, computer chips, storage containers for cells and biological fluids, and infection resistant surfaces [42, 144, 185-188]. Since the first report by Messersmith's group in 2007, mussel-inspired chemistry has opened an advanced strategy for surface modification [85, 189-190]. Modifications with PDA and PNE have been reported as material-independent surface functionalization strategies to form adherent films on virtually any material surfaces [92-93, 191-192].

There have been significant developments on the use of this technology for both material designs and biomedical applications [89, 90, 193-194]. Attempts are made to improve the properties surface coatings prepared by this material-independent strategy by incorporating various small molecules, synthetic polymers and biomacromolecules utilizing both covalent and non-covalent pathways [95-96]. For instance, in 2012, Lee's group first reported a one-step surface functionalization method by immersing diverse substrates into a solution of dopamine with other interested molecules including polymerization initiators, antibacterial agents, tertiary amines, growth factors and polysaccharides [94]. They believed that the interested molecules

were incorporated into the PDA coating *via* the covalent pathway. In 2014, Stadler's group investigated the interactions of several uncharged polymers with PDA during the coating assembly, in which the non-covalent pathway plays a decisive role [99]. The authors showed that polymers can be co-deposited onto the silicon wafer with PDA *via* the non-covalent interactions and the physical entrapments. Since then the dopamine-assisted co-deposition strategy has received more attention as a facile method to generate functional surfaces for diverse applications [120-122, 174-175, 195-197]. Although significant advances occurred on this versatile method of surface modification, in general, the mechanisms behind the co-assembly and co-deposition process of PDA with other molecules are still unclear and more investigations are needed. Such understanding will enhance our ability to design novel surfaces for both material and biomedical applications.

In this chapter, we systematically investigated the co-assembly of catecholamines with different hydrophilic polymers to understand the mechanism of the co-assembly to generate anti-adhesive surfaces using various surface analytical techniques. We paid attention on how the molecular weight and chemistry of the hydrophilic polymers as well as the catecholamine type affect their co-assembly in solution and subsequent deposition on the surface to form an efficient surface coating. The physicochemical properties of the nanoparticles formed by the co-assembly of catecholamines and hydrophilic polymers, its aggregation kinetics, stabilization, interfacial properties of the binary coating, and the performance of the coating as an anti-adhesive layer are investigated.

## 3.2 Materials and methods

### 3.2.1 Materials

Reagents were purchased from Sigma-Aldrich and used as received unless otherwise noted. Water was purified using a Milli-Q Plus water purification system (Milipore Corp., Bedford, MA) and used in all experiments. Monomers including *N*,*N*-dimethylacrylamide (DMA, 99%), 2-((methacryloyl)-oxy)ethyl phosphorylcholine (MPC, 97%), glycidol and polymers including polyethylene oxide (PEO, Mv=1,000,000), polyvinylpyrrolidone (PVP, Mw=1,300,000), poly(2-ethyl-2-oxazoline) (PEOX Mw=500,000) were purchased from Sigma-Aldrich. DMA and glycidol was purified by vacuum distillation and stored in a refrigerator at 4 °C before use. The single-side-polished silicon wafers were bought from University Wafer (Boston, MA). Polypropylene (PP) sheet with a thickness of 0.3 mm was purchased from Professional Plastics (CA, USA).

### 3.2.2 Polymer synthesis

The ultra-high molecular weight (uHMW) PDMA and PMPC were synthesized by aqueous ATRP. In a typical experiment, copper (II) chloride ($CuCl_2$, 2 mg), copper (I) chloride (CuCl, 15.9 mg), and 1, 1, 4, 7, 10, 10-hexamethyl triethylene tetramine (HMTETA, 96.2 μL) were added successively into a glass tube, followed by the addition of 20 mL of Milli-Q water. The solution was degassed with three freeze-pump-thaw cycles and then transferred into the glovebox. The catalyst solution (20 mL) was thoroughly mixed before the addition of monomers (2 g). The amount of methyl 2-chloropropionate in methanol added to the reaction mixture was controlled to change the molecular weight of the polymers, and the polymerization could proceed at room temperature (22 °C) for 24 h. The soluble polymer was finally collected by dialysis

(molecular weight cut-off: 1000) against water for 1 week. The ultra-high molecular weight HPG was synthesized according to our previous protocol.

### 3.2.3 Gel permeation chromatography

The molecular weight and polydispersity index (PDI) of the synthetic polymers were determined by gel permeation chromatography (GPC) on a Waters 2690 separation module fitted with a DAWN EOS multiangle laser light scattering detector from Wyatt Technology Corp. with 18 detectors placed at different angles and a refractive index detector (Optilab DSP from Wyatt Technology Corp.). An Ultrahydrogel linear column with a bead size of 6-13 μm (elution range $10^3$ to $5\times10^6$ Da) and an Ultrahydrogel 120 with a bead size of 6 μm (elution range 150 to $5\times10^3$ Da) from Waters were used. The dn/dc values of high molecular weight polymers in the mobile phase was determined at $\lambda = 620$ nm and was calculated to be 0.15 for the PDMA and 0.12 for the PMPC. The number average mean square radius moments were taken as the radius of gyration of the polymer. The detailed information about high molecular weight polymers was provided in **Appendix B1**.

### 3.2.4 Coating process

Silicon wafer pieces were exposed to oxygen plasma for 2 min to remove adventitious contamination. PP films were cleaned by ultrasonication in deionized water for 10 min and dried under a steam of nitrogen. For a typical coating preparation process, a mixture of 2 mg/mL catecholamine and 10 mg/mL polymer was prepared in 10 mM Tris-HCl buffer (pH= 8.5) [85]. The substrates were then immersed in either catecholamine alone or catecholamine-polymer solution and were kept for 24 h without stirring. Afterward, the modified samples were rinsed with Tris-HCl buffer and deionized water and dried in a steam of nitrogen. The modified substrates were used for further characterization.

### 3.2.5 Dynamic light scattering and zeta potential

Dynamic light scattering (DLS) and zeta potential measurements of the final solutions containing either polycatecholamine alone or polymer alone or binary components were performed using a Zetasizer NanoZS instrument (Malvern Instruments, UK) at the end the reaction. The final solution was diluted 75-fold using tris buffer for measuring the particle size and zeta potential. The measurements were performed with an equilibration time of 1 min at room temperature. Each measurement was repeated for three times, and the average value was accepted as the final hydrodynamic size or zeta potential.

### 3.2.6 Transmission electron microscopy

Samples of the final binary components were prepared for transmission electron microscopy (TEM) by adsorbing 4 μL of the undiluted mixture onto a carbon film mounted on 300 mesh copper grids. The specimen was applied as a droplet to the grid and left for 5 min of incubation on the surface to aid adsorption. The grid was blotted and left to air dry. Negative staining agent uranyl acetate was applied on all the samples. The formed binary nanoparticles were either viewed on a Hitachi H7600 PC-TEM (Hitachi) at an accelerating voltage of 80 kV or viewed on a FEI Tecnai G2 200 kV. The images were either recorded with an AMT XR50 CCD camera or recorded with a high-resolution FEI Eagle 4K bottom mount CCD camera.

### 3.2.7 UV-Vis spectroscopy

The dopamine concentration was kept 2 mg/mL for the initial mixing and was diluted 40-fold before the measurement of ultraviolet-visible (UV-Vis) spectrum. The UV-Vis spectra were recorded at room temperature in a Varian Cary 4000 spectrophotometer at the wavelengths from 200 to 800 nm using a 1 cm path length quartz cell.

### 3.2.8 Ellipsometry analysis

The variable-angle spectroscopic ellipsometry (VASE) spectra were collected on an M-2000 V spectroscopic ellipsometer (J.A. Woollam, Lincoln, NE) at 50°, 60°, and 70° at wavelengths from 480 to 700 nm with an M-2000 50W quartz tungsten halogen light source. The VASE spectra were then fitted with a multilayer model utilizing WVASE32 analysis software based on the optical properties of a generalized Cauchy layer to obtain the dry thickness of the deposited layers. Silicon wafer was used as the substrate.

### 3.2.9 Attenuated total reflectance Fourier transform infrared analysis

Attenuated total reflectance Fourier transform infrared (ATR-FTIR) spectra were recorded using a Thermo-Nicolet Nexus FTIR spectrometer (Nicolet Instrument, Waltham, MA) with an MCT/A liquid nitrogen cooled detector, KBr beam splitter and MKII Golden Gate Single Refection ATR accessory (Specac Inc. Woodstock, GA). Spectra were recorded at 4 $cm^{-1}$ resolution and 64 scans were collected for each sample. PP films were used as the substrate and the atmosphere was used for background collection.

### 3.2.10 X-ray photoelectron spectroscopy analysis

X-ray photoelectron spectroscopy (XPS) was performed using a Leybold LH Max 200 surface analysis system (Leybold, Cologne, Germany) equipped with a Mg Kα source at a power of 200 W. Elements were identified from survey spectra. High-resolution spectra were collected at 48 eV pass energy. Silicon wafer was used as the substrate for sample preparation.

### 3.2.11 Water contact angle measurements

For water contact angle (WCA) measurements, digital images of a 10 µL water droplet on the surface were taken using a digital camera (Retiga 1300, Q-imaging Co.), and analyzed using Northern Eclipse software. Six different spots on the uncoated and

polycatecholamine/uHMW polymer coated PP films were tested for each sample and the average value was reported.

### 3.2.12 Scanning electron microscopy analysis

The surface morphology of the coatings on silicon wafer was investigated by scanning electron microscopy (SEM) using a Hitachi S-4700 field emission scanning electron microscope. The samples were dried under high vacuum and coated with a 1 nm gold layer by using a sputter coater.

### 3.2.13 Atomic force microscopy

Atomic force microscopy (AFM) measurements were performed on a commercially available multimode system with an atomic head of 130×130 $\mu m^2$ scan range which used a NanoScope IIIa controller (Digital Instruments, Santa Barbara, CA). Surface morphology was examined under PBS buffer in contact mode using a commercially manufactured V-shaped silicon nitride ($Si_3N_4$) cantilever with gold on the back for laser beam reflection (Veeco, NP-S20). The spring constant of the AFM cantilever was measured using the thermal equipartition theorem. Force measurements were performed in PBS buffer. On tip approach, the onset of the region of constant compliance was used to determine the zero distance. On retraction, the region in which force was unchanged was used to determine the zero force. The rate of tip-sample approach or retraction was typically 1 μm/s. The raw AFM force data were converted into force *vs.* separation using custom Matlab v.5.3 software. The software converts the cantilever deflection *vs.* linear voltage displacement transformer signal into restoring force *vs.* tip substrate separation using user input trigger and spring constant values. We followed our previously published protocols for the calculation of the adhesive force and rupture distance. Silicon wafer was used as the substrate for testing.

### 3.2.14 Surface zeta potential measurements

The surface zeta potential of different coatings on PP films was determined with a Malvern surface zeta potential cell ZEN1020. The cell consists of a height-adjustable sample barrel in which the sample is placed on a sample holder and is held between two palladium electrodes. A series of zeta potential measurements were performed in a conventional cuvette and the measurement position within the cell was controlled by adjusting the height of the sample barrel. The final surface zeta potential was then calculated.

## 3.3 Results and discussion

### 3.3.1 Mechanism of the binary PDA/PDMA-795K coating formation

We initially performed investigations to understand the mechanism behind the optimized PDA/PDMA coating formation. Specifically, we were interested in determining how uHMW PDMA interacts with PDA in the solution, how uHMW PDMA is incorporated into the coating (described in Chapter 2), as well as the possible structure of the binary coating that provides long-term antifouling properties. To probe these facts, we initially investigated the particle formation in solution using DLS and TEM measurements. The hydrodynamic size of the PDA particles without the PDMA was several micrometers as determined by DLS (**Figure 3.1a**). The aggregation of PDA particles following dopamine oxidation is prevented in presence of PDMA, as evidenced by the smaller size of PDA particles formed under this condition. The hydrodynamic size of the PDA particles decreased to a few hundred nanometers in the presence of uHMW PDMA. The TEM studies showed that PDA particles formed in the presence of PDMA-795K are evenly dispersed nanoparticles compared to the highly aggregated particles formed in the case of PDA alone (**Figure 3.5a**) [198-200]. Furthermore, TEM analysis showed the formation of core-shell particles containing a dense PDA-core surrounded by a light shell

layer of PDMA chains (**Figure 3.1b**) [201-202]. As suggested by previous reports, supramolecular interactions between PDA and PDMA might be contributing to the formation of the uniform dispersed particles [99, 195, 203-204]. The PDMA incorporated into PDA particles via hydrogen bonding and formed a core-shell structure with PDMA shell and PDA core. In addition, it appears that the generated core-shell nanoparticle contains multiple nanoaggregates.

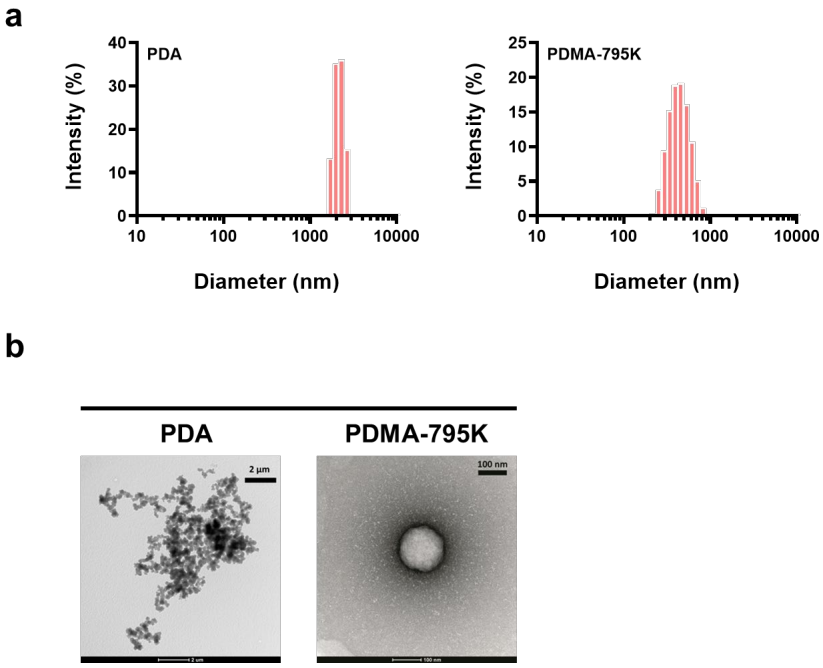


**Figure 3.1 Nanoparticle particle formation in solution.**

**(a) Hydrodynamic size distribution of particles formed in a Tris-HCl buffered solution of PDA alone and PDA/PDMA-795 K. (b) Representative TEM images of particles assembled using PDA alone and PDA/PDMA-795 K.**

To investigate the coating morphology, we used high-resolution SEM analysis. Our analyses of the PDA and PDA/PDMA coating by SEM point to the following process in the formation of the binary coating. In the case of PDA alone coating, we observed a two-layer coating: the top layer contains PDA nanoparticles about 100-200 nm in size, while the bottom

layer contains much smaller PDA nanoaggregates (**Figure 3.2a**) demonstrating a rough morphology. The coating became very uniform with low surface roughness in the presence of uHMW PDMA; the deposited layer only contains ultra-small nanoaggregates as revealed by SEM micrographs obtained at high resolution. AFM imaging also confirms similar surface structures in wet conditions (**Figure 3.2b**).

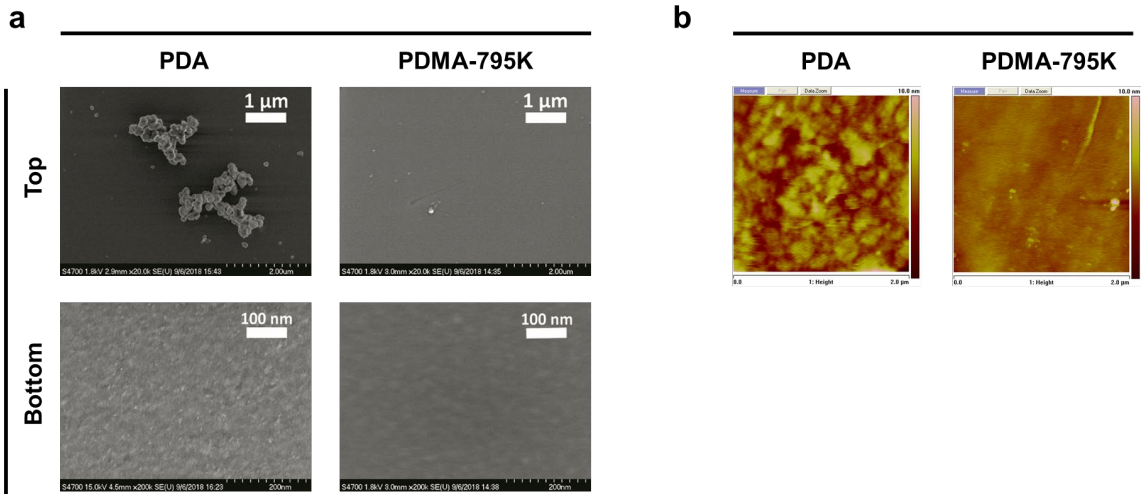


**Figure 3.2 Particle deposition on surface.**

**(a) Representative SEM images of deposited coating using PDA alone and PDA/PDMA-795 K. (b) Surface morphology of PDA coated silicon wafer, and PDA/PDMA-795K coated silicon wafer determined by AFM in wet conditions. The scan size is 2 µm × 2 µm.**

The PDA chemistry is still evolving and is under very active investigation. The most recent findings suggest that dopamine initially generates oligomers *via* oxidation and then forms PDA particles *via* a progressive self-assembly process [205-206]. Based on this information and our current data, we propose a mechanism for the formation of thin coating in PDA alone and binary coating composed of PDA and uHMW PDMA (**Figure 3.3**). We believe that the nanoscale coating formed on the substrate in our experimental conditions is during the dynamic

assembly process in PDA polymerization. Our data from an experiment where we added PDMA-795K after the formation of PDA particles failed to generate a coating with sufficient thickness supports this argument (**Table 2.1**). The dopamine initially forms oligomers after oxidation *via* a covalent pathway, and the presence of uHMW PDMA does not affect this process. In the next stage, the monomeric species and small oligomers initialize the surface anchoring along with the assembly in solution in an orderly manner to form nanoaggregates (about 2-20 nm). We suspect that this process might be influenced by the presence of uHMW PDMA. In the absence of PDMA, PDA nanoaggregates deposit onto the surface to form a tightly adhered bottom PDA layer and concurrently assemble in solution to form large PDA particles (about 100-200 nm in our system). The large PDA particles further deposit onto the surface to form a top layer with rough structures. The process of aggregation is uncontrolled in solution and forms ultralarge PDA aggregates (1000-10000 nm). However, in the presence of uHMW PDMA, the PDA nanoaggregates deposit onto the surface together with PDMA which further reorganize and form a stable layer on the surface. The PDA/PDMA nanoaggregates continue the self-assembly process in aqueous solution, resulting in nanoparticles with a core-shell structure (about 100 nm in the optimized system). The PDMA shell layer prevents the particles from further deposition and growth of a rough layer. The PDMA shell layer also prevents further aggregation of the PDA particles. Rearrangement of PDMA chains within the coating occurs during the surface bonding process, resulting in overall enrichment of PDMA on the surface due to high hydrophilicity of PDMA compared to PDA. The evidence here reveals that the uHMW PDMA is not simply incorporated into the coating, but its presence dramatically changed the self-assembly process of the PDA and facilitates the formation of a uniform layer with PDMA.

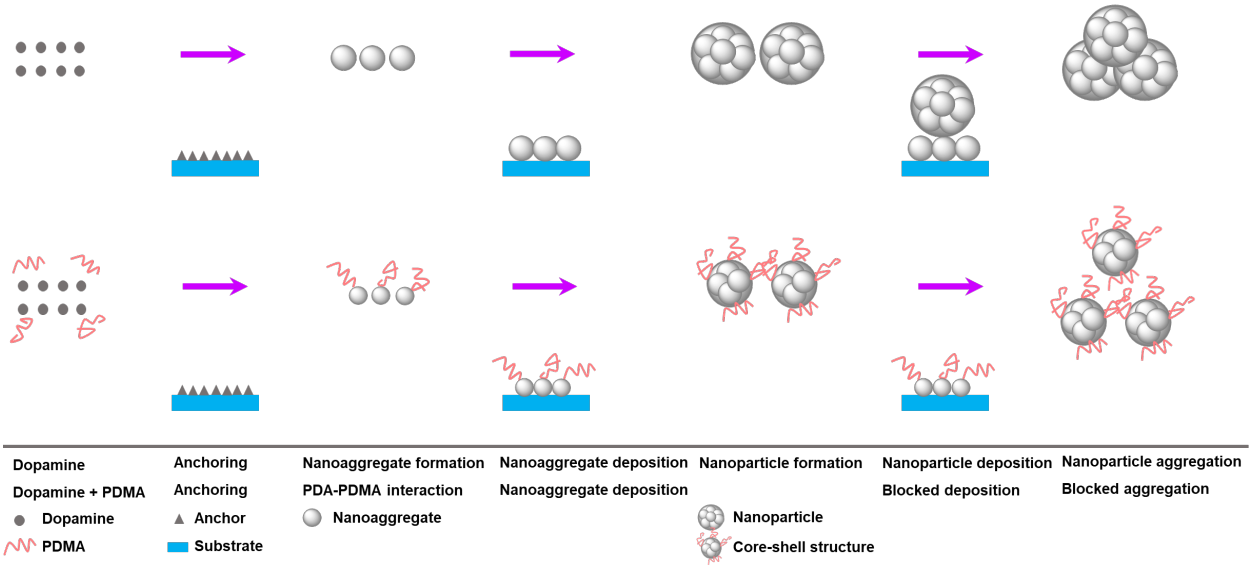


**Figure 3.3 Schematic illustration of possible mechanism of PDA alone and binary coating formation.**

### 3.3.2 Influence of molecular weight on the binary coating formation

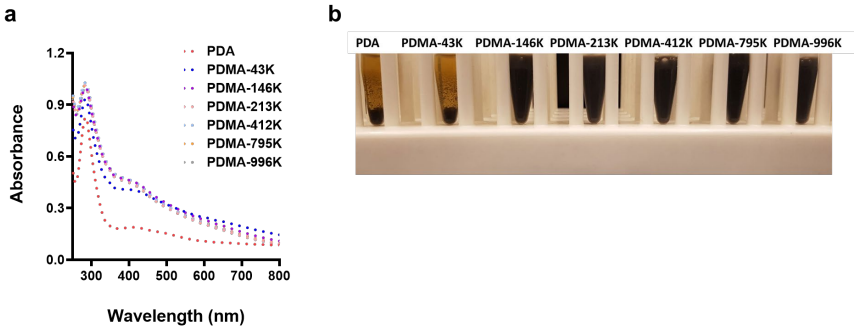


**Figure 3.4 Influence of molecular weight on the amount of PDA particle formation.**

**(a) UV spectra of particles formed in a Tris buffered solution of dopamine and different molecular weight PDMAs. (b) Photographs of dopamine, dopamine/PDMA-43K, dopamine/PDMA-146K, dopamine/PDMA-213K, dopamine/PDMA-412, dopamine/PDMA-795K and dopamine/PDMA-996K solution after 24 h reaction. As noted, dopamine and dopamine/PDMA-43K solution precipitated during the storage suggesting the poor suspension stability.**

The results shown in Chapter 2 demonstrate that molecular weight of PDMA plays a critical role on the coating's antibiofilm activity. Thus, we investigated the formation of PDA

particles in the presence of different molecular weight PDMAs. The amount of PDA generated in the presence of PDMA is increased, as evident from the increase in spectral intensity between 300 and 800 nm in the UV-vis spectra (**Figure 3.4a**) [89, 207]. This may be explained by the fact that dopamine alone generates PDA precipitates within several hours, which blocks further polymerization and aggregation (**Figure 3.4b**).

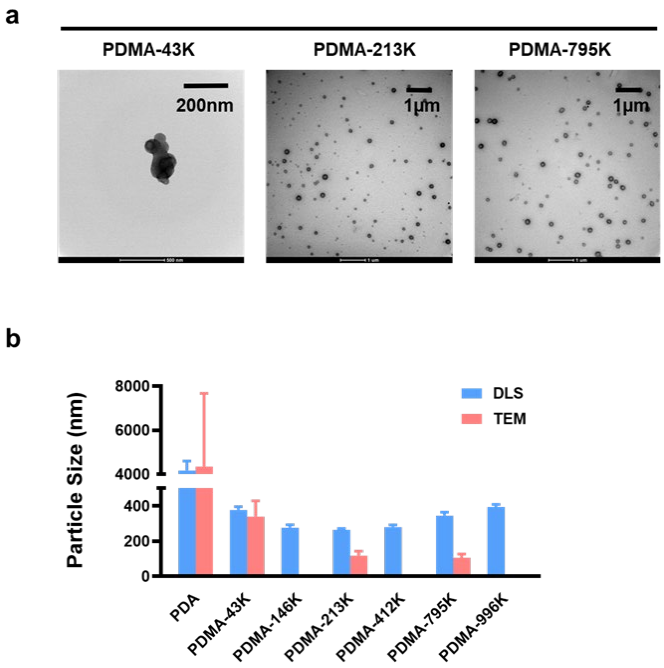


**Figure 3.5 Influence of molecular weight on the formed particle size.**

**(a) Representative TEM images of nanoparticles assembled using dopamine with different molecular weight PDMAs. (b) hydrodynamic size and dry size of particles formed in a Tris buffered solution of dopamine and different molecular weight PDMAs.**

The DLS and TEM analyses (**Figure 3.5**) further proved that PDA particle aggregation was not completely blocked by using polymers with molecular weights around 43 kDa. This resulted in the formation of large PDA aggregates in the coating prepared in the presence of

PDMA-43K (**Figure 3.6**). Only uHMW PDMAs can prevent the aggregation and control the PDA self-assembly process, resulting in a much thinner and smoother antibiofilm coating.

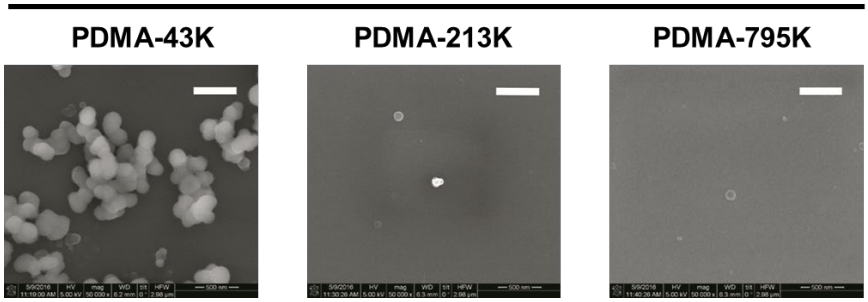


**Figure 3.6 Influence of molecular weight on surface morphology.**

**Representative SEM images of the deposited coatings using dopamine with different molecular weight PDMAs on silicon wafers. The scale bar is 500 nm.**

To probe this further, we utilized AFM force measurements to determine the surface structure of the binary PDA/PDMA coating in wet conditions (**Figure 3.7**). AFM approach curves showed a typical approach profile for steric repulsion exerted by polymer chains grafted on the surface (**Figure 3.7a**); remanence of a brush layer [208-209]. The equilibrium thickness of the coating increased with increasing MW of PDMA: reaching 25 nm, 45 nm, and 90 nm, respectively, for PDMA-43K, PDMA-213K, PDMA-795K. The AFM retraction curve gave a characteristic profile of looplike assembly of PDMA chains on the surface, and the adhesive force was found to decrease with increasing molecular weight of PDMA (**Figure 3.7b**). Further, the extension length increased with increasing molecular weight of PDMA (**Figure 3.7c**). Together these data support the hypothesis that the rearrangement of PDMA chains within the coating is occurring during the surface bonding process, resulting in overall enrichment of PDMA on the surface. Since PDMA is not covalently bound to PDA, the chains could rearrange to generate its optimal conformation. The increased content of PDMA chains on the surface of

the coating generated the desired antifouling property. We have previously shown that PDMA is an excellent candidate to generate nonfouling surfaces [210-212]. The PDA self-assembly in water and concurrent surface deposition depend on the molecular weight of PDMA. uHMW PDMA is crucial to generate looplike assembly of hydrophilic chains to avoid fouling on the surface, and polymers without uHMW (e.g., PDMA-43K) lack this property resulting in the generation a poor antifouling surface.

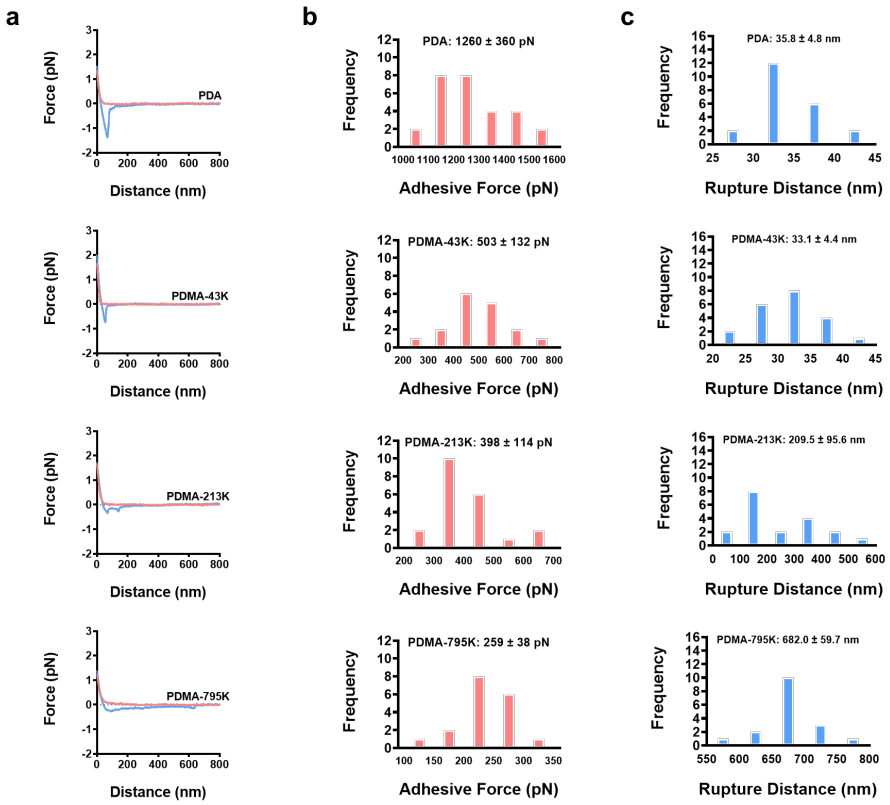


**Figure 3.7 AFM force measurement of PDA coated, /PDMA-43K coated, PDMA-213 K coated, and PDMA-795K coated silicon wafer pieces.**

**(a) Representative approach (blue line) and retraction (red line) force curves are shown. (b) Distribution of the adhesive force. (c) Distribution of the rupture distance.**

### 3.3.3 Influence of polymer chemistry on binary coating formation

We further used five different neutral hydrophilic polymers (PMPC, PEO, HPG, PVP, and PEOX) having uHMW ranged from 500 kDa to 1600 kDa in comparison with PDMA-795K to investigate the influence of polymer chemistry on the binary coating formation. As shown in **Figure 3.8**, the polymers have diverse chemistry and architecture. The experimental conditions for their co-assembly with dopamine in solution and surface deposition are based on previously described protocol (10 mg/mL of hydrophilic polymer and 2 mg/mL dopamine at pH 8.5 in Tris-HCl buffer) [85].

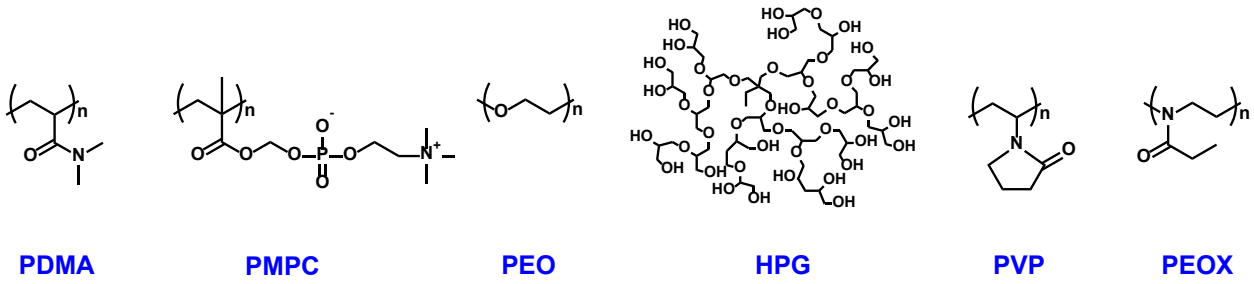


**Figure 3.8 Chemical structures of the catecholamines and uncharged uHMW polymers.**

**Hydrophilic polymers include PDMA: Poly(*N*,*N*-dimethylacrylamide); PMPC: Poly(2-methacryloyloxyethyl phosphorylcholine); PEO: Poly(ethylene oxide); HPG: Hyperbranched polyglycerol; PVP: Polyvinylpyrrolidone; and PEOX: Poly(2-ethyl-2-oxazoline) .**

#### 3.3.3.1 Analysis of formation of nanoparticles by the co-assembly in solution

Initially, we investigated the formation of PDA in the presence of uHMW polymers. As shown in **Figure 3.9a**, the amount of PDA generated in the presence of different polymers did not show marked change as evident from the similar spectral intensity between 300 and 800 nm in the UV-vis spectra. The data suggest that the nucleation of PDA aggregation is similar in presence of the uHMW hydrophilic polymers in the molecular weight range.

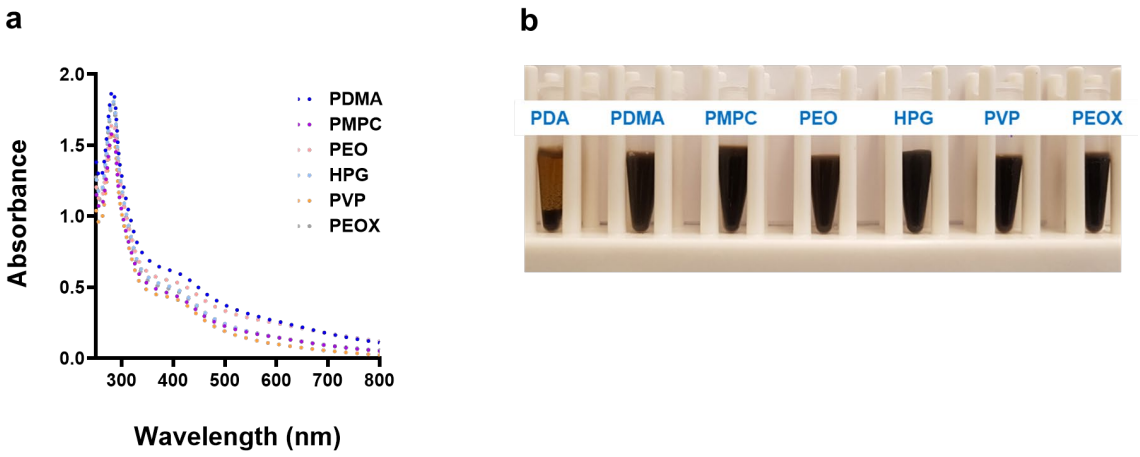


**Figure 3.9 Influence of molecular weight on the amount of PDA particle formation.**

**(a) UV spectra of the Tris buffered solution after mixing dopamine and different polymers for 24 h. (b) Optical photographs of dopamine, dopamine/PDMA, dopamine/PMPC, dopamine/PEO, dopamine/HPG, dopamine/PVP and dopamine/PEOX Tris buffered solution after 24 h reaction. As noted, dopamine solution without polymers precipitated during the storage suggesting the poor suspension stability.**

We next investigated the formation of nanostructures in solution by the co-assembly process. TEM analysis showed the formation of core-shell nanoparticles containing a dense PDA-core surrounded by a light layer of hydrophilic polymer for all the polymers studied except for PVP. Nanoparticles composed of PDA and the uHMW hydrophilic polymers with average diameters of 123.5 nm, 84.6 nm, 178.1 nm, 54.0 nm and 41.4 nm respectively for PDMA, PMPC, PEO, HPG and PEOX were visualized (**Figure 3.10**). However, the presence of nanoparticles was not visualized in the presence of PVP.

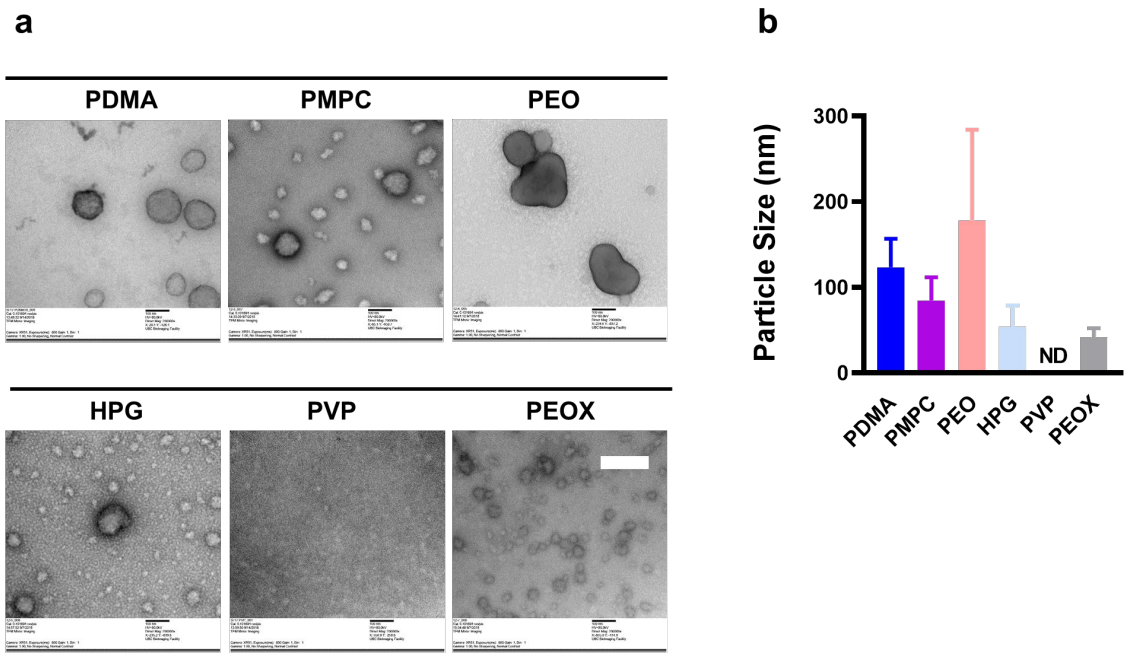


**Figure 3.10 Influence of polymer chemistry on the assembled nanoparticle size.**

**(a) Representative TEM images of nanoparticles formed by the co-assembly of dopamine and uHMW polymers with diverse chemistry. The scale bar is 200 nm. (b) The calculated number-averaged particle size based on TEM images.**

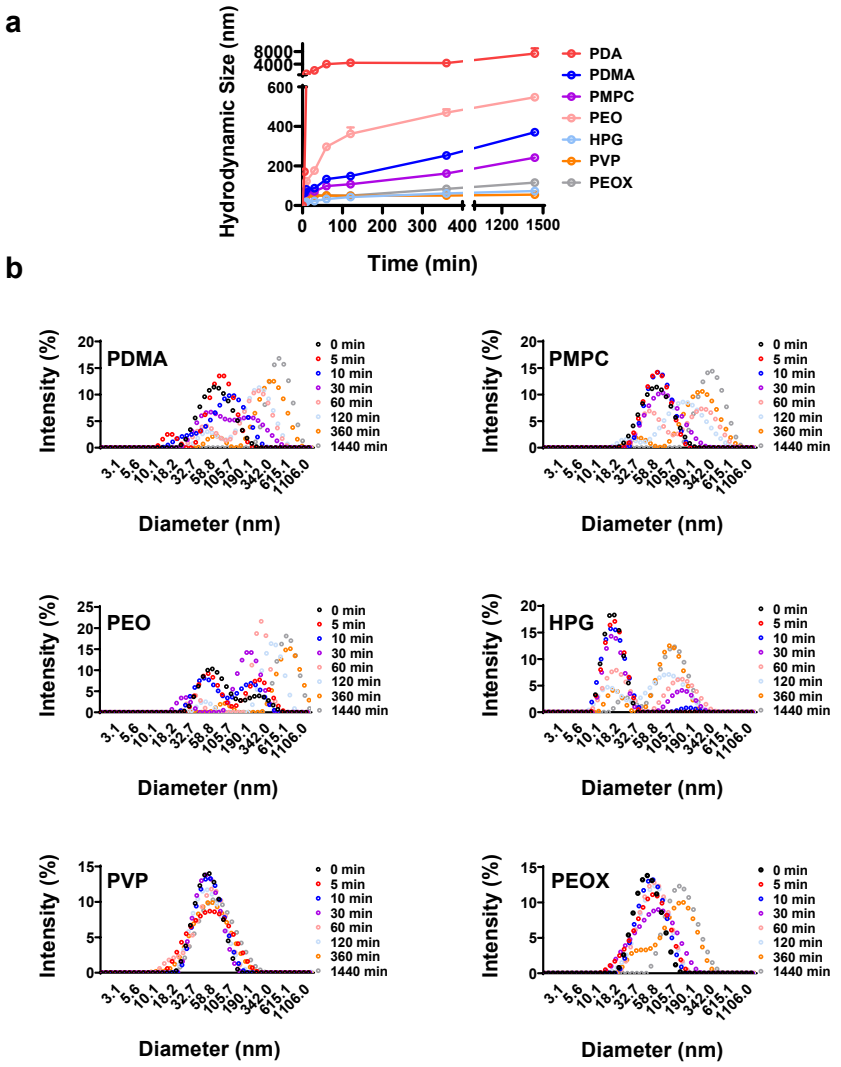


**Figure 3.11 Kinetics of nanoparticle formation in the presence of polymers with different chemistry.**

**(a) Change in hydrodynamic size during the oxidative process of dopamine in the absence or in the presence of hydrophilic polymers. (b) Hydrodynamic size distribution at various elapsed times during the oxidative process of dopamine in the absence or in the presence of hydrophilic polymers.**

We then investigated the hydrodynamic size and formation kinetics of nanoparticles formed using DLS measurements. In the absence of uHMW polymers, the hydrodynamic size of the particles formed increased to >1000 nm as soon as the initiation of dopamine oxidation/polymerization process was started. The addition of neutral uHMW polymers with

dopamine markedly decreased the particle growth, evident from the changes in hydrodynamic size with time (**Figure 3.11a**). The suspension of PDA nanoparticles and uHMW polymers are more stable than PDA alone . In the absence of uHMW polymer, PDA particles precipitated out of the suspension suggesting the formation of large particles and agrees with the DLS data (**Figure 3.9b**). The change in hydrodynamic size of the formed aggregates depends on the chemistry of uHMW polymer (**Figure 3.11b**). In the presence of PDMA, two aggregate populations were detected, the first distribution (Rh=60 nm) corresponding to the PDMA itself and the second distribution (Rh=400 nm) attributable to the core-shell nanoparticles. In the case of PEO group, 3 separated peaks were discovered, including the peak from PEO itself (Rh=60 nm), the peak from core-shell nanoparticles (Rh=300 nm), and the peak from aggregated particles (Rh=700 nm). A surprise observation was that the inhibition on PDA aggregation in the presence of PVP even when the reaction time was extended beyond 24 h. As seen from the time dependent DLS measurements, monomodal size distribution was observed for PVP system unlike other uHMW polymers.

We further investigated the zeta potential of binary nanoparticles formed by the co-assembly, as this will provide information regarding steric stabilization and surface coverage by uHMW polymers on PDA particles. The naked PDA particles has a high negative charge at the measurement conditions, however, most of the co-assembled PDA/uHMW polymer nanoparticles have near neutral surface charge (**Figure 3.12**). Since the PDA particles are negatively charged and the hydrophilic polymers are neutral, the data indicates the formation of core-shell type PDA/uHMW polymer nanoparticles with surface enriched with uHMW polymers. The uHMW polymers are shielding the negative charge of the PDA particles.

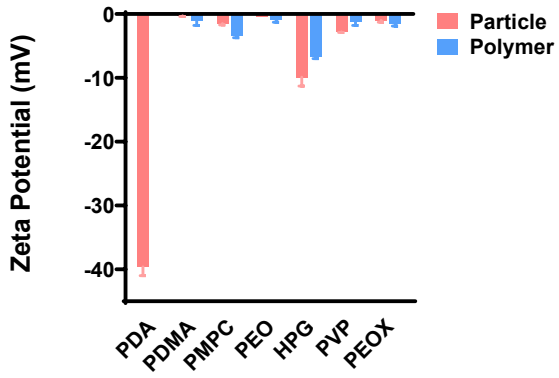


**Figure 3.12 The zeta potential of the nanoparticles formed by the co-assembly of uncharged uHMW polymers with dopamine.**

**Particle: PDA/uHMW polymer or PDA. Polymer: uHMW polymer alone. The pure hydrophilic polymers were used as controls.**

Based on these data, the following information can be deduced regarding the PDA/uHMW polymer nanoparticle assembly process (**Figure 3.13**). (1) Upon oxidation, the dopamine initially forms PDA nanoaggregates and interacts with hydrophilic uHMW polymers depending on their chemistry, (2) The PDA/uHMW polymer nanoaggregates continue the self-assembly process in aqueous solution resulting in nanoparticles with a core-shell structure with PDA core and uHMW polymer shell. The average size of the generated core-shell nanoparticles depends on the chemistry of the uHMW polymers, (3) PVP is a well-recognized strong hydrogen acceptor [65] which strongly interacts with PDA nanoaggregates *via* hydrogen bonding thereby forming very small nanoparticles under the detection limit. PEO, a weak hydrogen acceptor due to its ether groups, forms aggregated nanoparticles without offering steric stabilization. By moderately interacting with PDA through hydrogen bonding, PDMA generated well-distributed and uniform nanoparticles with medium size.

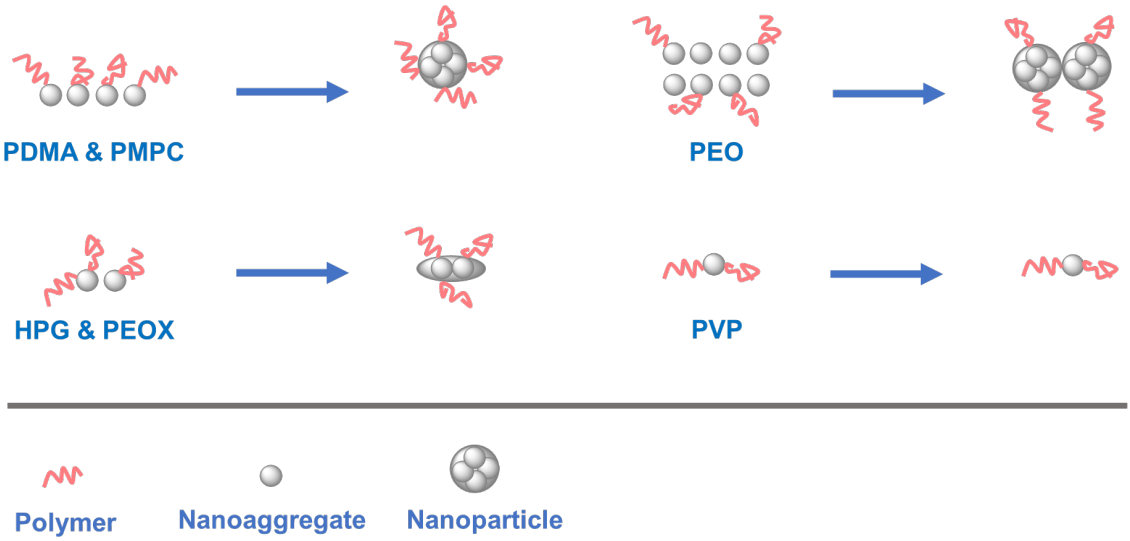


**Figure 3.13 A cartoon representing the mechanism of the core-shell structure formation.**

### 3.3.3.2 Surface deposition of aggregates and formation of an antiadhesive layer

Next, we investigated whether the presence of uHMW polymers during dopamine oxidation and self-assembly process influence the formation of a stable surface coating. The successful deposition and incorporation of PDA and uHMW hydrophilic polymers are confirmed by ellipsometry, XPS, ATR-FTIR spectroscopy, AFM, surface zeta potential and water contact angle measurements. Pieces of silicon wafer and PP film were immersed in dopamine/uHMW polymer solution for 24 h followed by a thorough washing of the substrate with Tris-HCl buffer and then with pure water. Dried samples were then used for further characterization.

Based on ellipsometry analysis, PDMA, PMPC, PEO, HPG and PEOX co-assembly with PDA resulted in coatings with dry thickness 17.5 ± 0.3 nm, 10.5 ± 0.5 nm, 10.2 ± 1.7 nm, 13.9 ± 1.4 nm and 10.7 ± 0.8 nm, respectively, while PVP co-assembly generated the thinnest coating with a thickness of 3.3 ± 0.5 nm (**Table 3.1**).

| Polymer Coating | [1]Thickness (nm) | [2]Si (At%) | [2]C (At%) | [2]N (At%) | [2]O (At%) | [2]P (At%) | [3]N/C | [4]N/O |
|---|---|---|---|---|---|---|---|---|
| PDA | 26.8 ± 1.8 | 0.51 | 74.41 | 6.93 | 18.15 | 0.00 | 0.093 | 0.382 |
| PDMA | 17.5 ± 0.3 | 0.92 | 74.07 | 9.63 | 15.64 | 0.00 | 0.130 | 0.616 |
| PMPC | 10.5 ± 0.5 | 3.53 | 63.23 | 5.97 | 25.13 | 2.14 | 0.094 | 0.237 |
| PEO | 10.2 ± 1.7 | 5.00 | 64.36 | 5.76 | 24.88 | 0.00 | 0.090 | 0.232 |
| HPG | 13.9 ± 1.4 | 1.61 | 63.91 | 4.51 | 29.97 | 0.00 | 0.071 | 0.150 |
| PVP | 3.3 ± 0.5 | 27.63 | 42.03 | 6.12 | 24.05 | 0.00 | 0.145 | 0.254 |
| PEOX | 10.7 ± 0.8 | 3.10 | 68.10 | 10.15 | 18.65 | 0.00 | 0.149 | 0.544 |

**Table 3.1 Dry thickness and chemical composition of the binary coatings prepared by different polymers.**

**1- from ellipsometry measurements; 2- from XPS analysis; 3- The theoretical N/C values of PDA, PDMA, PMPC, PEO, HPG, PVP, PEOX are 0.125, 0.200, 0.091, 0.000, 0.000, 0.167, 0.200; 4- The theoretical N/O values of PDA, PDMA, PMPC, PEO, HPG, PVP, PEOX are 0.500, 1.000, 0.167, 0.000, 0.000, 1.000, 1.000.**

The surface composition analysis by XPS clearly show the incorporation of uHMW polymers into the surface coatings. This is evident from the change in the ratio of N/C, N/O (**Figure 3.14**) and high-resolution O1s, N1s scans (**Figure 3.15**). Detailed analysis of PDA/PDMA binary coating provided the following information. Increased ratios of N/C (from 0.093 to 0.130) and N/O (from 0.382 to 0.616) compared to the PDA control were observed for

the PDMA/PDA coating. In the high-resolution spectrum, a marked increase in the intensity of C=O peak in O1s was observed. In comparison to the PDA control, a slight decrease in $NH_2$ component in N1s detail spectrum was also detected. All these data confirmed the successful incorporation of PDMA within the binary coating. Similar data were obtained for other uHWM polymers incorporated binary coatings.

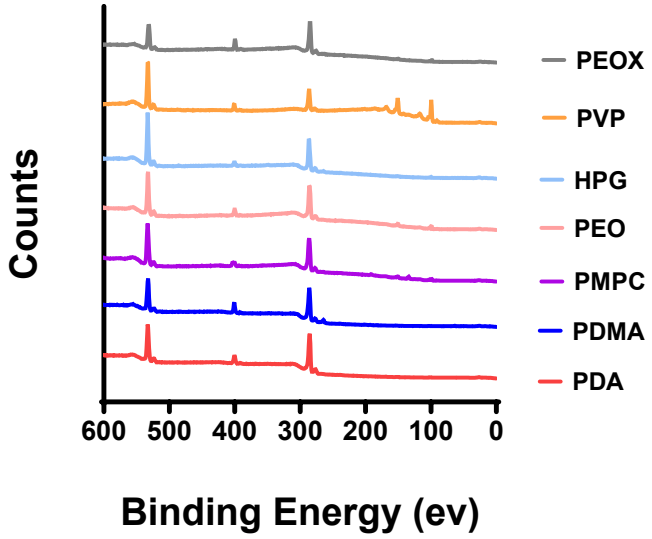


**Figure 3.14 Wide scans of PDMA, PMPC, PEO, HPG, PVP and PEOX coated silicon wafer pieces obtained using XPS.**

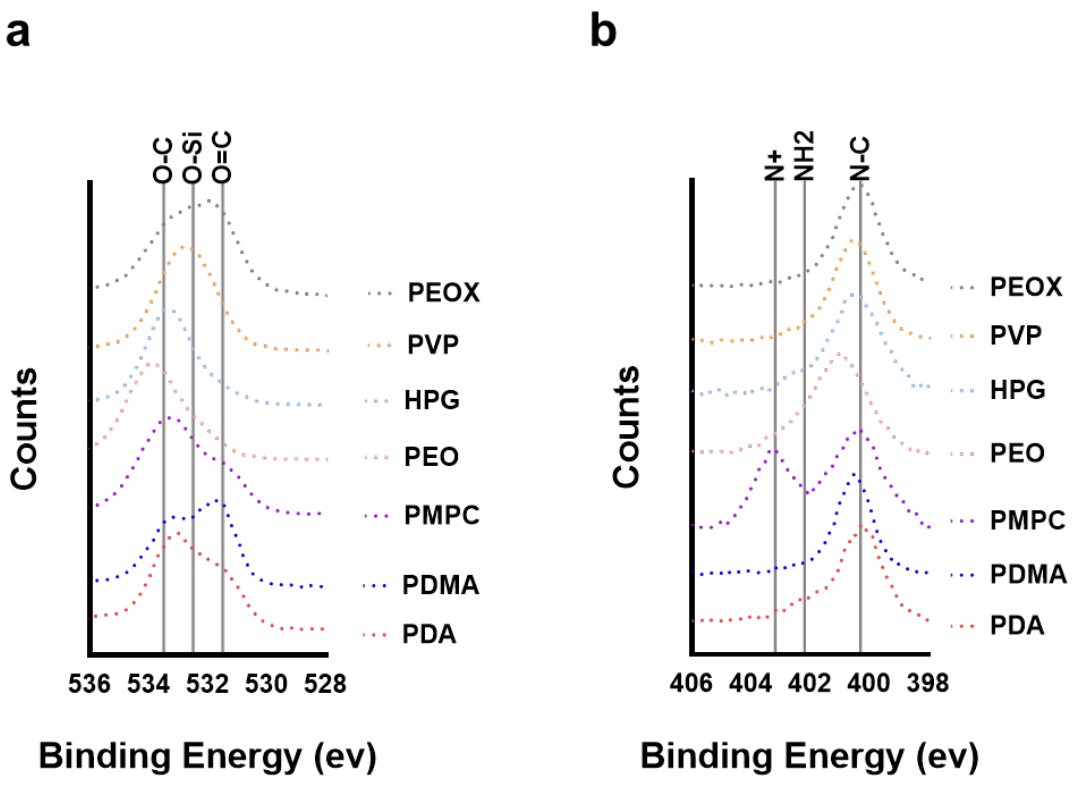


**Figure 3.15 Detailed scans of PDMA, PMPC, PEO, HPG, PVP and PEOX coated silicon wafer pieces obtained using XPS.**

**(a) Detailed O1s XPS scan of the coatings prepared by the co-assembly of PDA and PDMA, PMPC, PEO, HPG, PVP and PEOX on silicon wafer pieces. (b) Detailed N1s XPS scan of the coatings prepared by the co-assembly of PDA and PDMA, PMPC, PEO, HPG, PVP and PEOX on silicon wafer pieces.**

ATR-FTIR spectroscopy analysis also supported the findings that uHWM polymers were incorporated into the coatings (**Figure 3.16**). However, the incorporation of PEO and HPG was not significant based on the spectral intensity. The surface morphology of the coating on silicon wafers was investigated by AFM in wet conditions. Nanoaggregate-like structures were seen on the surface for all the PDA/uHMW polymer coating (**Figure 3.17**) consistent with previous reports on PDA nanoaggregates. Though the binary PDA/PDMA coating showed the highest dry thickness (**Table 3.1**), this coating had a smooth morphology under wet condition.

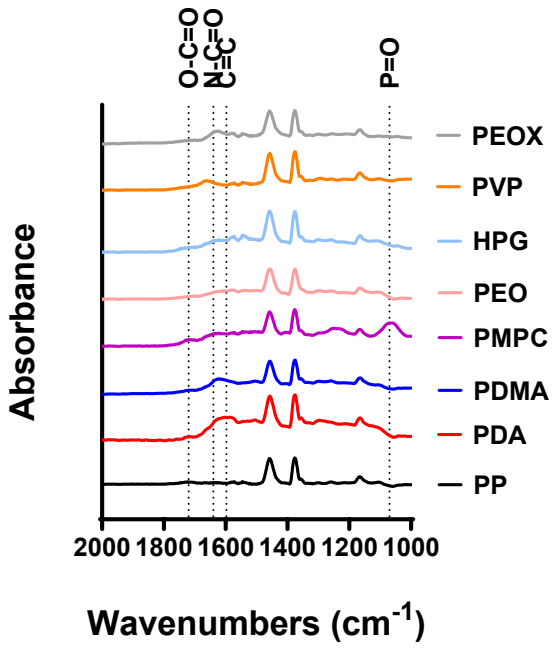


**Figure 3.16 ATR-FTIR spectra of binary PDMA, PMPC, PEO, HPG, PVP, and PEOX coatings on PP films.**

**The increased peaks at 1623 $cm^{-1}$, 1640 $cm^{-1}$, and 1660 $cm^{-1}$ of the coatings indicate the incorporation of PDMA, PEOX, and PVP. The increased peaks at 1080 $cm^{-1}$ and 1730 $cm^{-1}$ of the coating indicates the incorporation of PMPC.**

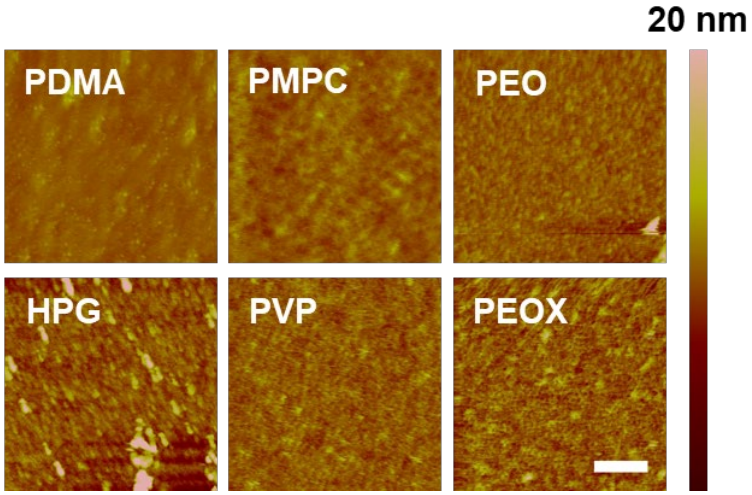


**Figure 3.17 AFM images of different PDA/uHMW polymers coated silicon wafers in wet conditions.**

Due to the surface enrichment of the hydrophilic polymer, the wettability of the surface was greatly improved for coating formed by the co-assembly of the polymers and PDA compared to the uncoated substrates. Lower contact angle values were obtained for the binary coatings prepared by PDMA or PMPC with PDA (**Figure 3.18a**), indicating the formation of stable and fully covered substrate at these conditions. Next, we looked at the surface zeta potential of the coating to understand the shielding of PDA by the neutral uHMW polymer. The surface charge could provide information regarding surface coverage and the ability of uHMW polymer to protect the PDA layer. For the measurements, we modified the surface of PP films with different coatings, and the surface charge was measured using a special cell. The surface zeta potential values ranged from -35.3 mV for PDA coating to -2.6 mV for PDA/PDMA coating. The uHMW PDMA was able to efficiently protect the high negative charge of the PDA unlike other uHMW polymers (**Figure 3.18b**). The low surface charge of PDA/PDMA coating demonstrates that the co-assembly of PDA/PDMA resulting in the formation of hydrophilic polymer enriched coating compared to other systems studied. Taken together, the data demonstrate that the chemistry of the polymers and their architecture have significant influence on the co-assembly of the PDA/uHMW polymer system, its deposition on the surface, formation of the coating and its stabilization. Only selected systems could generate a neutral surface coating from the deposition of co-assembled PDA and hydrophilic uHMW polymer, and in our case, it is PDA and uHMW PDMA system. The co-assembly of the PDA and PVP resulted in very small highly stabilized nanoaggregates (evident from TEM images and DLS profiles) due to the strong interaction of PVP with PDA, which prevented from its deposition on to the surface. This further opens avenues to optimize the surface deposition and coating by altering the PDA-polymer interaction.

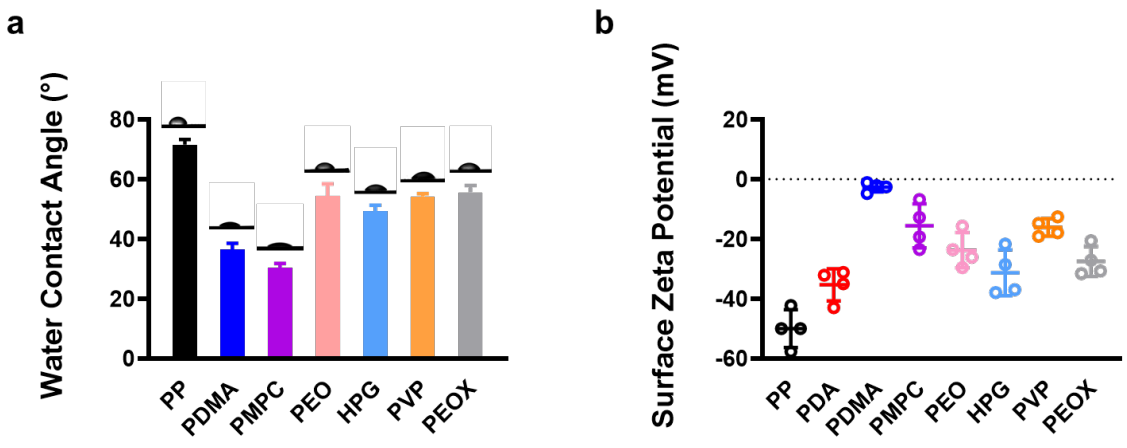


**Figure 3.18 Surface wettability and charge of the binary coatings with different polymer chemistry.**

**(a) Static water contact angles of binary PDA/ uHMW polymer coatings prepared using polymers with different chemistry on PP films. (b) The surface zeta potential of binary PDA/ uHMW polymer coatings prepared using polymers with different chemistry on PP films.**

### 3.3.3.3 The structure of the binary coating

To investigate the possible structure of the binary coatings, AFM force measurement was used. Typical force-distance curves for different surface coatings are shown in **Figure 3.19**. Nature of the force curves suggests that there are three different potential interactions are in existence at the AFM tip-surface coating interface. These include (1) a hydrophobic interaction between the AFM tip and the coating at short distances evident from the AFM retraction curve. (2) Steric repulsion offered by the uHMW polymers evident from the approach curve, and (3) attractive interactions at long distances between the AFM tip and the uHMW hydrophilic polymer possibly due to the adsorption of polymer chains on to the tip (evident from the retraction curve).

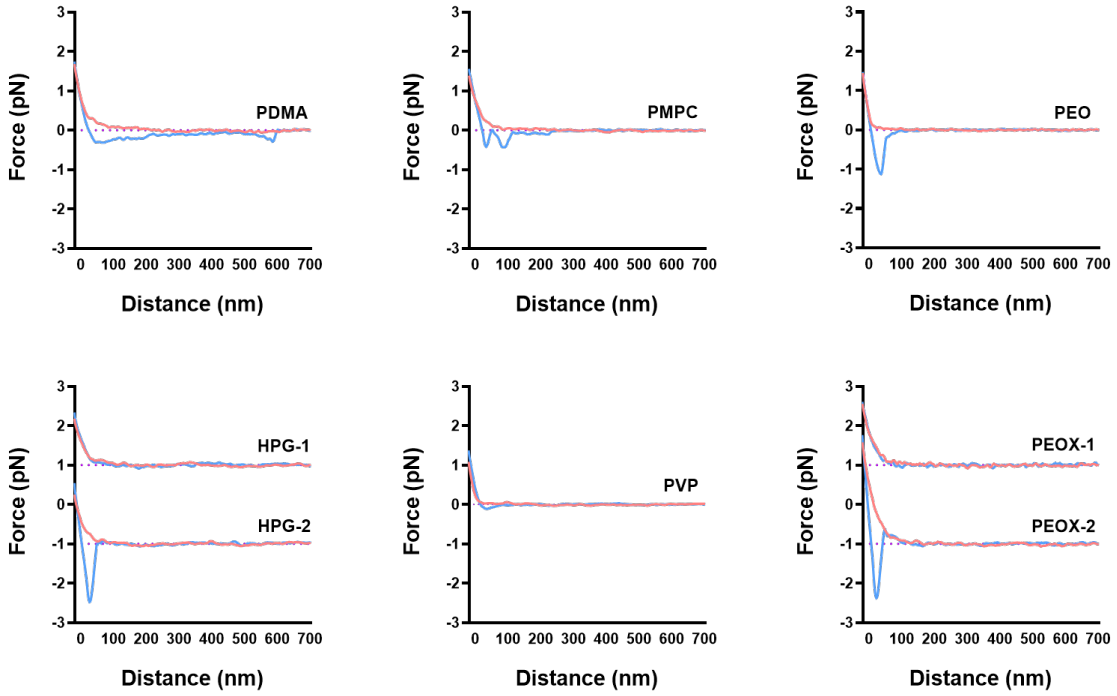


**Figure 3.19 AFM force curves of the coatings prepared by the co-assembly of dopamine with PDMA, PMPC, PEO, HPG, PVP, and PEOX on silicon wafer pieces.**

**The blue line indicates the approach curve, the red line indicates the retract curve.**

**Figure 3.20a** shows the maximum adhesive force distribution and wet thickness of the binary coatings. Significant adhesive forces were observed on PEO, HPG and PEOX binary coatings, while minimum adhesive forces were detected on PDMA, PMPC and PVP binary coatings. This indicates that the AFM tip has less chance to contact the PDA component in the case of PDMA, PMPC and PVP binary coatings, i.e., less PDA exposure on such coatings. The AFM approach curves for all binary coatings except for the PVP coating showed a typical approach profile for steric repulsion exerted by polymer chains grafted on the surface; reminiscence of a swollen hydrophilic brush layer [208-209]. The equilibrium thickness of the PDMA, PMPC, PEO, HPG, PVP and PEOX binary coatings reached 87 nm, 62 nm, 37 nm, 45 nm, 8 nm and 51 nm, respectively, in accordance with their dry thickness (**Figure 3.20b**). The

AFM retraction curve profiles also found evidence of weak attractive forces at long distances between the AFM tip and the coating composed of PDMA and PMPC. The data suggest that in the case of these samples, the polymer chains are getting detached from the AFM tip upon retraction. The data also suggest that the surface anchored polymer chains may be more flexible in these samples. The attractive force is due to the weak adsorption of polymer chains to the tip that are present until the tip retracts beyond their maximum extension.

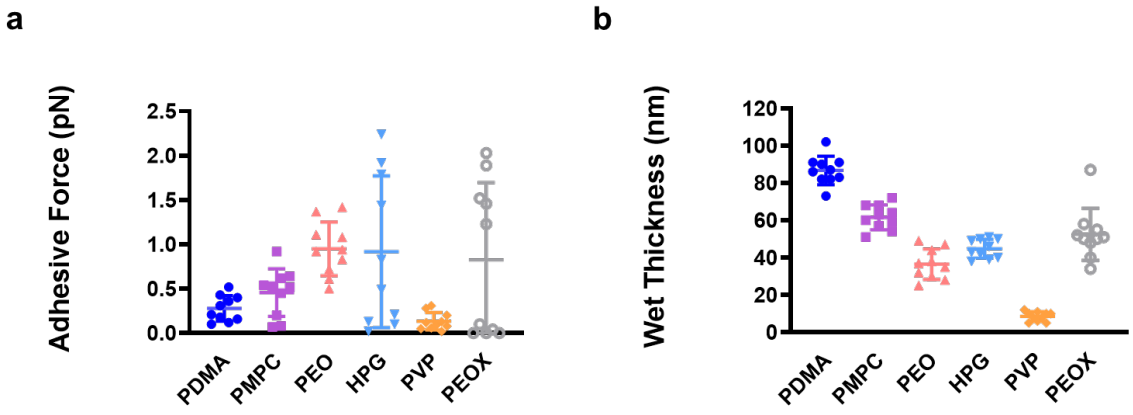


**Figure 3.20 Distribution of adhesive force and wet thickness of the coatings prepared by the co-assembly of PDA with PDMA, PMPC, PEO, HPG, PVP and PEOX on silicon wafers.**

Based on these observations, we propose a structure of the binary coating formed by PDA in the presence of different hydrophilic polymers in **Figure 3.21**. The PDMA and PMPC binary coatings demonstrate a structure that the hydrophilic polymers protect the PDA component, and the anchored hydrophilic polymer chains are flexible. The PEO binary coating shares a similar structure as that of PDA coating because of the poor incorporation of PEO in the coating. The HPG and PEOX binary coatings exhibit a structure that the PDA component is not totally covered by the uHMW polymers, and the polymer chains are less mobile. In the case of

PVP binary coating, due to the insufficient coating coverage, it showed similar characteristics as that of an uncoated silicon wafer.

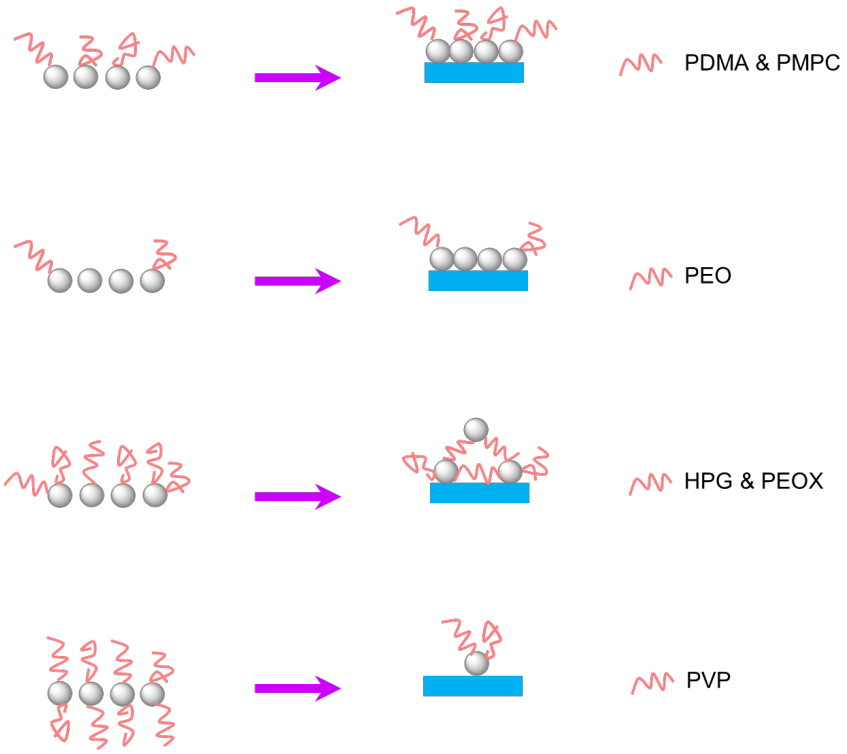


**Figure 3.21 A cartoon illustration of possible structure of the binary coatings with different polymer chemistry.**

### 3.3.4 Influence of catecholamine type on the binary coating formation

To investigate whether other catecholamines also behave similarly to dopamine in the co-assembly and surface deposition in presence of uHMW polymers, we then studied norepinephrine as it has shown to form a layer of thin coating upon oxidation similar to dopamine [213]. We used similar experimental conditions that was used in the case of dopamine (2 mg/mL of norepinephrine and 10 mg/mL uHMW polymer at a pH=8.5 in Tris-HCl buffer solution). As shown in **Appendix B2**, the amount of PNE generated in the presence of uHMW

polymers did not show marked change as evident from the similar spectral intensity between 300 and 800 nm in the UV-vis spectra. TEM images show that PNE aggregates differently than PDA, forming agglomerated nanoaggregates instead of aggregated nanoparticles. With the addition of uHMW PDMA, well-distributed core-shell nanoparticles were visualized in the case of PNE (**Figure 3.22a**). A more dispersed nanoaggregates were detected in the case of PNE in comparison to PDA. This indicates that the self-assembly process might be different for PNE in comparison to PDA. The zeta potential of the assembled particles from PNE/PDMA group was slight lower than the pure polymer from PDMA group, which may be attribute to these negatively charged dispersed PNE nanoaggregates (**Figure 3.22b**).

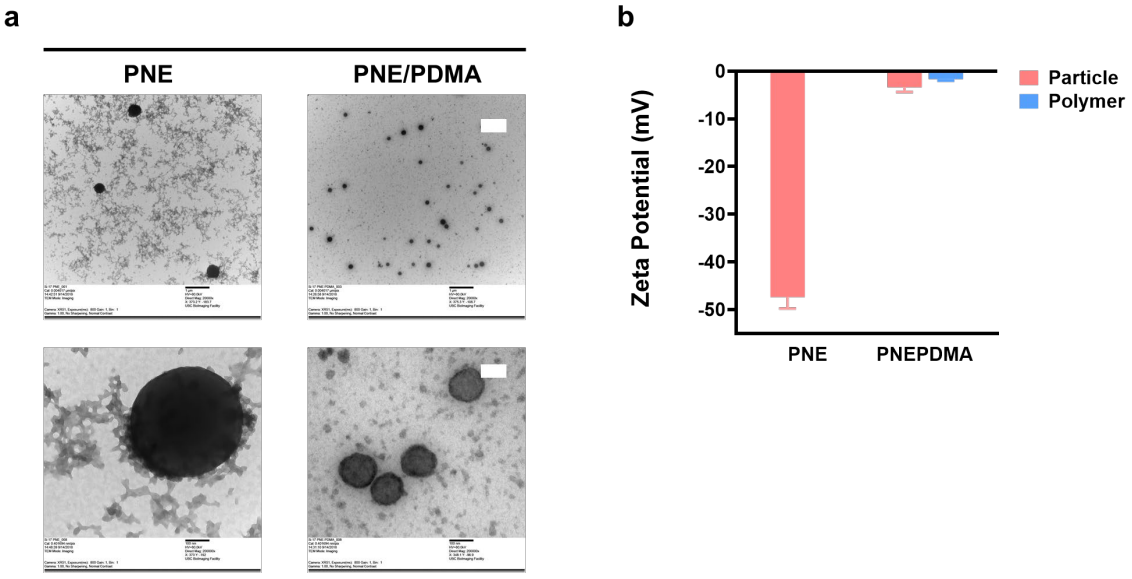


**Figure 3.22 Representative TEM images (a) and zeta potential (b) of particles assembled using norepinephrine alone or with uHMW PDMA.**

**The scale bars in TEM images are 1 µm, 100 nm for the top layer, the bottom layer, respectively.**

To probe this further, we collected the XPS spectra of the surface coating prepared by PNE alone or assembled with uHMW PDMA. The chemical composition from the XPS survey

scan showed an increase of N content from 6.4% to 7.5% and N/C ratio from 0.127 to 0.154, which indicates the enrichment of uHMW PDMA on the surface of the coating (**Figure 3.23, Table 3.2**). High-resolution O1s and N1s XPS analyses revealed that the PNE/uHMW PDMA coated surface showed higher C=O content and a lower $NH_2$ content compared to the surface coated with PNE alone, suggesting the successful incorporation of uHMW PDMA (**Figure 3.24**).

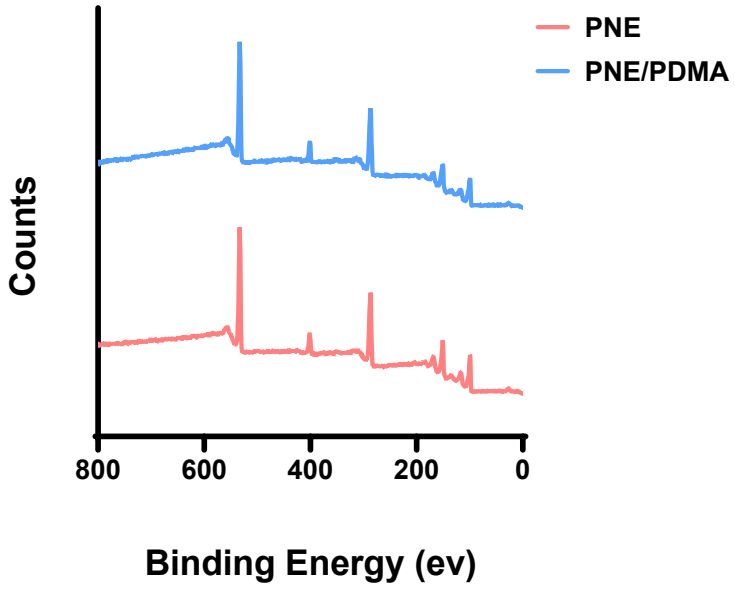


**Figure 3.23 Wide scans of PNE and PNE/uHMW PDMA coated silicon wafer pieces obtained using XPS.**

| Polymer Coating | [1]Thickness (nm) | [2]Si (At%) | [2]C (At%) | [2]N (At%) | [2]O (At%) | [3]N/C | [4]N/O |
|---|---|---|---|---|---|---|---|
| PNE | 44.1 ± 8.3 | 18.43 | 50.78 | 6.43 | 24.36 | 0.127 | 0.264 |
| PNE/uHMW PDMA | 14.7 ± 0.9 | 18.69 | 48.70 | 7.49 | 25.12 | 0.154 | 0.298 |

**Table 3.2 Dry thickness and chemical composition of the PNE and PNE/uHMW PDMA coatings.**

**1- from ellipsometry measurements; 2- from XPS analysis; 3- The theoretical N/C values of PNE, PDMA are 0.125, 0.250; 4- The theoretical N/O values of PNE, PDMA are 0.333, 1.000.**

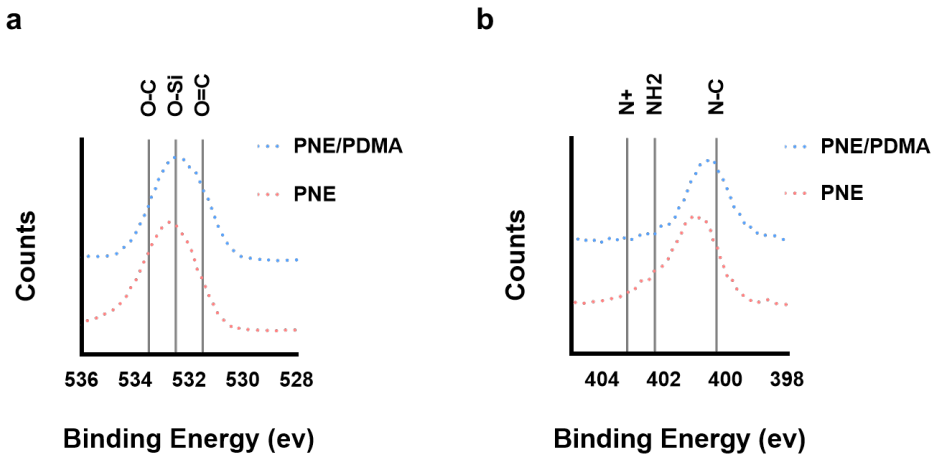


**Figure 3.24 High-resolution O1s (a) and N1s (b) scans of PNE and PNE/uHMW PDMA coated silicon wafer pieces obtained by XPS.**

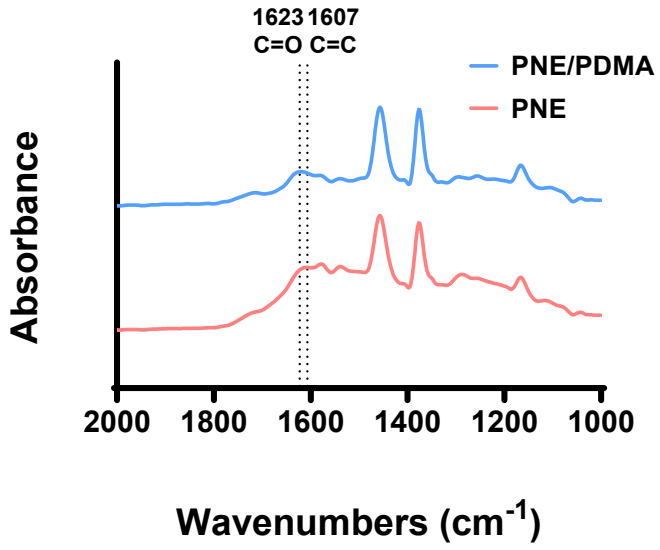


**Figure 3.25 ATR-FTIR spectra of PNE and PNE/uHMW PDMA coated PP films.**

**The increased peak at 1623 $cm^{-1}$ of the binary coatings indicates the successful incorporation of PDMA.**

ATR-FTIR analysis also supported the findings that the PDMA was incorporated into the binary coating on the PP film (**Figure 3.25**). The incorporation of uHMW PDMA results in a hydrophilic and neutral coating on PP films.

As shown in AFM images (**Appendix B3**), the PNE/PDMA binary coating demonstrated higher surface roughness compared to the PDA/PDMA binary coating. Water contact angle measurements gave a value 33.7° for the PNE/PDMA binary coating, which was lower than the contact angle 43.3° obtained for coating containing only PNE (**Figure 3.26a**). The surface zeta potential of the PNE/PDMA was -4.2 mV, which was significantly lower than the -39.5 mV of the PNE coating (**Figure 3.26b**).

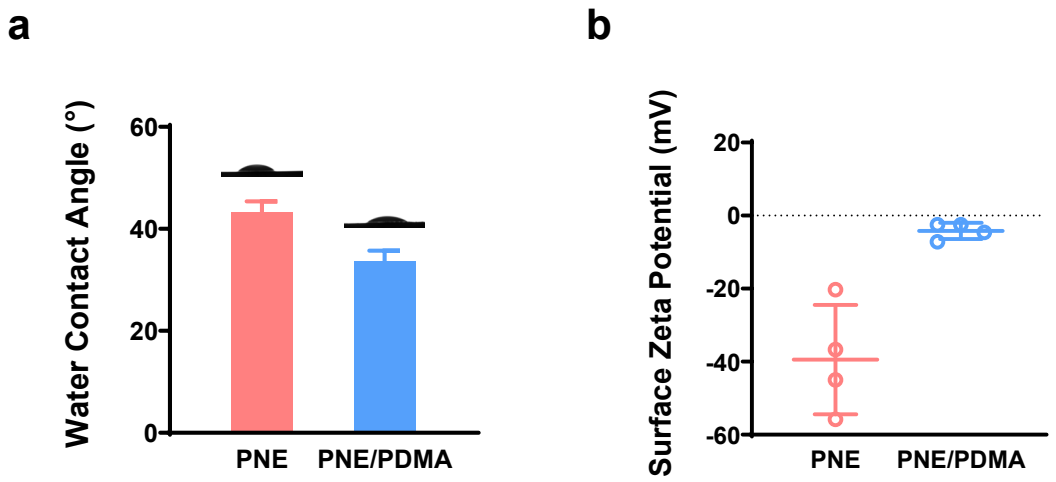


**Figure 3.26 Surface properties of the PNE and PNE/PDMA coatings on the PP films.**

**(a) Static water contact angles of the PNE and PNE/PDMA coated PP films. (b) The surface zeta potential of the PNE and PNE/PDMA coated PP films.**

Finally, we utilized AFM force measurements to determine the surface structure of the binary PNE/PDMA coating in wet conditions **(Figure 3.27**). AFM approach curves showed a similar approach profile for steric repulsion exerted by hydrophilic PDMA chains grafted on the surface, with an equilibrium thickness of 80 nm. The AFM retraction curve gave a characteristic profile of loop like assembly of PDMA chains on the surface similar to PDA/PDMA coating, and the adhesive force was reduced compared to the PNE coating. Together these data support the observation that the PNE/PDMA binary coating shares a similar structure as that of PDA/PDMA binary coating although the self-assembly process and surface morphology might be slightly different.

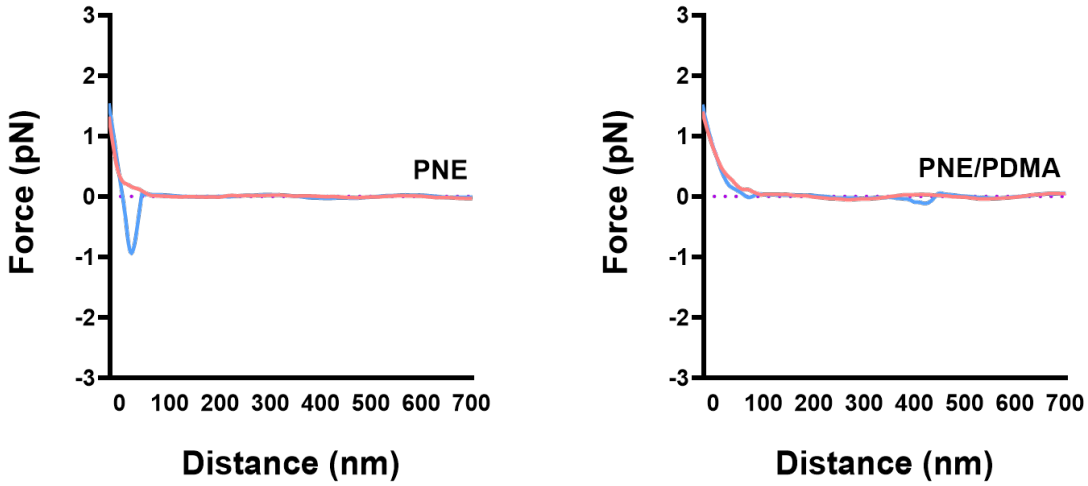


**Figure 3.27 AFM force curves of the PNE and PNE/PDMA coated silicon wafer pieces.**

**The blue line indicates the approach curve, the red line indicates the retract curve.**

## 3.4 Conclusions

We first investigated the mechanism of the optimized coating formation. Then, we employed three hydrophilic polymers with different molecular weights, six hydrophilic polymers with different chemistry, and two different catecholamines for investigating the co-assembly and co-deposition process. The molecular weight and chemistry of the hydrophilic polymers is found to influence the interaction between polycatecholamine and the hydrophilic polymers, thus plays an important role in the aqueous self-assembly in solution to nanoaggregates, its formation kinetics, steric stabilization, and subsequent surface deposition. The type of catecholamine influences the properties of the coating less in comparison to the molecular weight and chemistry of the hydrophilic polymer.

# Chapter 4: A universal antifouling coating with variable thickness based on layer-by-layer assembly

Studies in Chapter 2 & 3 clearly demonstrated that robust thin films can be prepared on diverse substrates with high stability and excellent antifouling properties. However, for applications that require the incorporation of bioactive agents and its sustained release over long-term, it is desirable to have thicker coating with antifouling activity. This would allow for the incorporation of high content of bioactive agents for its long-term action. Thus, in Chapter 4 we aim at developing a surface coating method utilizing a polyphenol and ultra-high molecular weight (uHMW) polymers which could potentially generate thicker films.

## 4.1 Introduction

Layer-by-layer (LbL) assembly is a simple and facile method for generating thickness-controlled coatings on substrates by the alternate immersion of substrates into interactive solutions [185]. A variety of coating materials, including synthetic polymers and biomacromolecules have been used to construct LbL multilayers *via* electrostatic interaction, hydrogen bonding, covalent interaction, coordination bonding or their combinations on substrates with all kinds of shapes and sizes. This technique has been widely explored and applied in electrical, optical, biomedical, and environmental devices [186].

Tannic acid (TA), a natural polyphenol, has recently attracted attention because of its unique potential as a coating material. It forms monolayers by itself or multilayers with ferric ions [144]. Since TA is negatively charged and can act as a hydrogen donor, it also forms multilayered films *via* LbL assembly with a wide range of materials. Neutral polymers such as

polyvinylpyrrolidone (PVP), polyethylene oxide (PEO), poly(*N*-vinylcaprolactam) (PVCL), poly(*N*-isopropylacrylamide) (PNIPAAM), poly(2-methyl-2-oxazoline) (PMOX), poly(2-ethyl-2-oxazoline) (PEOX) and poly(2-n-propyl-2-oxazoline) (PPROPOX) can interact with TA to form the hydrogen-bonded multilayered films [214]. Hoogenboom's group investigated the LbL multilayer films prepared by TA and poly(2-oxazoline)s with varying hydrophilicity, including PMOX, PEOX and PPROPOX. They demonstrated that smooth multilayer films were formed by LbL assembly of TA with all three poly(2-oxazoline)s [215].

Although there is a critical demand for fabricating stable and antifouling LbL multilayer films using TA, only a few studies reported in this area. Xu's group found that TA was able to assemble with zwitterionic polymer PSBMA, forming stable multilayers [216]. The 20 bilayers TA/PSBMA thin films exhibited good hydrophilicity and excellent resistance to a wide range of proteins, such as bovine serum albumin (BSA), hemoglobin (Hgb), and lysozyme (Lys). Caruso's group initially generated the TA/$Fe^{3+}$ MPN film by LbL assembly and used partially coordinated $Fe^{3+}$ as a means of adding specific functionality through the chelation of galloyl-terminated PEOX, which reduced protein adsorption by 79% and bacterial adhesion by 66% [74]. We anticipated that by optimizing the polymer chemistry and their interaction with TA, highly efficient antifouling surface coating could be achieved.

In this chapter, we systemically constructed the LbL multilayered films assembled by TA and a wide range of uHMW hydrophilic polymers utilizing hydrogen bonding and evaluated their antifouling activities. The finally optimized multilayer coating could also be used as an antifouling platform for incorporating antimicrobial agents.

## 4.2 Materials and methods

### 4.2.1 Materials

Reagents were purchased from Sigma-Aldrich and used as received unless otherwise noted. Water was purified using a Milli-Q Plus water purification system (Milipore Corp., Bedford, MA) and used in all experiments. Monomers including *N*,*N*-dimethylacrylamide (DMA, 99%), acrylamide (AM), *N*-hydroxyethyl acrylamide (HEA, 97%), *N*-[tris(hydroxymethyl) methyl]acrylamide (THMAM, 93%), [3-[(methacryloyl) amido]propyl]dimethyl(3-sulfopropyl) ammonium hydroxide inner salt (MPDSAH, 96%), 2-[(methacryloyl)-oxy]ethylphosphorylcholine (MPC, 97%), glycidol and polymers including polyethylene oxide (PEO, Mv=1,000,000), polyvinylpyrrolidone (PVP, Mw=1,300,000), poly(2-ethyl-2-oxazoline) (PEOX Mw=500,000), branched polyethyleneimine (BPEI, Mn=10,000) were purchased from Sigma-Aldrich. *N*-(2-hydroxypropyl)methacrylamide (HPMA) was purchased from Polysciences and dextran (Mw=500,000) was received from Pharmacia Fine Chemicals. *N*,*N*-Dimethylacrylamide and glycidol was purified by vacuum distillation and stored in a refrigerator at 4 °C before use. The single-side-polished silicon wafers were bought from University Wafer (Boston, MA).

### 4.2.2 Polymer synthesis

The uHMW PDMA, PAM, PHEA, PHPMA, PTHMAM, PMPDSAH, and PMPC were synthesized by aqueous ATRP. In a typical experiment, copper(II) chloride ($CuCl_2$, 2 mg), copper(I) chloride (CuCl, 15.9 mg), and 1, 1, 4, 7, 10, 10-hexamethyl triethylene tetramine (HMTETA, 96.2 μL) were added successively into a glass tube, followed by the addition of 20 mL of Milli-Q water. The solution was degassed with three freeze-pump-thaw cycles and then transferred into the glovebox. The catalyst solution (20 mL) was thoroughly mixed before the

addition of monomers (2 g). The amount of methyl 2-chloropropionate in methanol added to the reaction mixture was controlled to change the molecular weight of the polymers, and the polymerization could proceed at room temperature (22 °C) for 24 h. The soluble polymer was finally collected by dialysis (molecular weight cut-off: 1000) against water for 1 week. The uHMW HPG was synthesized according to our previous protocol.

### 4.2.3 Gel permeation chromatography

The molecular weight and PDI of the synthetic polymers were determined by gel permeation chromatography (GPC) on a Waters 2690 separation module fitted with a DAWN EOS multiangle laser light scattering detector from Wyatt Technology Corp. with 18 detectors placed at different angles and a refractive index detector (Optilab DSP from Wyatt Technology Corp.). An Ultrahydrogel linear column with a bead size of 6-13 μm (elution range $10^3$ to $5\times10^6$ Da) and an Ultrahydrogel 120 with a bead size of 6 μm (elution range 150 to $5\times10^3$ Da) from Waters were used. The dn/dc values of uHMW polymers in the mobile phase was determined at $\lambda = 620$ nm. The number average mean square radius moments were taken as the radius of gyration of the polymer. The detailed information about high molecular weight polymers was provided in **Appendix C1**.

### 4.2.4 Dynamic light scattering

Dynamic light scattering (DLS) measurement of the TA/uHMW polymer complex or uHMW polymer alone was performed using a Zetasizer NanoZS instrument (Malvern Instruments, UK). The final solution was diluted 75-fold using PBS buffer for measuring the particle size. The measurement was performed with an equilibration time of 1 min at room temperature. Each measurement was repeated for three times, and the averaged value was accepted as the final hydrodynamic size.

### 4.2.5 Deposition of multilayer films

LbL assembly process was used to deposit TA multilayers with different uHMW hydrophilic polymers on the surface of silicon wafer as a standard model. The concentration of TA was 0.5 mg/mL and that of uHMW polymers was 2 mg/mL in 0.01 M phosphate buffer at pH=7.4. To remove the dust, silicon wafer pieces were precleaned using oxygen plasma treatment for 2 min. To enhance the adhesion of multilayer films to the surface, a precursor layer of branched polyethyleneimine (BPEI) was deposited on the precleaned surface *via* dipping into 2 mg/mL BPEI solution for 15 min. LbL multilayer films were deposited using the dipping coating method. BPEI deposited silicon wafer pieces were alternately immersed into 0.5 mg/mL of TA and 2 mg/mL of uHMW polymer solutions at pH=7.4 for 10 min. After each deposition step, the substrates were thoroughly washed with phosphate buffer solution. Pieces of silicon wafer coated with 5 and 10 bilayers films were dried for further characterization.

### 4.2.6 Ellipsometry analysis

The variable-angle spectroscopic ellipsometry (VASE) spectra were collected on an M-2000 V spectroscopic ellipsometer (J.A. Woollam, Lincoln, NE) at 50°, 60°, and 70° at wavelengths from 480 to 700 nm with an M-2000 50W quartz tungsten halogen light source. The VASE spectra were then fitted with a multilayer model utilizing WVASE32 analysis software based on the optical properties of a generalized Cauchy layer to obtain the dry thickness of deposited layers. Silicon wafer was used as the substrate.

### 4.2.7 Attenuated total reflectance Fourier transform infrared analysis

Attenuated total reflectance Fourier transform infrared (ATR-FTIR) spectra were recorded using a Thermo-Nicolet Nexus FTIR spectrometer (Nicolet Instrument, Waltham, MA) with an MCT/A liquid nitrogen cooled detector, KBr beam splitter and MKII Golden Gate Single

Refection ATR accessory (Specac Inc. Woodstock, GA). Spectra were recorded at 4 $cm^{-1}$ resolution and 64 scans were collected for each sample. Silicon wafer pieces were used for background collection.

### 4.2.8 Water contact angle measurements

For water contact angle (WCA) measurements, digital images of a 10 μL water droplet on the surface were taken using a digital camera (Retiga 1300, Q-imaging Co.), and analyzed using Northern Eclipse software. Six different spots on the multilayer films coated silicon wafers were tested for each sample and the average value was reported.

### 4.2.9 Evaluation of early stage biofilm formation

For early stage biofilm formation assessment, silicon wafer pieces coated with BPEI or TA were used as controls, while pieces coated with multilayer films were used for evaluation. An overnight culture of *Staphylococcus aureus* (*S. aureus*) lux strain (Xen36 Lux) or *Pseudomonas aeruginosa* (*P. aeruginosa*) lux strain (PAO1 Tn7::Plac-lux) was first adjusted to $10^6$ CFU/mL in Lysogeny broth (LB) medium. The sterilized multilayer film coated silicon wafers were transferred into a 24-well plate. The concentration of bacteria (cultured overnight) was first adjusted to $10^6$ cells/mL in LB medium. Each sample was equilibrated in LB for 10 min and then immersed in 1 mL *S. aureus* lux or *P. aeruginosa* lux culture in a 24-well plate. The 24-well plate was incubated at 37 °C with shaking at 50 rpm. After 24 h incubation, suspension was removed, and the samples were washed with PBS to remove loosely adhered bacteria. For the assessment of surface adhered bacteria, SYTO 9, a green-fluorescent nucleic acid staining agent, was used to label all the bacterial cells by penetrating cells membranes. The washed samples were soaked in a dye solution at room temperature in the dark for 15 min. The stained bacterial cells were viewed under a fluorescent microscope using the FITC filter.

## 4.3 Results and discussion

### 4.3.1 Particle assembly and polymer film deposition

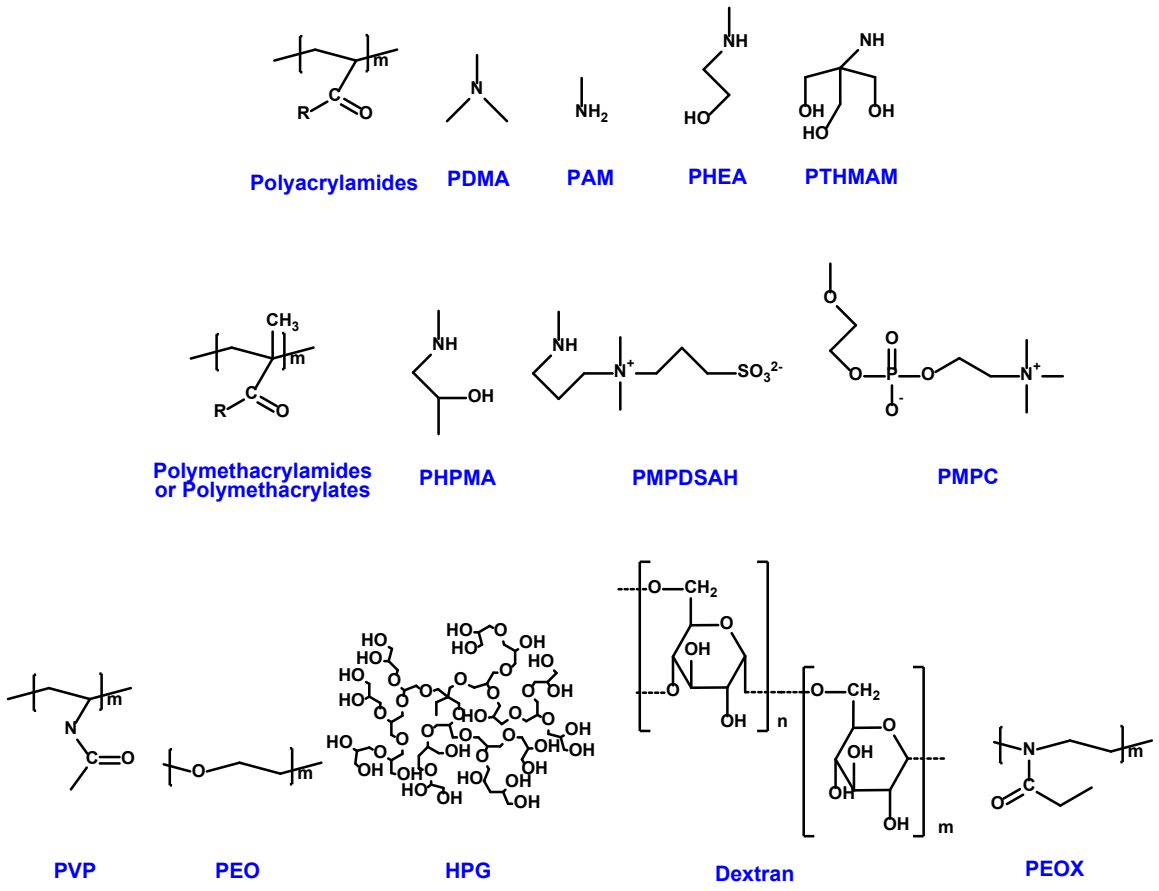


**Figure 4.1 Chemical structures of the hydrophilic polymers screened for LbL assembly.**

**PDMA: Poly(*N*,*N*-dimethylacrylamide), PAM: Polyacrylamide, PHEA: Poly(*N*-hydroxyethylacrylamide), PTHMAM: Poly(*N*-(tris(hydroxymethyl) methyl)acrylamide), PHPMA: Poly(*N*-(2-hydroxypropyl)methacrylamide), PMPDSAH: Poly(*N*-(3-(methacryloylamino) propyl)-*N*,*N*-dimethyl-*N*-(3-sulfopropyl) ammonium hydroxide), PMPC: Poly(2-methacryloyloxyethyl phosphorylcholine), HPG: Hyperbranched polyglycerol, PEO: Polyethylene oxide, PVP: Polyvinylpyrrolidone, Dextran, PEOX: Poly(2-ethyl-2-oxazoline).**

Before the investigation on the formation of LbL assembly by TA and uHMW polymer (**Figure 4.1**), we initially investigated the formation of complexes between TA and different

uHMW polymers based on the understanding the deposition of LbL films on the surface and the formation of their complexes in solution is related. The turbidimetric analysis and DLS measurement were used for monitoring the formation of water-insoluble complexes between TA and the uHMW polymers. Optical images of samples obtained by mixing TA (0.5 mg/mL) and different uHMW polymers (2 mg/mL) in PBS (0.01 M, pH=7.4) are shown in **Figure 4.2**. Among the uHMW polymers tested, PDMA, PMPC, PEO, PVP and PEOX formed cloudy solutions upon mixing with TA suggesting that these neutral polymers are interacting with TA and forming complexes. Other polymers formed clear solutions.

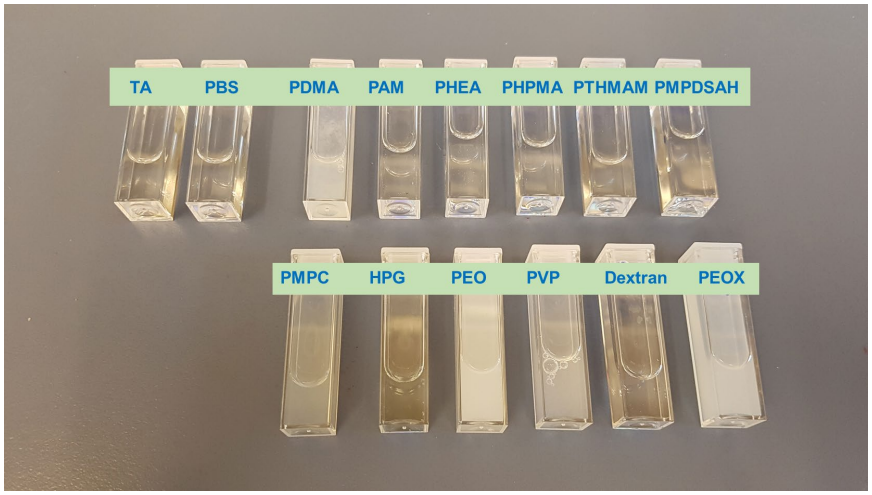


**Figure 4.2 Photographs of mixtures of TA and 12 uHMW polymers with different chemistry.**

**Figure 4.3** shows the turbidity data which further confirms this observation. The PDMA, PMPC, PEO, PVP, and PEOX showed clear increase in turbidity after mixing with TA suggesting their strong interactions with TA potentially *via* hydrogen bonding. This agrees with the previous findings that TA can at as a hydrogen donor to bind polymers (e.g. PEO, PVP) having hydrogen acceptors.

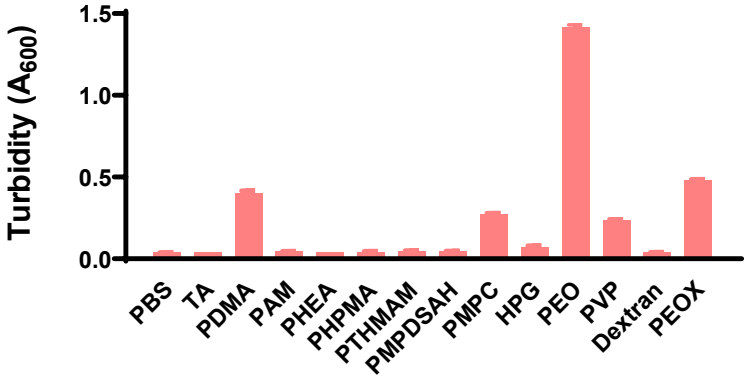


**Figure 4.3 Turbidimetric analysis of TA/uHMW polymer complexes.**

**Significant increase in turbidity was observed in complexes of TA and PDMA, PMPC, PEO, PVP and PEOX.**

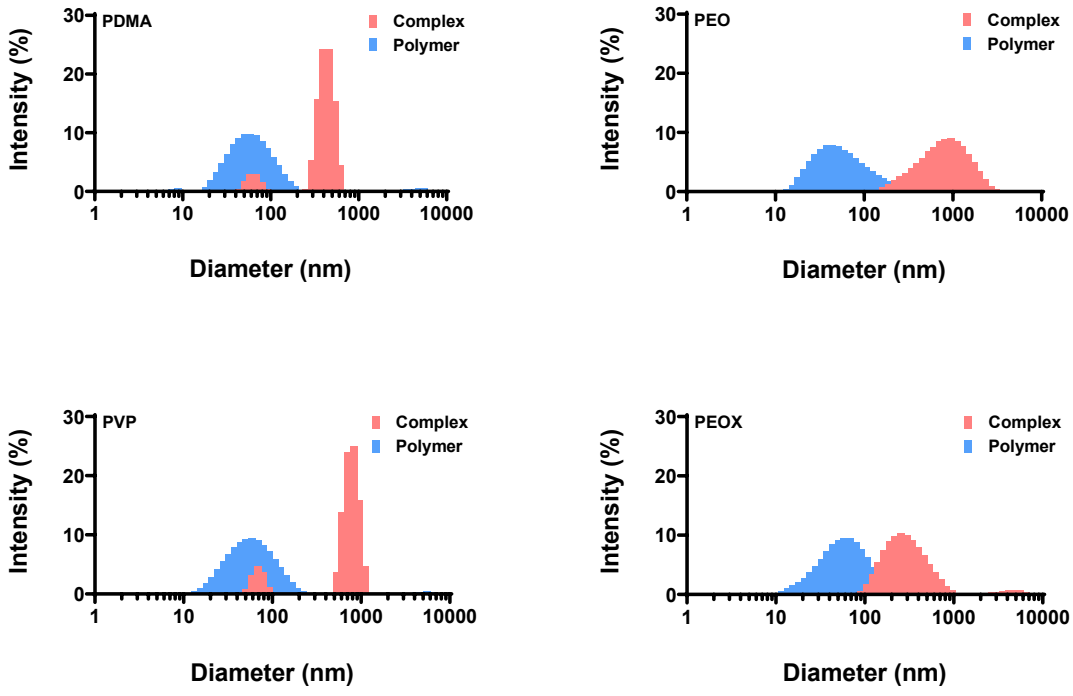


**Figure 4.4 Nanoparticle size distribution of TA/PDMA, TA/PEO, TA/PVP, and TA/PEOX complexes prepared in PBS buffer.**

The complexation of TA and uHMW polymers in the solution was further confirmed by DLS. The complex formation of TA and PDMA, PEO, PVP, and PEOX effectively occurred in PBS buffer as evidenced by the fact that a new peak appeared in the higher particle size region (**Figure 4.4)**. For instance, a new distinctive peak at 400-500 nm was appeared after TA was mixed with uHMW PDMA. This is obviously different from the unimodal peak at 60 nm observed for PDMA alone. In addition, when PMPC, PEO, PVP and PEOX were used for complexing with TA, the average hydrodynamic diameter increased from few tens of nanometers to few hundreds or thousands of nanometers (**Figure 4.5**). Other tested uHMW hydrophilic polymers showed no significant change in average hydrodynamic diameter after complexing with TA. These results demonstrate that only selected polymers can interact with TA under the conditions tested.

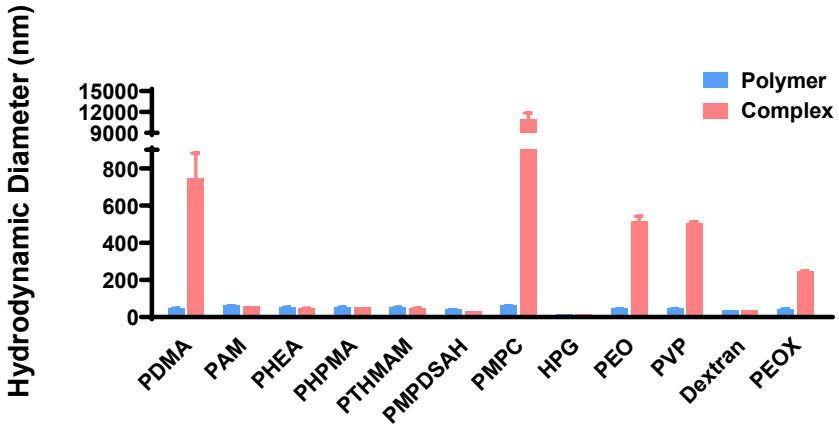


**Figure 4.5 Nanoparticle analysis TA/uHMW polymer complexes.**

**Average hydrodynamic size measured by DLS is shown. The size of the complexes is similar to the pure polymer for most of the groups. The polymers that formed complexes with TA are PDMA, PMPC, PEO, PVP, and PEOX.**

We further explored LbL deposition of TA/uHMW polymer films using five polymers selected from the turbidity and DLS measurements. The polymers that formed stable complexes as evidenced by the large sized complexes were used for LbL assembly. **Figure 4.6** illustrates thickness growth of multilayer thin films prepared *via* dip coating. All systems showed linear or exponential growth mode at pH=7.4 in PBS buffer, except for the TA/PMPC system. The surface multilayers showed an increase with increase in the number of bilayers with TA/PEO system reached a dry thickness about 150 nm at 10 bilayers. The TA/PMPC system exhibited a slow growth in the thickness of surface layer until the multilayer reached 5 bilayers. Unlike other polymers, the continued growth of the TA/PMPC system decreased, and the film showed unstable behavior. The instability of the TA/PMPC multilayers is possibly since PMPC can act as both hydrogen bonding donor and acceptor unlike other polymer systems studied. All other polymer system studied including PDMA, PEO, PVP, and PEOX, can only perform as hydrogen acceptor which is a distinguishable feature.

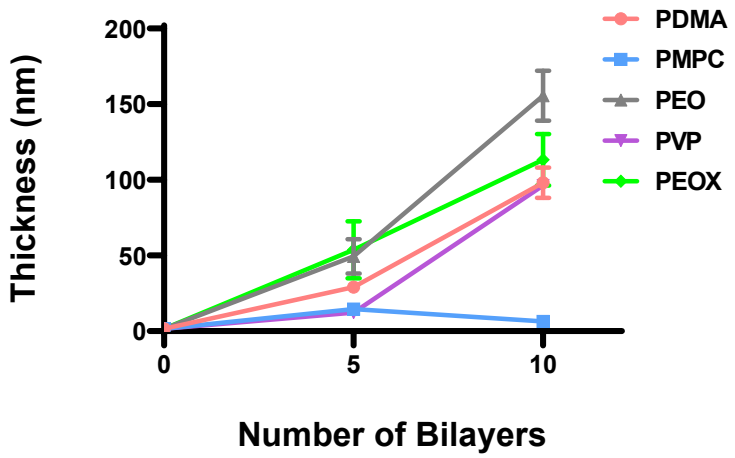


**Figure 4.6 The thickness of multilayer thin films.**

**LbL deposition of TA/PDMA, TA/PMPC, TA/PEO, TA/PVP, and TA/PEOX films on silicon wafer pieces at pH=7.4 monitored by ellipsometry. Multilayer thin films were dried after deposition.**

The successful assembly of TA/uHMW polymer multilayers was further confirmed by ATR-FTIR spectra. As shown in **Figure 4.7**, N-C=O peak from PDMA appear at 1620 $cm^{-1}$, O=P-$O^-$ and C-N-C peaks from PMPC appear at 1240 $cm^{-1}$ and $1080^{-1}$, C-O-C peak from PEO appears at 1100 $cm^{-1}$, N-C=O peak from PVP appears at 1650 $cm^{-1}$, N-C=O peak from PEOX appears at 1630 $cm^{-1}$. Taken together, these data demonstrated the incorporation of uHMW polymers into the multilayer films formed on the surface of silicon wafer pieces.

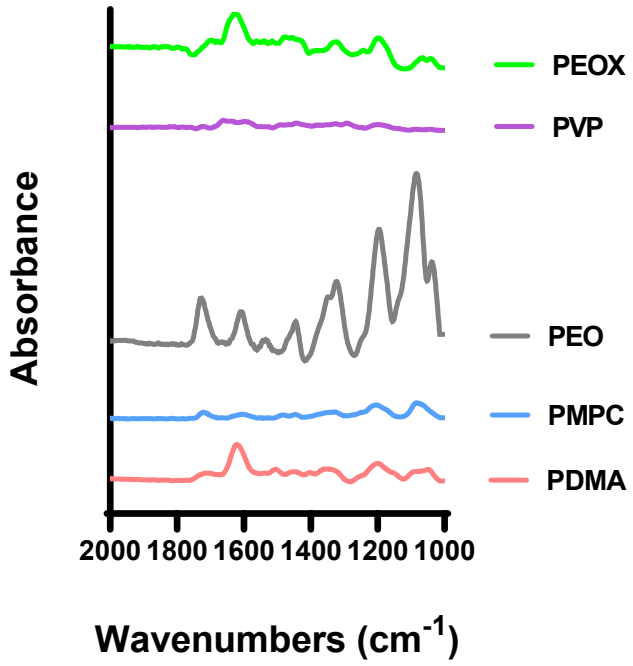


**Figure 4.7 ATR-FTIR spectra of the 5 bilayers of TA/PDMA, TA/PMPC, TA/PEO, TA/PVP and TA/PEOX multilayer films.**

**A silicon wafer piece coated with a single PEI layer was used as the background for subtraction.**

It is generally accepted that hydrophilic surfaces can form a hydrated layer, thus resisting protein adsorption and cell adhesion *via* repulsive hydration forces. Static water contact angle measurement was used to evaluate the surface wettability of TA/uHMW polymer multilayer thin films prepared using polymers with different chemistry and having different number of bilayers. In general, the water contact angles were below 40° for multilayers with TA and uHMW polymers when the uHMW polymers were used as the outer most layer. The water contact angle of the surface also depends on the nature of the uHMW polymers used. This is consistent with the fact that all the polymers used for the study are hydrophilic in nature. The 5 bilayers coating showed higher water contact angles than 10 bilayers coating which could be explained by the

high surface roughness of the thicker coating. The slightly higher water contact of 10 bilayer coating TA/PMPC is due to the instability of the coating as explained previously (**Figure 4.8**).

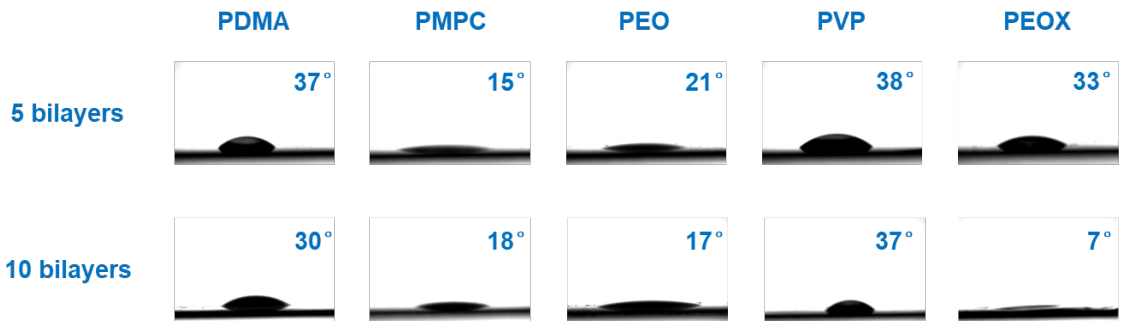


**Figure 4.8 Water contact angles of TA/uHMW multilayer thin films with different polymers.**

**5 bilayers and 10 bilayers prepared on silicon wafer pieces were used for the measurements.**

### 4.3.2 Bacterial adhesion resistance of the multilayer thin films

As discussed previously, the coating prepared with uHMW polymer as outer layer has excellent hydrophilicity, which is anticipated to inhibit the bacteria adhesion. *S. aureus* and *P. aeruginosa* were used to systematically evaluate the bacteria adhesion resistance properties of TA/uHMW polymer multilayers. The data given in **Figure 4.9** and **Figure 4.10** show the adhesion behaviors of *S. aureus* and *P. aeruginosa* on TA/uHMW polymer films prepared with different chemistry and bilayer numbers (n = 5 and 10).

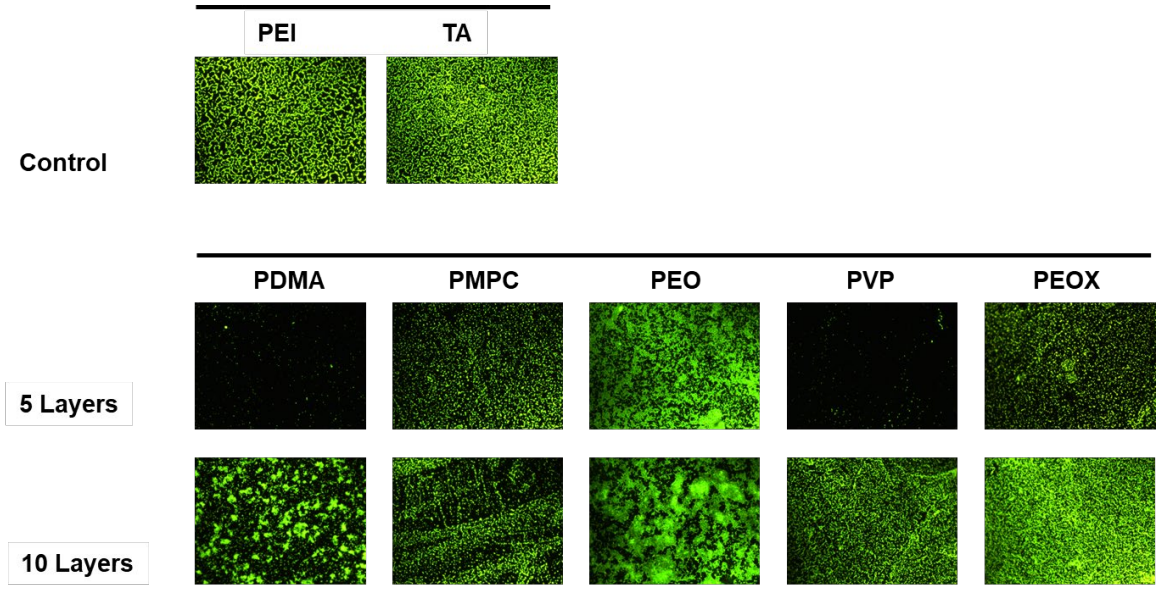


**Figure 4.9 Fluorescent microscopy images of 5 and 10 bilayers of TA/PDMA, TA/PMPC, TA/PEO, TA/PVP and TA/PEOX surfaces after 24 hours incubation in $10^6$ CFU/mL *S. aureus* suspension.**

In general, surfaces assembled with 5 bilayers films show significantly lower bacterial adhesion compared to 10 bilayers films. This could be explained by the high surface roughness of 10 bilayers coatings. The surface coatings prepared with uHMW PDMA and PVP layers have excellent bacterial adhesion resistance properties. The bacterial adhesion resistance obtained for PDMA and PVP multilayer films are similar to that obtained for previously studied thin layer coatings.

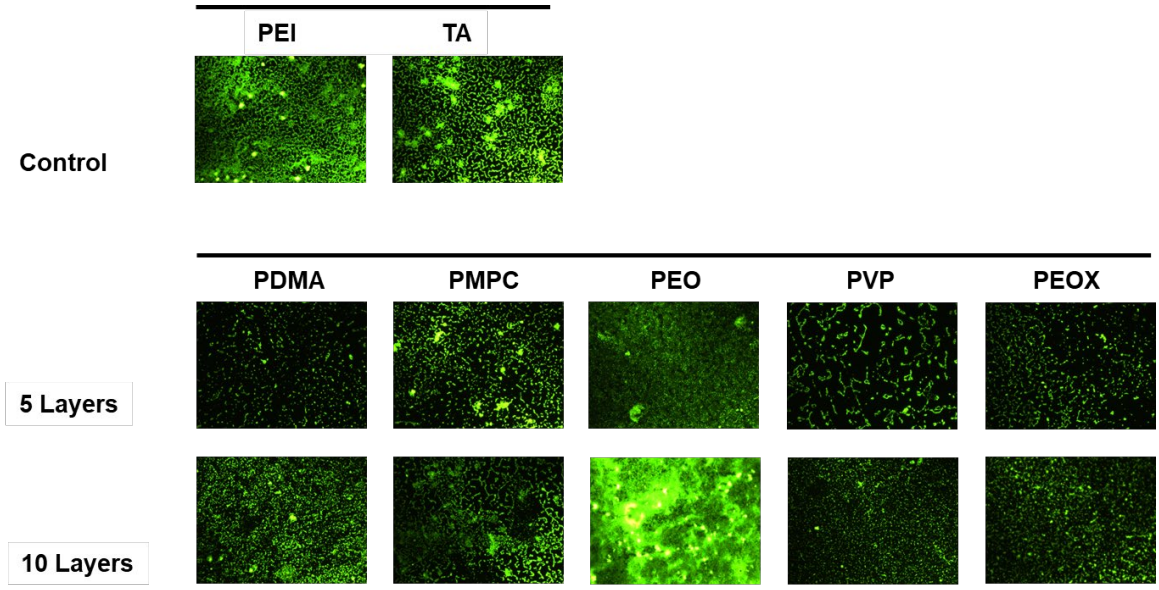


**Figure 4.10 Fluorescent microscopy images of 5 and 10 bilayers of TA/PDMA, TA/PMPC, TA/PEO, TA/PVP, and TA/PEOX surfaces after 24 hours incubation in $10^6$ CFU/mL *P. aeruginosa* suspension.**

## 4.4 Conclusions

In this Chapter, we studied the LBL assembly of hydrophilic polymers with a polyphenol named TA, towards the developed of thicker infection-resistant surfaces. The assembly process was monitored by ellipsometry, which confirmed the formation of multilayer films on silicon wafers. The surface chemical compositions were characterized by ATR-FTIR. Furthermore, all TA/uHMW polymer multilayered films show high hydrophilicity, with a water contact angle lower than 40°. In terms of preventing infection, multilayered films with selected polymer chemistry and less bilayer numbers demonstrated higher resistance towards bacterial colonization.

# Chapter 5: Conclusions and future directions

## 5.1 Conclusions

The common thread linking all chapters of this thesis together is the overall goal of generating universal antibiofilm coatings on catheter surfaces to inhibit bacterial adhesion and subsequent biofilm formation. To develop facile, universal and effective antifouling coating systems, uHMW antifouling polymers were synthesized and anchored onto substrates using different surface anchoring methods.

In Chapter 2, we developed a novel ultrathin coating with long-term antibiofilm activity based on mussel-inspired surface chemistry. We utilized the interaction between catecholamine and uHMW hydrophilic polymers to generate stable coatings with broad spectrum antibiofilm activity. We used bacterial adhesion assays as an initial screening method to identify coating compositions that give superior performance and found that only selected polymers, catecholamine and molecular weights gave promising antifouling activity. The optimized 19 nm coating demonstrated excellent antifouling and antibiofilm properties (>4 weeks) against diverse bacteria ($\sim 10^8$ CFU/mL) in shaking and flow conditions. The ultrathin coating is effective on diverse substrates including metals and polymeric substrates. The coating was successfully adapted to commercial catheters and demonstrated efficacy both *in vitro* and *in vivo*.

The one-step modification strategy we used to impart surface functionalities in Chapter 2 was the catecholamine-assisted co-deposition. Despite successful incorporation of numerous functional agents, little understanding has emerged regarding the mechanisms behind their co-assembly and co-deposition. In Chapter 3, we first investigated the mechanism of the optimized coating formation. Then, we employed 3 hydrophilic polymers with different molecular weights, 6 hydrophilic polymers with different chemistry, and 2 different catecholamines for investigating

the co-assembly and co-deposition process. The molecular weight and chemistry of the hydrophilic polymers is found to influence the interaction between polycatecholamine and the hydrophilic polymers, thus plays an important role in the aqueous self-assembly in solution to nanoaggregates, its formation kinetics, steric stabilization, and subsequent surface deposition. The type of catecholamine influences the properties of the coating less in comparison to the molecular weight and chemistry of the hydrophilic polymer.

In Chapter 4, we studied the LBL assembly of hydrophilic polymers with a polyphenol named TA, towards the developed of thicker infection-resistant surfaces. The assembly process was monitored by ellipsometry, which confirmed the formation of multilayer films on silicon wafers. The surface chemical compositions were characterized by ATR-FTIR. Furthermore, all TA/uHMW polymer multilayered films show high hydrophilicity, with a water contact angle lower than 40°. In terms of preventing infection, multilayered films with selected polymer chemistry and less bilayer numbers demonstrated higher resistance towards bacterial colonization.

## 5.2 Future directions

Although the findings in the conclusions upheld the stated hypothesis, further studies are still required to improve the coating's structure as well as validate the translational potential of the currently optimized coating.

### 5.2.1 Large animal studies for the optimized PDA/PDMA binary coating

In Chapter 2, we used our previously established mice model to study the efficacy of the PDA/uHMW PDMA binary coating against bacterial adhesion and biofilm [217]. The optimized antifouling coating reduced bacterial colonization on catheter in animal bladders for one week. To further evaluate the coating for human catheters, a porcine as the experimental animal and

UPEC as the infected bacteria should be selected for the *in vivo* experiments as they provide a realistic condition that mimics the human urinary tract infection and are accessible for laboratory testing.

### 5.2.2 Influence of polymer concentration on the binary coating formation

In Chapter 3, we systematically investigated the effects of molecular weight and chemistry of the hydrophilic polymers on the binary coating formation. As demonstrated in Chapter 2, polymer concentration of the mixing solution also affected the coating's antibiofilm activity. Further studies on how hydrophilic polymer concentration affects the coating's structure should be performed.

### 5.2.3 Construction of multifunctional coatings

In Chapter 4, we construct antifouling coatings with controllable thickness *via* LbL assembly. Since TA is negatively charged, it can interact with cationic antibiotics *via* electrostatic interaction. We can further introduce those positively charged antibiotics into the platform we built in Chapter 4 to construct multifunctional coatings containing both antifouling and antimicrobial components.

## Bibliography

1) Saint, S., Clinical and economic consequences of nosocomial catheter-related bacteriuria. American Journal of Infection Control 2000, 28 (1), 68-75.

2) Trautner, B. W.; Hull, R. A.; Darouiche, R. O., Prevention of catheter-associated urinary tract infection. Current Opinion in Infectious Diseases 2005, 18 (1), 37-41.

3) Singha, P.; Locklin, J.; Handa, H., A review of the recent advances in antimicrobial coatings for urinary catheters. Acta Biomaterialia 2017, 50, 20-40.

4) Lawrence, E. L.; Turner, I. G., Materials for urinary catheters: a review of their history and development in the UK. Medical Engineering & Physics 2005, 27 (6), 443-453.

5) Zhu, Z. L.; Wang, Z. P.; Li, S. H.; Yuan, X., Antimicrobial strategies for urinary catheters. Journal of Biomedical Materials Research Part A 2019, 107 (2), 445-467.

6) Foxman, B., The epidemiology of urinary tract infection. Nature Reviews Urology 2010, 7 (12), 653-660.

7) Meddings, J.; Rogers, M. A. M.; Krein, S. L.; Fakih, M. G.; Olmsted, R. N.; Saint, S., Reducing unnecessary urinary catheter use and other strategies to prevent catheter-associated urinary tract infection: an integrative review. BMJ Quality & Safety 2014, 23 (4), 277-289.

8) Francolini, I.; Donelli, G., Prevention and control of biofilm-based medical-device-related infections. FEMS Immunology and Medical Microbiology 2010, 59 (3), 227-238.

9) Lundeberg, T., Prevention of catheter-associated urinary-tract infections by use of silver-impregnated catheters. Lancet 1986, 2 (8514), 1031-1031.

10) Siddiq, D. M.; Darouiche, R. O., New strategies to prevent catheter-associated urinary tract infections. Nature Reviews Urology 2012, 9 (6), 305-314.

11) Lederer, J. W.; Jarvis, W. R.; Thomas, L.; Ritter, J., Multicenter cohort study to assess the impact of a silver-alloy and hydrogel-coated urinary catheter on symptomatic catheter-associated urinary tract infections. Journal of Wound Ostomy and Continence Nursing 2014, 41 (5), 473-480.

12) Stenzelius, K.; Laszlo, L.; Madeja, M.; Pessah-Rasmusson, H.; Grabe, M., Catheter-associated urinary tract infections and other infections in patients hospitalized for acute stroke: A prospective cohort study of two different silicone catheters. Scandinavian Journal of Urology 2016, 50 (6), 483-488.

13) Johnson, J. R.; Johnston, B.; Kuskowski, M. A., In vitro comparison of nitrofurazone- and silver alloy-coated foley catheters for contact-dependent and diffusible inhibition of urinary tract infection-associated microorganisms. Antimicrobial Agents and Chemotherapy 2012, 56 (9), 4969-4972.

14) Lee, S. J.; Kim, S. W.; Cho, Y. H.; Shin, W. S.; Lee, S. E.; Kim, C. S.; Hong, S. J.; Chung, B. Y. H.; Kim, J. J.; Yoon, M. S., A comparative multicentre study on the incidence of catheter-associated urinary tract infection between nitrofurazone-coated and silicone catheters. International Journal of Antimicrobial Agents 2004, 24, S65-S69.

15) Darouiche, R. O.; Smith, J. A.; Hanna, H.; Dhabuwala, C. B.; Steiner, M. S.; Babaian, R. J.; Boone, T. B.; Scardino, P. T.; Thornby, J. I.; Raad, II, Efficacy of antimicrobial-impregnated bladder catheters in reducing catheter-associated bacteriuria: A prospective, randomized, multicenter clinical trial. Urology 1999, 54 (6), 976-981.

16) Segev, G.; Bankirer, T.; Steinberg, D.; Duvdevani, M.; Shapur, N. K.; Friedman, M.; Lavy, E., Evaluation of urinary catheters coated with sustained-release varnish of chlorhexidine in

mitigating biofilm formation on urinary catheters in dogs. Journal of Veterinary Internal Medicine 2013, 27 (1), 39-46.

17) Hachem, R.; Reitzel, R.; Borne, A.; Jiang, Y.; Tinkey, P.; Uthamanthil, R.; Chandra, J.; Ghannoum, M.; Raad, I., Novel antiseptic urinary catheters for prevention of urinary tract infections: correlation of in vivo and in vitro test results. Antimicrobial Agents and Chemotherapy 2009, 53 (12), 5145-5149.

18) Li, X.; Li, P.; Saravanan, R.; Basu, A.; Mishra, B.; Lim, S. H.; Su, X. D.; Tambyah, P. A.; Leong, S. S. J., Antimicrobial functionalization of silicone surfaces with engineered short peptides having broad spectrum antimicrobial and salt-resistant properties. Acta Biomaterialia 2014, 10 (1), 258-266.

19) Lim, K. Y.; Chua, R. R. Y.; Bow, H.; Tambyah, P. A.; Hadinoto, K.; Leong, S. S. J., Development of a catheter functionalized by a polydopamine peptide coating with antimicrobial and antibiofilm properties. Acta Biomaterialia 2015, 15, 127-138.

20) Yu, K.; Lo, J. C. Y.; Yan, M.; Yang, X. Q.; Brooks, D. E.; Hancock, R. E. W.; Lange, D.; Kizhakkedathu, J. N., Anti-adhesive antimicrobial peptide coating prevents catheter associated infection in a mouse urinary infection model. Biomaterials 2017, 116, 69-81.

21) Curtin, J. J.; Donlan, R. M., Using bacteriophages to reduce formation of catheter-associated biofilms by Staphylococcus epidermidis. Antimicrobial Agents and Chemotherapy 2006, 50 (4), 1268-1275.

22) Lehman, S. M.; Donlan, R. M., Bacteriophage-mediated control of a two-species biofilm formed by microorganisms causing catheter-associated urinary tract infections in an in vitro urinary catheter model. Antimicrobial Agents and Chemotherapy 2015, 59 (2), 1127-1137.

23) Regev-Shoshani, G.; Ko, M.; Miller, C.; Av-Gay, Y., Slow release of nitric oxide from charged catheters and its effect on biofilm formation by Escherichia coli. Antimicrobial Agents and Chemotherapy 2010, 54 (1), 273-279.

24) Regev-Shoshani, G.; Ko, M.; Crowe, A.; Av-Gay, Y., Comparative efficacy of commercially available and emerging antimicrobial urinary catheters against bacteriuria caused by E.coli In vitro. Urology 2011, 78 (2), 334-339.

25) Tunney, M. M.; Gorman, S. P., Evaluation of a poly(vinyl pyrollidone)-coated biomaterial for urological use. Biomaterials 2002, 23 (23), 4601-4608.

26) Park, J. H.; Cho, Y. W.; Kwon, I. C.; Jeong, S. Y.; Bae, Y. H., Assessment of PEO/PTMO multiblock copolymer/segmented polyurethane blends as coating materials for urinary catheters: in vitro bacterial adhesion and encrustation behavior. Biomaterials 2002, 23 (19), 3991-4000.

27) Blanco, C. D.; Ortner, A.; Dimitrov, R.; Navarro, A.; Mendoza, E.; Tzanov, T., Building an antifouling zwitterionic coating on urinary catheters using an enzymatically triggered bottom-up approach. ACS Applied Materials & Interfaces 2014, 6 (14), 11385-11393.

28) Ruggieri, M. R.; Hanno, P. M.; Levin, R. M., Reduction of bacterial adherence of catheter surface with heparin. Journal of Urology 1987, 138 (2), 423-426.

29) Cloutier, M.; Mantovani, D.; Rosei, F., Antibacterial coatings: challenges, perspectives, and opportunities. Trends in Biotechnology 2015, 33 (11), 637-652.

30) Coad, B. R.; Griesser, H. J.; Peleg, A. Y.; Traven, A., Anti-infective surface coatings: design and therapeutic promise against device-associated infections. Plos Pathogens 2016, 12 (6). 1005598.

31) Campoccia, D.; Montanaro, L.; Arciola, C. R., A review of the biomaterials technologies for infection-resistant surfaces. Biomaterials 2013, 34 (34), 8533-8554.

32) Banerjee, I.; Pangule, R. C.; Kane, R. S., Antifouling coatings: recent developments in the design of surfaces that prevent fouling by proteins, bacteria, and marine Organisms. Advanced Materials 2011, 23 (6), 690-718.

33) Rana, D.; Matsuura, T., Surface modifications for antifouling membranes. Chemical Reviews 2010, 110 (4), 2448-2471.

34) Chen, S. F.; Li, L. Y.; Zhao, C.; Zheng, J., Surface hydration: Principles and applications toward low-fouling/nonfouling biomaterials. Polymer 2010, 51 (23), 5283-5293.

35) Howell, C.; Grinthal, A.; Sunny, S.; Aizenberg, M.; Aizenberg, J., Designing liquid-infused surfaces for medical applications: A review. Advanced Materials 2018, 30 (50), 1802724.

36) Kugel, A.; Stafslien, S.; Chisholm, B. J., Antimicrobial coatings produced by "tethering" biocides to the coating matrix: A comprehensive review. Progress in Organic Coatings 2011, 72 (3), 222-252.

37) Hasan, J.; Crawford, R. J.; Lvanova, E. P., Antibacterial surfaces: the quest for a new generation of biomaterials. Trends in Biotechnology 2013, 31 (5), 31-40.

38) Lejars, M.; Margaillan, A.; Bressy, C., Fouling Release Coatings: A nontoxic alternative to biocidal antifouling coatings. Chemical Reviews 2012, 112 (8), 4347-4390.

39) Hetrick, E. M.; Schoenfisch, M. H., Reducing implant-related infections: active release strategies. Chemical Society Reviews 2006, 35 (9), 780-789.

40) Wei, T.; Yu, Q.; Chen, H., Responsive and synergistic antibacterial coatings: Fighting against bacteria in a smart and effective way. Advanced Healthcare Materials 2019, 8 (3), 1801381.

41) Yu, Q. A.; Zhang, Y. X.; Wang, H. W.; Brash, J.; Chen, H., Anti-fouling bioactive surfaces. Acta Biomaterialia 2011, 7 (4), 1550-1557.

42) Wei, Q.; Haag, R., Universal polymer coatings and their representative biomedical applications. Materials Horizons 2015, 2 (6), 567-577.
43) Chu, P. K.; Chen, J. Y.; Wang, L. P.; Huang, N., Plasma-surface modification of biomaterials. Materials Science & Engineering R-Reports 2002, 36 (5-6), 143-206.
44) Wise, S. G.; Waterhouse, A.; Kondyurin, A.; Bilek, M. M.; Weiss, A. S., Plasma-based biofunctionalization of vascular implants. Nanomedicine 2012, 7 (12), 1907-1916.
45) Morent, R.; De Geyter, N.; Desmet, T.; Dubruel, P.; Leys, C., Plasma surface modification of biodegradable polymers: A review. Plasma Processes and Polymers 2011, 8 (3), 171-190.
46) Desmet, T.; Morent, R.; De Geyter, N.; Leys, C.; Schacht, E.; Dubruel, P., Nonthermal plasma technology as a versatile strategy for polymeric biomaterials surface modification: A review. Biomacromolecules 2009, 10 (9), 2351-2378.
47) Jhong, J. F.; Venault, A.; Hou, C. C.; Chen, S. H.; Wei, T. C.; Zheng, J.; Huang, J.; Chang, Y., Surface Zwitterionization of expanded poly(tetrafluoroethylene) membranes via atmospheric plasma-induced polymerization for enhanced skin wound healing. ACS Applied Materials & Interfaces 2013, 5 (14), 6732-6742.
48) Li, M.; Neoh, K. G.; Kang, E. T.; Lau, T.; Chiong, E., Surface modification of silicone with covalently immobilized and crosslinked agarose for potential application in the inhibition of infection and omental wrapping. Advanced Functional Materials 2014, 24 (11), 1631-1643.
49) Yao, C.; Li, X. S.; Neoh, K. G.; Shi, Z. L.; Kang, E. T., Surface modification and antibacterial activity of electrospun polyurethane fibrous membranes with quaternary ammonium moieties. Journal of Membrane Science 2008, 320 (1-2), 259-267.

50) Yao, C.; Li, X. S.; Neoh, K. G.; Shi, Z. L.; Kang, E. T., Antibacterial activities of surface modified electrospun poly(vinylidene fluoride-co-hexafluoropropylene) (PVDF-HFP) fibrous membranes. Applied Surface Science 2009, 255 (6), 3854-3858.

51) Yao, C.; Li, X. S.; Neoh, K. G.; Shi, Z. L.; Kang, E. T., Antibacterial poly(D,L-lactide) (PDLLA) fibrous membranes modified with quaternary ammonium. Chinese Journal of Polymer Science 2010, 28 (4), 581-588.

52) Vreuls, C.; Zocchi, G.; Thierry, B.; Garitte, G.; Griesser, S. S.; Archambeau, C.; Van de Weerdt, C. V.; Martial, J.; Griesser, H., Prevention of bacterial biofilms by covalent immobilization of peptides onto plasma polymer functionalized substrates. Journal of Materials Chemistry 2010, 20 (37), 8092-8098.

53) Vasilev, K.; Sah, V.; Anselme, K.; Ndi, C.; Mateescu, M.; Dollmann, B.; Martinek, P.; Ys, H.; Ploux, L.; Griesser, H. J., Tunable antibacterial coatings that support mammalian cell growth. Nano Letters 2010, 10 (1), 202-207.

54) Fielding, G. A.; Roy, M.; Bandyopadhyay, A.; Bose, S., Antibacterial and biological characteristics of silver containing and strontium doped plasma sprayed hydroxyapatite coatings. Acta Biomaterialia 2012, 8 (8), 3144-3152.

55) Zhi, Z. L.; Su, Y. J.; Xi, Y. W.; Tian, L.; Xu, M.; Wang, Q. Q.; Padidan, S.; Li, P.; Huang, W., Dual-functional polyethylene glycol-b-polyhexanide surface coating with in vitro and in vivo antimicrobial and antifouling activities. ACS Applied Materials & Interfaces 2017, 9 (12), 10383-10397.

56) Gao, Q.; Yu, M.; Su, Y. J.; Xie, M. H.; Zhao, X.; Li, P.; Ma, P. X., Rationally designed dual functional block copolymers for bottlebrush-like coatings: In vitro and in vivo antimicrobial, antibiofilm, and antifouling properties. Acta Biomaterialia 2017, 51, 112-124.

57) Decher, G.; Hong, J. D.; Schmitt, J., Buildup of ultrathin multilayer films by a self-assembly process. 3. Consecutively alternating adsorption of anionic and cationic polyelectrolytes on charged surfaces. Thin Solid Films 1992, 210 (1-2), 831-835.
58) Zhang, X. L.; Xu, Y.; Zhang, X.; Wu, H.; Shen, J. B.; Chen, R.; Xiong, Y.; Li, J.; Guo, S. Y., Progress on the layer-by-layer assembly of multilayered polymer composites: Strategy, structural control and applications. Progress in Polymer Science 2019, 89, 76-107.
59) Xiao, F. X.; Pagliaro, M.; Xu, Y. J.; Liu, B., Layer-by-layer assembly of versatile nanoarchitectures with diverse dimensionality: a new perspective for rational construction of multilayer assemblies. Chemical Society Reviews 2016, 45 (11), 3088-3121.
60) Shiratori, S. S.; Rubner, M. F., pH-dependent thickness behavior of sequentially adsorbed layers of weak polyelectrolytes. Macromolecules 2000, 33 (11), 4213-4219.
61) Ren, K. F.; Wang, Y. X.; Ji, J.; Lin, Q. K.; Shen, J. C., Construction and deconstruction of PLL/DNA multilayered films for DNA delivery: Effect of ionic strength. Colloids and Surfaces B-Biointerfaces 2005, 46 (2), 63-69.
62) Stockton, W. B.; Rubner, M. F., Molecular-level processing of conjugated polymers. 4. Layer-by-layer manipulation of polyaniline via hydrogen-bonding interactions. Macromolecules 1997, 30 (9), 2717-2725.
63) Sukhishvili, S. A.; Granick, S., Layered, erasable polymer multilayers formed by hydrogen-bonded sequential self-assembly. Macromolecules 2002, 35 (1), 301-310.
64) Sukhishvili, S. A.; Granick, S., Layered, erasable, ultrathin polymer films. Journal of the American Chemical Society 2000, 122 (39), 9550-9551.
65) Erel-Unal, I.; Sukhishvili, S. A., Hydrogen-bonded multilayers of a neutral polymer and a polyphenol. Macromolecules 2008, 41 (11), 3962-3970.

66) An, Q.; Huang, T.; Shi, F., Covalent layer-by-layer films: chemistry, design, and multidisciplinary applications. Chemical Society Reviews 2018, 47 (13), 5061-5098.
67) Lee, H.; Lee, Y.; Statz, A. R.; Rho, J.; Park, T. G.; Messersmith, P. B., Substrate-independent layer-by-layer assembly by using mussel-adhesive-inspired polymers. Advanced Materials 2008, 20 (9), 1619-1623.
68) Such, G. K.; Quinn, J. F.; Quinn, A.; Tjipto, E.; Caruso, F., Assembly of ultrathin polymer multilayer films by click chemistry. Journal of the American Chemical Society 2006, 128 (29), 9318-9319.
69) Rahim, M. A.; Ejima, H.; Cho, K. L.; Kempe, K.; Mullner, M.; Best, J. P.; Caruso, F., Coordination-driven multistep assembly of metal-polyphenol films and capsules. Chemistry of Materials 2014, 26 (4), 1645-1653.
70) Kim, S.; Kim, D. S.; Kang, S. M., Reversible layer-by-layer deposition on solid substrates inspired by mussel byssus cuticle. Chemistry-an Asian Journal 2014, 9 (1), 63-66.
71) Boulmedais, F.; Frisch, B.; Etienne, O.; Lavalle, P.; Picart, C.; Ogier, J.; Voegel, J. C.; Schaaf, P.; Egles, C., Polyelectrolyte multilayer films with pegylated polypeptides as a new type of anti-microbial protection for biomaterials. Biomaterials 2004, 25 (11), 2003-2011.
72) Tang, L.; Gu, W. Y.; Yi, P.; Bitter, J. L.; Hong, J. Y.; Fairbrother, D. H.; Chen, K. L., Bacterial anti-adhesive properties of polysulfone membranes modified with polyelectrolyte multilayers. Journal of Membrane Science 2013, 446, 201-211.
73) Zhu, X. Y.; Guo, S. F.; Janczewski, D.; Velandia, F. J. P.; Teo, S. L. M.; Vancso, G. J., Multilayers of fluorinated amphiphilic polyions for marine fouling prevention. Langmuir 2014, 30 (1), 288-296.

74) Tardy, B. L.; Richardson, J. J.; Nithipipat, V.; Kempe, K.; Guo, J. L.; Cho, K. L.; Rahim, M. A.; Ejima, H.; Caruso, F., Protein adsorption and coordination-based end-tethering of functional polymers on metal-phenolic network films. Biomacromolecules 2019, 20 (3), 1421-1428.
75) Cerkez, I.; Kocer, H. B.; Worley, S. D.; Broughton, R. M.; Huang, T. S., N-Halamine biocidal coatings via a layer-by-layer assembly technique. Langmuir 2011, 27 (7), 4091-4097.
76) Tang, Y. W.; Zhao, Y.; Wang, H. X.; Gao, Y.; Liu, X.; Wang, X. G.; Lin, T., Layer-by-layer assembly of antibacterial coating on interbonded 3D fibrous scaffolds and its cytocompatibility assessment. Journal of Biomedical Materials Research Part A 2012, 100A (8), 2071-2078.
77) Chuang, H. F.; Smith, R. C.; Hammond, P. T., Polyelectrolyte multilayers for tunable release of antibiotics. Biomacromolecules 2008, 9 (6), 1660-1668.
78) Moskowitz, J. S.; Blaisse, M. R.; Samuel, R. E.; Hsu, H. P.; Harris, M. B.; Martin, S. D.; Lee, J. C.; Spector, M.; Hammond, P. T., The effectiveness of the controlled release of gentamicin from polyelectrolyte multilayers in the treatment of Staphylococcus aureus infection in a rabbit bone model. Biomaterials 2010, 31 (23), 6019-6030.
79) Zhuk, I.; Jariwala, F.; Attygalle, A. B.; Wu, Y.; Libera, M. R.; Sukhishvili, S. A., Self-defensive layer-by-layer films with bacteria-triggered antibiotic release. ACS Nano 2014, 8 (8), 7733-7745.
80) Pavlukhina, S.; Lu, Y. M.; Patimetha, A.; Libera, M.; Sukhishvili, S., Polymer multilayers with pH-triggered release of antibacterial agents. Biomacromolecules 2010, 11 (12), 3448-3456.
81) Pavlukhina, S.; Zhuk, I.; Mentbayeva, A.; Rautenberg, E.; Chang, W.; Yu, X. J.; van de Belt-Gritter, B.; Busscher, H. J.; van der Mei, H. C.; Sukhishvili, S. A., Small-molecule-hosting nanocomposite films with multiple bacteria-triggered responses. NPG Asia Materials 2014, 6, e121.

82) Cado, G.; Aslam, R.; Seon, L.; Garnier, T.; Fabre, R.; Parat, A.; Chassepot, A.; Voegel, J. C.; Senger, B.; Schneider, F.; Frere, Y.; Jierry, L.; Schaaf, P.; Kerdjoudj, H.; Metz-Boutigue, M. H.; Boulmedais, F., Self-defensive biomaterial coating against bacteria and yeasts: Polysaccharide multilayer film with embedded antimicrobial peptide. Advanced Functional Materials 2013, 23 (38), 4801-4809.

83) Fu, J. H.; Ji, J.; Yuan, W. Y.; Shen, J. C., Construction of anti-adhesive and antibacterial multilayer films via layer-by-layer assembly of heparin and chitosan. Biomaterials 2005, 26 (33), 6684-6692.

84) Yang, W. J.; Pranantyo, D.; Neoh, K. G.; Kang, E. T.; Teo, S. L. M.; Rittschof, D., Layer-by-layer click deposition of functional polymer coatings for combating marine biofouling. Biomacromolecules 2012, 13 (9), 2769-2780.

85) Lee, H.; Dellatore, S. M.; Miller, W. M.; Messersmith, P. B., Mussel-inspired surface chemistry for multifunctional coatings. Science 2007, 318 (5849), 426-430.

86) Ball, V.; Del Frari, D.; Toniazzo, V.; Ruch, D., Kinetics of polydopamine film deposition as a function of pH and dopamine concentration: Insights in the polydopamine deposition mechanism. Journal of Colloid and Interface Science 2012, 386, 366-372.

87) Della Vecchia, N. F.; Luchini, A.; Napolitano, A.; D'Errico, G.; Vitiello, G.; Szekely, N.; d'Ischia, M.; Paduano, L., Tris buffer modulates polydopamine growth, aggregation, and paramagnetic properties. Langmuir 2014, 30 (32), 9811-9818.

88) Ponzio, F.; Barthes, J.; Bour, J.; Michel, M.; Bertani, P.; Hemmerle, J.; d'Ischia, M.; Ball, V., Oxidant control of polydopamine surface chemistry in acids: A mechanism-based entry to superhydrophilic-superoleophobic coatings. Chemistry of Materials 2016, 28 (13), 4697-4705.

89) Du, X.; Li, L. X.; Li, J. S.; Yang, C. W.; Frenkel, N.; Welle, A.; Heissler, S.; Nefedov, A.; Grunze, M.; Levkin, P. A., UV-triggered dopamine polymerization: Control of polymerization, surface coating, and photopatterning. Advanced Materials 2014, 26 (47), 8029-8033.
90) Lee, M.; Lee, S. H.; Oh, I. K.; Lee, H., Microwave-accelerated rapid, chemical oxidant-free, material-independent surface chemistry of poly(dopamine). Small 2017, 13 (4), 1600443.
91) Della Vecchia, N. F.; Avolio, R.; Alfe, M.; Errico, M. E.; Napolitano, A.; d'Ischia, M., Building-block diversity in polydopamine underpins a multifunctional eumelanin-type platform tunable through a quinone control point. Advanced Functional Materials 2013, 23 (10), 1331-1340.
92) Kang, S. M.; Rho, J.; Choi, I. S.; Messersmith, P. B.; Lee, H., Norepinephrine: material-independent, multifunctional surface modification reagent. Journal of the American Chemical Society 2009, 131 (37), 13224-13225.
93) Hong, S.; Kim, J.; Na, Y. S.; Park, J.; Kim, S.; Singha, K.; Im, G. I.; Han, D. K.; Kim, W. J.; Lee, H., Poly(norepinephrine): Ultrasmooth material-independent surface chemistry and nanodepot for nitric oxide. Angewandte Chemie-International Edition 2013, 52 (35), 9187-9191.
94) Kang, S. M.; Hwang, N. S.; Yeom, J.; Park, S. Y.; Messersmith, P. B.; Choi, I. S.; Langer, R.; Anderson, D. G.; Lee, H., One-step multipurpose surface functionalization by adhesive catecholamine. Advanced Functional Materials 2012, 22 (14), 2949-2955.
95) Qiu, W. Z.; Yang, H. C.; Xu, Z. K., Dopamine-assisted co-deposition: An emerging and promising strategy for surface modification. Advances in Colloid and Interface Science 2018, 256, 111-125.

96) Yang, H. C.; Liao, K. J.; Huang, H.; Wu, Q. Y.; Wan, L. S.; Xu, Z. K., Mussel-inspired modification of a polymer membrane for ultra-high water permeability and oil-in-water emulsion separation. Journal of Materials Chemistry A 2014, 2 (26), 10225-10230.
97) Lv, Y.; Yang, S. J.; Du, Y.; Yang, H. C.; Xu, Z. K., Co-deposition kinetics of polydopamine/ polyethyleneimine coatings: Effects of solution composition and substrate surface. Langmuir 2018, 34 (44), 13123-13131.
98) Kang, S. M.; Ryou, M. H.; Choi, J. W.; Lee, H., Mussel- and diatom-inspired silica coating on separators yields improved power and safety in Li-ion batteries. Chemistry of Materials 2012, 24 (17), 3481-3485.
99) Zhang, Y.; Thingholm, B.; Goldie, K. N.; Ogaki, R.; Stadler, B., Assembly of poly(dopamine) films mixed with a nonionic polymer. Langmuir 2012, 28 (51), 17585-17592.
100) Mateescu, M.; Metz-Boutigue, M. H.; Bertani, P.; Ball, V., Polyelectrolytes to produce nanosized polydopamine. Journal of Colloid and Interface Science 2016, 469, 184-190.
101) Liu, Y.; Qiu, W. Z.; Yang, H. C.; Qian, Y. C.; Huang, X. J.; Xu, Z. K., Polydopamine-assisted deposition of heparin for selective adsorption of low-density lipoprotein. RSC Advances 2015, 5 (17), 12922-12930.
102) You, I.; Kang, S. M.; Byun, Y.; Lee, H., Enhancement of blood compatibility of poly(urethane) substrates by mussel-inspired adhesive heparin coating. Bioconjugate Chemistry 2011, 22 (7), 1264-1269.
103) Park, J. Y.; Yeom, J.; Kim, J. S.; Lee, M.; Lee, H.; Nam, Y. S., Cell-repellant dextran coatings of porous titania using mussel adhesion chemistry. Macromolecular Bioscience 2013, 13 (11), 1511-1519.

104) Hong, S.; Yang, K.; Kang, B.; Lee, C.; Song, I. T.; Byun, E.; Park, K. I.; Cho, S. W.; Lee, H., Hyaluronic acid catechol: A biopolymer exhibiting a pH-dependent adhesive or cohesive property for human neural stem cell engineering. Advanced Functional Materials 2013, 23 (14), 1774-1780.

105) Hong, D.; Bae, K.; Hong, S. P.; Park, J. H.; Choi, I. S.; Cho, W. K., Mussel-inspired, perfluorinated polydopamine for self-cleaning coating on various substrates. Chemical Communications 2014, 50 (79), 11649-11652.

106) Lee, H.; Lee, K. D.; Pyo, K. B.; Park, S. Y., Catechol-grafted poly(ethylene glycol) for PEGylation on versatile substrates. Langmuir 2010, 26 (6), 3790-3793.

107) Mizrahi, B.; Khoo, X.; Chiang, H. H.; Sher, K. J.; Feldman, R. G.; Lee, J. J.; Irusta, S.; Kohane, D. S., Long-lasting antifouling coating from multi-armed polymer. Langmuir 2013, 29 (32), 10087-10094.

108) Wei, Q.; Becherer, T.; Mutihac, R. C.; Noeske, P. L. M.; Paulus, F.; Haag, R.; Grunwald, I., Multivalent anchoring and cross-linking of mussel-inspired antifouling surface coatings. Biomacromolecules 2014, 15 (8), 3061-3071.

109) Wei, Q.; Becherer, T.; Noeske, P. L. M.; Grunwald, I.; Haag, R., A universal approach to crosslinked hierarchical polymer multilayers as stable and highly effective antifouling coatings. Advanced Materials 2014, 26 (17), 2688-2693.

110) Sundaram, H. S.; Han, X.; Nowinski, A. K.; Brault, N. D.; Li, Y. T.; Ella-Menye, J. R.; Amoaka, K. A.; Cook, K. E.; Marek, P.; Senecal, K.; Jiang, S. Y., Achieving one-step surface coating of highly hydrophilic poly(carboxybetaine methacrylate) polymers on hydrophobic and hydrophilic surfaces. Advanced Materials Interfaces 2014, 1 (6), 1400071.

111) Sundaram, H. S.; Han, X.; Nowinski, A. K.; Ella-Menye, J. R.; Wimbish, C.; Marek, P.; Senecal, K.; Jiang, S. Y., One-step dip coating of zwitterionic sulfobetaine polymers on hydrophobic and hydrophilic surfaces. ACS Applied Materials & Interfaces 2014, 6 (9), 6664-6671.
112) Lee, H.; Rho, J.; Messersmith, P. B., Facile conjugation of biomolecules onto surfaces via mussel adhesive protein inspired coatings. Advanced Materials 2009, 21 (4), 431-434.
113) Li, X.; Cai, T.; Chung, T. S., Anti-fouling behavior of hyperbranched polyglycerol-grafted poly(ether sulfone) hollow fiber membranes for osmotic power generation. Environmental Science & Technology 2014, 48 (16), 9898-9907.
114) Cui, J. W.; Ju, Y.; Liang, K.; Ejima, H.; Lorcher, S.; Gause, K. T.; Richardson, J. J.; Caruso, F., Nanoscale engineering of low-fouling surfaces through polydopamine immobilisation of zwitterionic peptides. Soft Matter 2014, 10 (15), 2656-2663.
115) Karkhanechi, H.; Takagi, R.; Matsuyama, H., Enhanced antibiofouling of RO membranes via polydopamine coating and polyzwitterion immobilization. Desalination 2014, 337, 23-30.
116) Miller, D. J.; Araujo, P. A.; Correia, P. B.; Ramsey, M. M.; Kruithof, J. C.; van Loosdrecht, M. C. M.; Freeman, B. D.; Paul, D. R.; Whiteley, M.; Vrouwenvelder, J. S., Short-term adhesion and long-term biofouling testing of polydopamine and poly(ethylene glycol) surface modifications of membranes and feed spacers for biofouling control. Water Research 2012, 46 (12), 3737-3753.
117) Kim, S.; Moon, J. M.; Choi, J. S.; Cho, W. K.; Kang, S. M., Mussel-inspired approach to constructing robust multilayered alginate films for antibacterial applications. Advanced Functional Materials 2016, 26 (23), 4099-4105.

118) Kim, S.; Girn, T.; Jeong, Y.; Ryu, J. H.; Kang, S. M., Facile construction of robust multilayered PEG films on polydopamine-coated solid substrates for marine antifouling applications. ACS Applied Materials & Interfaces 2018, 10 (9), 7626-7631.
119) Sin, M. C.; Sun, Y. M.; Chang, Y., Zwitterionic-based stainless steel with well-defined polysulfobetaine brushes for general bioadhesive control. ACS Applied Materials & Interfaces 2014, 6 (2), 861-873.
120) Chang, C. C.; Kolewe, K. W.; Li, Y. Y.; Kosif, I.; Freeman, B. D.; Carter, K. R.; Schiffman, J. D.; Emrick, T., Underwater superoleophobic surfaces prepared from polymer zwitterion/dopamine composite coatings. Advanced Materials Interfaces 2016, 3 (6), 1500521.
121) Kolewe, K. W.; Dobosz, K. M.; Rieger, K. A.; Chang, C. C.; Emrick, T.; Schiffman, J. D., Antifouling electrospun nanofiber mats functionalized with polymer zwitterions. ACS Applied Materials & Interfaces 2016, 8 (41), 27585-27593.
122) Dobosz, K. M.; Kuo-LeBlanc, C. A.; Emrick, T.; Schiffman, J. D., Antifouling ultrafiltration membranes with retained pore size by controlled deposition of zwitterionic polymers and poly(ethylene glycol). Langmuir 2019, 35 (5), 1872-1881.
123) Kirschner, A. Y.; Chang, C. C.; Kasemset, S.; Emrick, T.; Freeman, B. D., Fouling-resistant ultrafiltration membranes prepared via co-deposition of dopamine/zwitterion composite coatings. Journal of Membrane Science 2017, 541, 300-311.
124) Zhang, C.; Li, H. N.; Du, Y.; Ma, M. Q.; Xu, Z. K., $CuSO_4/H_2O_2$-triggered polydopamine /poly(sulfobetaine methacrylate) coatings for antifouling membrane surfaces. Langmuir 2017, 33 (5), 1210-1216.

125) Hadjesfandiari, N.; Weinhart, M.; Kizhakkedathu, J. N.; Haag, R.; Brooks, D. E., Development of antifouling and bactericidal coatings for platelet storage bags using dopamine chemistry. Advanced Healthcare Materials 2018, 7 (5), 1700839.
126) Liu, X. Y.; Deng, J.; Ma, L.; Cheng, C.; Nie, C. X.; He, C.; Zhao, C. S., Catechol chemistry inspired approach to construct self-cross-linked polymer nanolayers as versatile biointerfaces. Langmuir 2014, 30 (49), 14905-14915.
127) Liu, C. H.; Lee, J.; Ma, J.; Elimelech, M., Antifouling thin-film composite membranes by controlled architecture of zwitterionic polymer brush layer. Environmental Science & Technology 2017, 51 (4), 2161-2169.
128) He, S.; Zhou, P.; Wang, L. X.; Xiong, X. L.; Zhang, Y. F.; Deng, Y.; Wei, S. C., Antibiotic-decorated titanium with enhanced antibacterial activity through adhesive polydopamine for dental/bone implant. Journal of the Royal Society Interface 2014, 11 (95), 20140169.
129) Shalev, T.; Gopin, A.; Bauer, M.; Stark, R. W.; Rahimipour, S., Non-leaching antimicrobial surfaces through polydopamine bio-inspired coating of quaternary ammonium salts or an ultrashort antimicrobial lipopeptide. Journal of Materials Chemistry 2012, 22 (5), 2026-2032.
130) Han, H.; Wu, J. F.; Avery, C. W.; Mizutani, M.; Jiang, X. M.; Kamigaito, M.; Chen, Z.; Xi, C. W.; Kuroda, K., Immobilization of amphiphilic polycations by catechol functionality for antimicrobial coatings. Langmuir 2011, 27 (7), 4010-4019.
131) Son, H. Y.; Ryu, J. H.; Lee, H.; Nam, Y. S., Silver-polydopamine hybrid coatings of electrospun poly(vinyl alcohol) nanofibers. Macromolecular Materials and Engineering 2013, 298 (5), 547-554.

132) Liu, Z. Y.; Hu, Y. X.; Liu, C. F.; Zhou, Z. Y., Surface-independent one-pot chelation of copper ions onto filtration membranes to provide antibacterial properties. Chemical Communications 2016, 52 (82), 12245-12248.
133) Yang, Z.; Wu, Y. C.; Wang, J. Q.; Cap, B.; Tang, C. Y. Y., In situ reduction of silver by polydopamine: A novel antimicrobial modification of a thin-film composite polyamide membrane. Environmental Science & Technology 2016, 50 (17), 9543-9550.
134) Ding, X.; Yang, C.; Lim, T. P.; Hsu, L. Y.; Engler, A. C.; Hedrick, J. L.; Yang, Y. Y., Antibacterial and antifouling catheter coatings using surface grafted PEG-b-cationic polycarbonate diblock copolymers. Biomaterials 2012, 33 (28), 6593-6603.
135) Yang, W. J.; Cai, T.; Neoh, K. G.; Kang, E. T.; Dickinson, G. H.; Teo, S. L. M.; Rittschof, D., Biomimetic anchors for antifouling and antibacterial polymer brushes on stainless steel. Langmuir 2011, 27 (11), 7065-7076.
136) Yang, C.; Ding, X.; Ono, R. J.; Lee, H.; Hsu, L. Y.; Tong, Y. W.; Hedrick, J.; Yang, Y. Y., Brush-like polycarbonates containing dopamine, cations, and PEG providing a broad-spectrum, antibacterial, and antifouling surface via one-stepc. Advanced Materials 2014, 26 (43), 7346-7351.
137) Wang, B. L.; Jin, T. W.; Han, Y. M.; Shen, C. H.; Li, Q.; Lin, Q. K.; Chen, H., Bio-inspired terpolymers containing dopamine, cations and MPC: a versatile platform to construct a recycle antibacterial and antifouling surface. Journal of Materials Chemistry B 2015, 3 (27), 5501-5510.
138) Sileika, T. S.; Kim, H. D.; Maniak, P.; Messersmith, P. B., Antibacterial performance of polydopamine-modified polymer surfaces containing passive and active components. ACS Applied Materials & Interfaces 2011, 3 (12), 4602-4610.

139) Sadrearhami, Z.; Shafiee, F. N.; Ho, K. K. K.; Kumar, N.; Krasowska, M.; Blencowe, A.; Wong, E. H. H.; Boyer, C., Antibiofilm nitric oxide-releasing polydopamine coatings. ACS Applied Materials & Interfaces 2019, 11 (7), 7320-7329.

140) Sileika, T. S.; Barrett, D. G.; Zhang, R.; Lau, K. H. A.; Messersmith, P. B., Colorless multifunctional coatings inspired by polyphenols found in tea, chocolate, and wine. Angewandte Chemie-International Edition 2013, 52 (41), 10766-10770.

141) Barrett, D. G.; Sileika, T. S.; Messersmith, P. B., Molecular diversity in phenolic and polyphenolic precursors of tannin-inspired nanocoatings. Chemical Communications 2014, 50 (55), 7265-7268.

142) Hong, S.; Yeom, J.; Song, I. T.; Kang, S. M.; Lee, H., Pyrogallol 2-aminoethane: A plant flavonoid-inspired molecule for material-independent surface chemistry. Advanced Materials Interfaces 2014, 1 (4), 1400113.

143) Behboodi-Sadabad, F.; Zhang, H. J.; Trouillet, V.; Welle, A.; Plumere, N.; Levkin, P. A., UV-triggered polymerization, deposition, and patterning of plant phenolic compounds. Advanced Functional Materials 2017, 27 (22), 1700127.

144) Ejima, H.; Richardson, J. J.; Liang, K.; Best, J. P.; van Koeverden, M. P.; Such, G. K.; Cui, J. W.; Caruso, F., One-step assembly of coordination complexes for versatile film and particle engineering. Science 2013, 341 (6142), 154-157.

145) Guo, J. L.; Ping, Y.; Ejima, H.; Alt, K.; Meissner, M.; Richardson, J. J.; Yan, Y.; Peter, K.; von Elverfeldt, D.; Hagemeyer, C. E.; Caruso, F., Engineering multifunctional capsules through the assembly of metal-phenolic networks. Angewandte Chemie-International Edition 2014, 53 (22), 5546-5551.

146) Rahim, M. A.; Kempe, K.; Mullner, M.; Ejima, H.; Ju, Y.; van Koeverden, M. P.; Suma, T.; Braunger, J. A.; Leeming, M. G.; Abrahams, B. F.; Caruso, F., Surface-confined amorphous films from metal-coordinated simple phenolic ligands. Chemistry of Materials 2015, 27 (16), 5825-5832.

147) Pranantyo, D.; Xu, L. Q.; Neoh, K. G.; Kang, E. T.; Teo, S. L. M., Antifouling coatings via tethering of hyperbranched polyglycerols on biomimetic anchors. Industrial & Engineering Chemistry Research 2016, 55 (7), 1890-1901.

148) Pranantyo, D.; Xu, L. Q.; Neoh, K. G.; Kang, E. T.; Ng, Y. X.; Teo, S. L. M., Tea stains-inspired initiator primer for surface grafting of antifouling and antimicrobial polymer brush coatings. Biomacromolecules 2015, 16 (3), 723-732.

149) Xu, L. Q.; Pranantyo, D.; Neoh, K. G.; Kang, E. T.; Fu, G. D., Thiol reactive maleimido-containing tannic acid for the bioinspired surface anchoring and post-functionalization of antifouling coatings. ACS Sustainable Chemistry & Engineering 2016, 4 (8), 4264-4272.

150) Xu, L. Q.; Pranantyo, D.; Neoh, K. G.; Kang, E. T., Tea stains-inspired antifouling coatings based on tannic acid-functionalized agarose. ACS Sustainable Chemistry & Engineering 2017, 5 (4), 3055-3062.

151) Kim, H. J.; Kim, D. G.; Yoon, H.; Choi, Y. S.; Yoon, J.; Lee, J. C., Polyphenol/$Fe^{III}$ complex coated membranes having multifunctional properties prepared by a one-step fast assembly. Advanced Materials Interfaces 2015, 2 (14), 1500298.

152) Kim, S.; Gim, T.; Kang, S. M., Versatile, tannic acid-mediated surface PEGylation for marine antifouling applications. ACS Applied Materials & Interfaces 2015, 7 (12), 6412-6416.

153) Kim, S.; Jeong, Y.; Kang, S. M., Marine antifouling surface coatings using tannic acid and poly(N-vinylpyrrolidone). Bulletin of the Korean Chemical Society 2016, 37 (3), 404-407.

154) Chen, S. Q.; Xie, Y.; Xiao, T. J.; Zhao, W. F.; Li, J. S.; Zhao, C. S., Tannic acid-inspiration and post-crosslinking of zwitterionic polymer as a universal approach towards antifouling surface. Chemical Engineering Journal 2018, 337, 122-132.
155) Dong, C. X.; Wang, Z.; Wu, J. H.; Wang, Y.; Wang, J. X.; Wang, S. C., A green strategy to immobilize silver nanoparticles onto reverse osmosis membrane for enhanced anti-biofouling property. Desalination 2017, 401, 32-41.
156) Busscher, H. J.; van der Mei, H. C.; Subbiahdoss, G.; Jutte, P. C.; van den Dungen, J.; Zaat, S. A. J.; Schultz, M. J.; Grainger, D. W., Biomaterial-associated infection: Locating the finish line in the race for the surface. Science Translational Medicine 2012, 4, 153rv10.
157) Busscher, H. J.; van der Mei, H. C., How do bacteria know they are on a surface and regulate their response to an adhering state? Plos Pathogens 2012, 8 (1). e1002440.
158) Davies, D., Understanding biofilm resistance to antibacterial agents. Nature Reviews Drug Discovery 2003, 2 (2), 114-122.
159) Hook, A. L.; Chang, C. Y.; Yang, J.; Luckett, J.; Cockayne, A.; Atkinson, S.; Mei, Y.; Bayston, R.; Irvine, D. J.; Langer, R.; Anderson, D. G.; Williams, P.; Davies, M. C.; Alexander, M. R., Combinatorial discovery of polymers resistant to bacterial attachment. Nature Biotechnology 2012, 30 (9), 868-875.
160) Campoccia, D.; Montanaro, L.; Arciola, C. R., A review of the clinical implications of anti-infective biomaterials and infection-resistant surfaces. Biomaterials 2013, 34 (33), 8018-8029.
161) Asri, L.; Crismaru, M.; Roest, S.; Chen, Y.; Ivashenko, O.; Rudolf, P.; Tiller, J. C.; van der Mei, H. C.; Loontjens, T. J. A.; Busscher, H. J., A shape-adaptive, antibacterial-coating of immobilized quaternary-ammonium compounds tethered on hyperbranched polyurea and its mechanism of action. Advanced Functional Materials 2014, 24 (3), 346-355.

162) Muszanska, A. K.; Busscher, H. J.; Herrmann, A.; van der Mei, H. C.; Norde, W., Pluronic-lysozyme conjugates as anti-adhesive and antibacterial bifunctional polymers for surface coating. Biomaterials 2011, 32 (26), 6333-6341.

163) Ahn, B. K.; Das, S.; Linstadt, R.; Kaufman, Y.; Martinez-Rodriguez, N. R.; Mirshafian, R.; Kesselman, E.; Talmon, Y.; Lipshutz, B. H.; Israelachvili, J. N.; Waite, J. H., High-performance mussel-inspired adhesives of reduced complexity. Nature Communications 2015, 6, 8663.

164) Ryu, J. H.; Messersmith, P. B.; Lee, H., Polydopamine surface chemistry: A decade of discovery. ACS Applied Materials & Interfaces 2018, 10 (9), 7523-7540.

165) Han, L.; Lu, X.; Liu, K. Z.; Wang, K. F.; Fang, L. M.; Weng, L. T.; Zhang, H. P.; Tang, Y. H.; Ren, F. Z.; Zhao, C. C.; Sun, G. X.; Liang, R.; Li, Z. J., Mussel-inspired adhesive and tough hydrogel based on nanoclay confined dopamine polymerization. ACS Nano 2017, 11 (3), 2561-2574.

166) Liu, X. S.; Cao, J. M.; Li, H.; Li, J. Y.; Jin, Q.; Ren, K. F.; Ji, J., Mussel-inspired polydopamine: A biocompatible and ultrastable coating for nanoparticles in vivo. ACS Nano 2013, 7 (10), 9384-9395.

167) d'Ischia, M.; Napolitano, A.; Ball, V.; Chen, C. T.; Buehler, M. J., Polydopamine and eumelanin: From structure-property relationships to a unified tailoring strategy. Accounts of Chemical Research 2014, 47 (12), 3541-3550.

168) Jiang, J. H.; Zhu, L. P.; Zhu, L. J.; Zhang, H. T.; Zhu, B. K.; Xu, Y. Y., Antifouling and antimicrobial polymer membranes based on bioinspired polydopamine and strong hydrogen-bonded poly(N-vinyl pyrrolidone). ACS Applied Materials & Interfaces 2013, 5 (24), 12895-12904.

169) Zhao, Y. H.; Wu, Y.; Wang, L.; Zhang, M. M.; Chen, X.; Liu, M. J.; Fan, J.; Liu, J. Q.; Zhou, F.; Wang, Z. K., Bio-inspired reversible underwater adhesive. Nature Communications 2017, 8, 2218.

170) Li, L.; Yan, B.; Yang, J. Q.; Chen, L. Y.; Zeng, H. B., Novel mussel-inspired injectable self-healing hydrogel with anti-biofouling property. Advanced Materials 2015, 27 (7), 1294-1299.

171) Ma, Y. F.; Ma, S. H.; Wu, Y.; Pei, X. W.; Gorb, S. N.; Wang, Z. K.; Liu, W. M.; Zhou, F., Remote control over underwater dynamic attachment/detachment and locomotion. Advanced Materials 2018, 30, 1801595.

172) Kang, T.; Banquy, X.; Heo, J. H.; Lim, C. N.; Lynd, N. A.; Lundberg, P.; Oh, D. X.; Lee, H. K.; Hong, Y. K.; Hwang, D. S.; Waite, J. H.; Israelachvili, J. N.; Hawker, C. J., Mussel-inspired anchoring of polymer loops that provide superior surface lubrication and antifouling properties. ACS Nano 2016, 10 (1), 930-937.

173) Han, L. B.; Gong, L.; Chen, J. S.; Zhang, J. W.; Xiang, L.; Zhang, L.; Wang, Q.; Yan, B.; Zeng, H. B., Universal mussel-inspired ultrastable surface-anchoring strategy via adaptive synergy of catechol and cations. ACS Applied Materials & Interfaces 2018, 10 (2), 2166-2173.

174) Zhou, R.; Ren, P. F.; Yang, H. C.; Xu, Z. K., Fabrication of antifouling membrane surface by poly(sulfobetaine methacrylate)/polydopamine co-deposition. Journal of Membrane Science 2014, 466, 18-25.

175) Huang, R. L.; Liu, X.; Ye, H. J.; Su, R. X.; Qi, W.; Wang, L. B.; He, Z. M., Conjugation of hyaluronic acid onto surfaces via the interfacial polymerization of dopamine to prevent protein adsorption. Langmuir 2015, 31 (44), 12061-12070.

176) Hwang, G. B.; Page, K.; Patir, A.; Nair, S. P.; Allan, E.; Parkin, I. P., The anti-biofouling properties of superhydrophobic surfaces are short-lived. ACS Nano 2018, 12 (6), 6050-6058.
177) Yu, K.; Kizhakkedathu, J. N., Synthesis of functional polymer brushes containing carbohydrate residues in the pyranose form and their specific and nonspecific interactions with proteins. Biomacromolecules 2010, 11 (11), 3073-3085.
178) Yu, K.; Lai, B. F. L.; Kizhakkedathu, J. N., Carbohydrate structure dependent hemocompatibility of biomimetic functional polymer brushes on surfaces. Advanced Healthcare Materials 2012, 1 (2), 199-213.
179) Kizhakkedathu, J. N.; Brooks, D. E., Synthesis of poly(N,N-dimethylacrylamide) brushes from charged polymeric surfaces by aqueous ATRP: Effect of surface initiator concentration. Macromolecules 2003, 36 (3), 591-598.
180) ul-Haq, M. I.; Shenoi, R. A.; Brooks, D. E.; Kizhakkedathu, J. N., Solvent-assisted anionic ring opening polymerization of glycidol: Toward medium and high molecular weight hyperbranched polyglycerols. Journal of Polymer Science Part A-Polymer Chemistry 2013, 51 (12), 2614-2621.
181) Yu, K.; Andruschak, P.; Yeh, H. H.; Grecov, D.; Kizhakkedathu, J. N., Influence of dynamic flow conditions on adsorbed plasma protein corona and surface-induced thrombus generation on antifouling brushes. Biomaterials 2018, 166, 79-95.
182) Elwood, C. N.; Lo, J.; Chou, E.; Crowe, A.; Arsovska, O.; Adomat, H.; Miyaoka, R.; Tomlinson-Guns, E.; Monga, M.; Chew, B. H.; Lange, D., Understanding urinary conditioning film components on ureteral stents: profiling protein components and evaluating their role in bacterial colonization. Biofouling 2013, 29 (9), 1115-1122.

183) Canales, B. K.; Higgins, L.; Markowski, T.; Anderson, L.; Li, Q. A.; Monga, M., Presence of five conditioning film proteins are highly associated with early stent encrustation. Journal of Endourology 2009, 23 (9), 1437-1442.

184) Janssen, C.; Lo, J.; Jager, W.; Moskalev, I.; Law, A.; Chew, B. H.; Lange, D., A high throughput, minimally invasive, ultrasound guided model for the study of catheter associated urinary tract infections and device encrustation in mice. Journal of Urology 2014, 192 (6), 1856-1863.

185) Richardson, J. J.; Bjornmalm, M.; Caruso, F., Technology-driven layer-by-layer assembly of nanofilms. Science 2015, 348 (6233), aaa2491.

186) Tang, Z. Y.; Wang, Y.; Podsiadlo, P.; Kotov, N. A., Biomedical applications of layer-by-layer assembly: From biomimetics to tissue engineering. Advanced Materials 2006, 18 (24), 3203-3224.

187) Rahim, M. A.; Kristufek, S. L.; Pan, S. J.; Richardson, J. J.; Caruso, F., Phenolic building blocks for the assembly of functional materials. Angewandte Chemie-International Edition 2019, 58 (7), 1904-1927.

188) Zhong, Q. Z.; Li, S. Y.; Chen, J. Q.; Xie, K.; Pan, S. J.; Richardson, J. J.; Caruso, F., Oxidation-mediated kinetic strategies for engineering metal-phenolic networks. Angewandte Chemie-International Edition 2019, Doi: 10.1002/anie.201907666.

189) Lee, B. P.; Messersmith, P. B.; Israelachvili, J. N.; Waite, J. H., Mussel-inspired adhesives and coatings. Annual Review of Materials Research 2011, 41, 99-132.

190) Liu, Y. L.; Ai, K. L.; Lu, L. H., Polydopamine and its derivative materials: Synthesis and promising applications in energy, environmental, and biomedical fields. Chemical Reviews 2014, 114 (9), 5057-5115.

191) Delparastan, P.; Malollari, K. G.; Lee, H.; Messersmith, P. B., Direct evidence for the polymeric nature of polydopamine. Angewandte Chemie-International Edition 2019, 58 (4), 1077-1082.

192) Lim, C.; Huang, J.; Kim, S.; Lee, H.; Zeng, H.; Hwang, D. S., Nanomechanics of poly(catecholamine) coatings in aqueous solutions. Angewandte Chemie-International Edition 2016, 55 (10), 3342-3346.

193) Wang, B.; Wang, G. C.; Zhao, B. J.; Chen, J. J.; Zhang, X. Y.; Tang, R. K., Antigenically shielded universal red blood cells by polydopamine-based cell surface engineering. Chemical Science 2014, 5 (9), 3463-3468.

194) Kang, S. M.; You, I.; Cho, W. K.; Shon, H. K.; Lee, T. G.; Choi, I. S.; Karp, J. M.; Lee, H., One-step modification of superhydrophobic surfaces by a mussel-inspired polymer coating. Angewandte Chemie-International Edition 2010, 49 (49), 9401-9404.

195) Yu, X.; Fan, H. L.; Wang, L.; Jin, Z. X., Formation of polydopamine nanofibers with the aid of folic acid. Angewandte Chemie-International Edition 2014, 53 (46), 12600-12604.

196) Liu, Y. X.; Chang, C. P.; Sun, T., Dopamine-assisted deposition of dextran for nonfouling applications. Langmuir 2014, 30 (11), 3118-3126.

197) Mei, Y.; Yu, K.; Lo, J. C. Y.; Takeuchi, L. E.; Hadjesfandiari, N.; Yazdani-Ahmadabadi, H.; Brooks, D. E.; Lange, D.; Kizhakkedathu, J. N., Polymer-nanoparticle interaction as a design principle in the development of a durable ultrathin universal binary antibiofilm coating with long-term Activity. ACS Nano 2018, 12 (12), 11881-11891.

198) Ju, K. Y.; Lee, Y.; Lee, S.; Park, S. B.; Lee, J. K., Bioinspired polymerization of dopamine to generate melanin-like nanoparticles having an excellent free-radical-scavenging property. Biomacromolecules 2011, 12 (3), 625-632.

199) Ai, K. L.; Liu, Y. L.; Ruan, C. P.; Lu, L. H.; Lu, G. Q., $Sp^2$ C-dominant N-doped carbon sub-micrometer spheres with a tunable size: A versatile platform for highly efficient oxygen-reduction catalysts. Advanced Materials 2013, 25 (7), 998-1003.
200) Li, Y. W.; Xie, Y. J.; Wang, Z.; Zang, N. Z.; Carniato, F.; Huang, Y. R.; Andolina, C. M.; Parent, L. R.; Ditri, T. B.; Walter, E. D.; Botta, M.; Rinehart, J. D.; Gianneschi, N. C., Structure and function of iron-loaded synthetic melanin. ACS Nano 2016, 10 (11), 10186-10194.
201) Bergtold, C.; Hauser, D.; Chaumont, A.; El Yakhlifi, S.; Mateescu, M.; Meyer, F.; Metz-Boutigue, M. H.; Frisch, B.; Schaaf, P.; Ihiawakrim, D.; Ersen, O.; Monnier, C. A.; Petri-Fink, A.; Rothen-Rutishauser, B.; Ball, V., Mimicking the chemistry of natural eumelanin synthesis: The KE sequence in polypeptides and in proteins allows for a specific control of nanosized functional polydopamine formation. Biomacromolecules 2018, 19 (9), 3693-3704.
202) Chassepot, A.; Ball, V., Human serum albumin and other proteins as templating agents for the synthesis of nanosized dopamine-eumelanin. Journal of Colloid and Interface Science 2014, 414, 97-102.
203) Hong, S.; Na, Y. S.; Choi, S.; Song, I. T.; Kim, W. Y.; Lee, H., Non-covalent self-assembly and covalent polymerization co-contribute to polydopamine formation. Advanced Functional Materials 2012, 22, 4711-4717.
204) Ponzio, F.; Bertani, P.; Ball, V., Role of surfactants in the control of dopamine-eumelanin particle size and in the inhibition of film deposition at solid-liquid interfaces. Journal of Colloid and Interface Science 2014, 431, 176-179.
205) Hong, S.; Wang, Y.; Park, S. Y.; Lee, H., Progressive fuzzy cation-$\pi$ assembly of biological catecholamines. Science Advances 2018, 4, eaat7457.

206) Jiang, J. H.; Zhu, L. P.; Zhu, L. J.; Zhu, B. K.; Xu, Y. Y., Surface characteristics of a self-polymerized dopamine coating deposited on hydrophobic polymer films. Langmuir 2011, 27 (23), 14180-14187.

207) Zhang, C.; Ou, Y.; Lei, W. X.; Wan, L. S.; Ji, J.; Xu, Z. K., $CuSO_4/H_2O_2$-induced rapid deposition of polydopamine coatings with high uniformity and enhanced stability. Angewandte Chemie-International Edition 2016, 55 (9), 3054-3057.

208) Yu, K.; Creagh, A. L.; Haynes, C. A.; Kizhakkedathu, J. N., Lectin interactions on surface-grafted glycostructures: Influence of the spatial distribution of carbohydrates on the binding kinetics and rupture forces. Analytical Chemistry 2013, 85 (16), 7786-7793.

209) Goodman, D.; Kizhakkedathu, J. N.; Brooks, D. E., Evaluation of an atomic force microscopy pull-off method for measuring molecular weight and polydispersity of polymer brushes: Effect of grafting density. Langmuir 2004, 20 (15), 6238-6245.

210) Yu, K.; Lo, J. C. Y.; Mei, Y.; Haney, E. F.; Siren, E.; Kalathottukaren, M. T.; Hancock, R. E. W.; Lange, D.; Kizhakkedathu, J. N., Toward infection-resistant surfaces: Achieving high antimicrobial peptide potency by modulating the functionality of polymer brush and peptide. ACS Applied Materials & Interfaces 2015, 7 (51), 28591-28605.

211) Gao, G. Z.; Lange, D.; Hilpert, K.; Kindrachuk, J.; Zou, Y. Q.; Cheng, J. T. J.; Kazemzadeh-Narbat, M.; Yu, K.; Wang, R. Z.; Straus, S. K.; Brooks, D. E.; Chew, B. H.; Hancock, R. E. W.; Kizhakkedathu, J. N., The biocompatibility and biofilm resistance of implant coatings based on hydrophilic polymer brushes conjugated with antimicrobial peptides. Biomaterials 2011, 32 (16), 3899-3909.

212) Lai, B. F. L.; Creagh, A. L.; Janzen, J.; Haynes, C. A.; Brooks, D. E.; Kizhakkedathu, J. N., The induction of thrombus generation on nanostructured neutral polymer brush surfaces. Biomaterials 2010, 31 (26), 6710-6718.

213) Iwasaki, T.; Tamai, Y.; Yamamoto, M.; Taniguchi, T.; Kishikawa, K.; Kohri, M., Melanin precursor influence on structural colors from artificial melanin particles: PolyDOPA, polydopamine, and polynorepinephrine. Langmuir 2018, 34 (39), 11814-11821.

214) Kozlovskaya, V.; Kharlampieva, E.; Drachuk, I.; Cheng, D.; Tsukruk, V. V., Responsive microcapsule reactors based on hydrogen-bonded tannic acid layer-by-layer assemblies. Soft Matter 2010, 6 (15), 3596-3608.

215) Sundaramurthy, A.; Vergaelen, M.; Maji, S.; Auzely-Velty, R.; Zhang, Z. Y.; De Geest, B. G.; Hoogenboom, R., Hydrogen bonded multilayer films based on poly(2-oxazoline)s and tannic acid. Advanced Healthcare Materials 2014, 3 (12), 2040-2047.

216) Ren, P. F.; Yang, H. C.; Liang, H. Q.; Xu, X. L.; Wan, L. S.; Xu, Z. K., Highly stable, protein-resistant surfaces via the layer-by-layer assembly of poly(sulfobetaine methacrylate) and tannic acid. Langmuir 2015, 31 (21), 5851-5858.

217) Mandakhalikar, K. D.; Wang, R.; Rahmat, J. N.; Chiong, E.; Neoh, K. G.; Tambyah, P. A., Restriction of in vivo infection by antifouling coating on urinary catheter with controllable and sustained silver release: a proof of concept study. BMC Infectious Diseases 2018, 18, 370.

# Appendices

## Appendix A

### A.1 Polymers used for generating binary coatings in Chapter 2

| Polymers | dn/dc | Mn | Mw | PDI | Hydrodynamic radius (nm) | Source |
|---|---|---|---|---|---|---|
| PEG-H | ND | 35,000 | ND | ND | ND | Commercial |
| PVP-H | ND | ND | 40,000 | ND | ND | Commercial |
| PAAEGal-H | 0.16 | 55,900 | 150,000 | 2.69 | 7.7 | ATRP |
| PDMA-H<br>PDMA-43K | 0.15 | 43,000 | 102,000 | 2.38 | 6.2 | ATRP |
| PDMA-146K | 0.15 | 146,000 | 209,000 | 1.43 | 12.9 | ATRP |
| PDMA-213K | 0.15 | 213,000 | 356,000 | 1.67 | 15.4 | ATRP |
| PDMA-412K | 0.15 | 412,000 | 555,000 | 1.35 | 18.7 | ATRP |
| PDMA-UH<br>PDMA-795K | 0.15 | 795,000 | 1260,000 | 1.58 | 28.1 | ATRP |
| PDMA-996K | 0.15 | 996,000 | 1290,000 | 1.30 | 29.8 | ATRP |
| PAM-UH | 0.16 | 441,000 | 614,000 | 1.39 | 21.4 | ATRP |
| PHMA-UH | 0.14 | 503,000 | 120,0000 | 2.38 | 23.9 | ATRP |
| PHEA-UH | 0.12 | 932,000 | 1290,000 | 1.38 | 33.4 | ATRP |
| PTHMAM-UH | 0.17 | 632,000 | 1050,000 | 1.66 | 22.4 | ATRP |
| PHPMA-UH | 0.17 | 824,000 | 1150,000 | 1.39 | 23.7 | ATRP |
| PMPDSAH-UH | 0.15 | 968,000 | 1160,000 | 1.19 | 16.2 | ATRP |
| PMPC-UH | 0.15 | 1310,000 | 1600,000 | 1.22 | ND | ATRP |
| PVP-UH | ND | ND | 1300,000 | ND | ND | Commercial |
| PEO-UH | ND | ND | 900,000 (Mv) | ND | ND | Commercial |
| HPG-UH | 0.12 | 703,000 | 865,000 | 1.23 | ND | ROMBP |
| Dextran-UH | ND | 705,000 | 1190,000 | 1.68 | ND | Commercial |
| PEOX-UH | ND | ND | 500,000 | 3-4 | ND | Commercial |

**H- high molecular weight; UH- ultrahigh molecular weight; ROMBP- ring-opening multibranching polymerization.**

## A.2 Calculation of protein adsorption

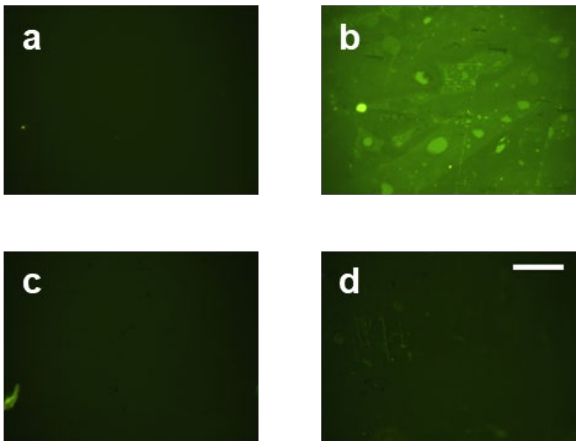


**Representative fluorescence microscopy images of uncoated PP film (a) before and (b) after BSA adsorption, PDA/PDMA-795K coated PP film (c) before and (d) after BSA adsorption. The scale bar is 100 µm. Uncoated and coated PP films were incubated with 1 mg/ml BSA for 2 h and thoroughly washed. The relative BSA adsorption on PDMA-795K coating was calculated as: (Intensity D - Intensity C)/(Intensity B - Intensity A).**

## A.3 Experimental set-up for long-term biofilm formation

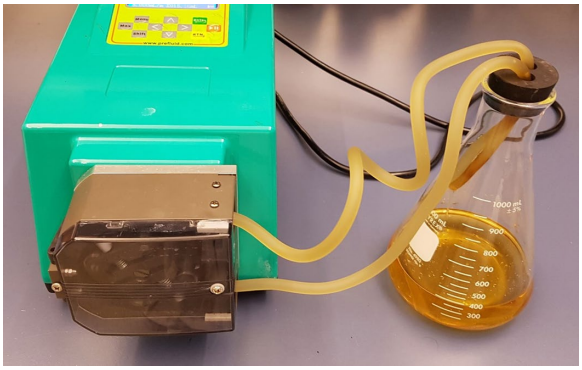

**The bacterial culture was circulated through the peristaltic roller pump (WF300-TH16, PreFluid) for different periods of time at 37 °C. Experimentation was performed using a flow rate of 114 mL/min, exposing uncoated and PDA/PDMA-795K coated titanium to *S. aureus* culture. The model was developed using silicone tubing (Tygon 3350 Sanitary Silicone Tubing) with an inner diameter of 6.4 mm. The uncoated and coated samples were placed in the tube near the outlet in the flask.**

# Appendix B

## B.1 Polymers used for generating binary coatings in Chapter 3

| Polymer | dn/dc | Mn | Mw | PDI | Source |
|---|---|---|---|---|---|
| PDMA | 0.15 | 795,000 | 1260,000 | 1.58 | ATRP |
| PMPC | 0.15 | 1310,000 | 1600,000 | 1.22 | ATRP |
| PEO | ND | ND | 1000,000 | ND | Commercial |
| HPG | 0.12 | 703,000 | 865,000 | 1.23 | ROMBP |
| PVP | ND | ND | 1300,000 | ND | Commercial |
| PEOX | ND | ND | 500,000 | 3-4 | Commercial |

## B.2 Influence of catecholamine type on the amount of PDA particle formation

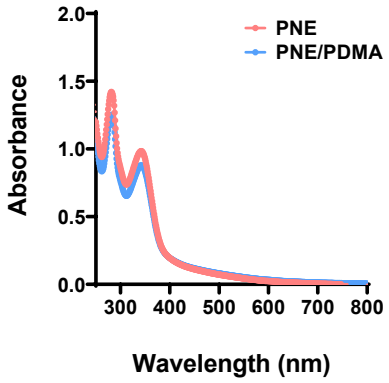


**UV spectra of particles formed in a Tris buffered solution of norepinephrine alone or with PDMA-795K.**

## B.3 Surface morphology of the PNE/PDMA-795K coating

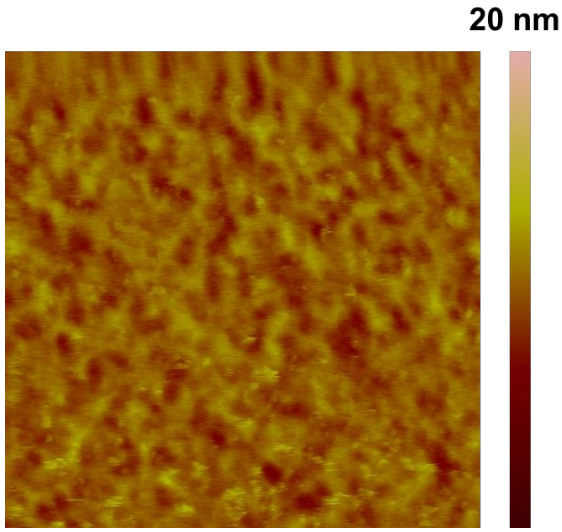


**Surface morphology of PNE/PDMA-795K coated silicon wafer determined by AFM in wet conditions. The scan size is 2 µm × 2 µm.**

## Appendix C

### C.1 Polymers used for generating multilayer films in Chapter 4

| Polymers | dn/dc | Mn | Mw | PDI | Hydrodynamic radius (nm) | Source |
|---|---|---|---|---|---|---|
| PDMA | 0.15 | 795,000 | 1260,000 | 1.58 | 28.1 | ATRP |
| PAM | 0.16 | 441,000 | 614,000 | 1.39 | 21.4 | ATRP |
| PHEA | 0.12 | 932,000 | 1290,000 | 1.38 | 33.4 | ATRP |
| PTHMAM | 0.17 | 632,000 | 1050,000 | 1.66 | 22.4 | ATRP |
| PHPMA | 0.17 | 824,000 | 1150,000 | 1.39 | 23.7 | ATRP |
| PMPDSAH | 0.15 | 968,000 | 1160,000 | 1.19 | 16.2 | ATRP |
| PMPC | 0.15 | 1310,000 | 1600,000 | 1.22 | ND | ATRP |
| PVP | ND | ND | 1300,000 | ND | ND | Commercial |
| PEO | ND | ND | 1000,000 (Mv) | ND | ND | Commercial |
| HPG | 0.12 | 703,000 | 865,000 | 1.23 | ND | ROMBP |
| Dextran | ND | ND | 500,000 | ND | ND | Commercial |
| PEOX | ND | ND | 500,000 | 3-4 | ND | Commercial |